RESEARCH ON CONSTELLATION DESIGN FOR VISIBLE LIGHT COMMUNICATION SYSTEMS

DISSERTATION

for the Degree of

DOCTOR OF PHILOSOPHY
(Electrical, Electronic and Computer Engineering)

MANH LE-TRAN

DECEMBER 2021

RESEARCH ON CONSTELLATION DESIGN FOR VISIBLE LIGHT COMMUNICATION SYSTEMS

DISSERTATION

for the Degree of

Doctor of Philosophy

(Electrical, Electronic and Computer Engineering)

MANH LE-TRAN

December 2021

RESEARCH ON CONSTELLATION DESIGN FOR VISIBLE LIGHT COMMUNICATION SYSTEMS

DISSERTATION

Submitted in Partial Fulfillment
of the Requirements for the
Degree of

DOCTOR OF PHILOSOPHY
(Electrical, Electronic and Computer Engineering)

at the

UNIVERSITY OF ULSAN

by

Manh Le-Tran
Supervisor: Professor Sunghwan Kim
December 2021

Publication No._____

Research on constellation design for visible light communication systems

Approved by Supervisory Committee:

Prof. Sungoh Kwon, *chair*

Prof. Jin-Ghoo Choi

Prof. Sungyoon Jung

Prof. Jiho Song

Prof. Sunghwan Kim, *adviser*

Department of Electrical, Electronic and

Computer Engineering, University of Ulsan

December, 2021

VITA

Manh Le-Tran was born in Thanh Hoa, Vietnam on August 28, 1992. He received the B.S. degree from the Posts and Telecommunications Institute of Technology, in 2015. After graduation, he was a mobile network engineer at Viettel Group, Vietnam, from 2015 to 2016. In March 2017, he started pursuing the combined M.S. and Ph.D. degrees as a researcher at the University of Ulsan, South Korea under the supervision of professor Sunghwan Kim. His main research interests include 5G communication, visible light communication, and modulation techniques.

Dedicated to my family

for their belief, love and support

ACKNOWLEDGMENTS

This thesis would not have been possible without the unquestionable support of many people. I would like to express my gratitude to everyone who contributed to this thesis.

To begin, I would like to express my profound gratitude to my advisor, Prof. Sunghwan Kim, for giving me the opportunity to join the Coding and Information Theory (CIT) lab and for his excellent guidance during weekly meetings, which supported me in accomplishing my work. I am really appreciative of his unwavering support, consistent encouragement, and advice in both research and life.

Additionally, I would like to express my gratitude to my committee members for numerous constructive discussions and for offering their broad perspectives to refining the ideas in this dissertation. I am thankful to my lab-mate and friends at the University of Ulsan for their genuine friendship, passionate assistance, and happiness throughout my time in Ulsan, Korea.

I am deeply appreciative of the University of Ulsan for providing me through BK21+ programs with such an excellent research environment and financial support. Even more, UOU has given us the opportunity to pursue a variety of valuable topics with outstanding lecturers that will equip me with the skills need to research and work properly for the rest of my life.

Finally, but certainly not least, I am appreciative to my parents and fiance for their unconditional love and support. I would not be who I am now without their support.

ABSTRACT

RESEARCH ON CONSTELLATION DESIGN FOR VISIBLE LIGHT COMMUNICATION SYSTEMS

by: **Manh Le-Tran**

Advisor: **Prof. Sunghwan Kim**

Submitted in Partial Fulfillment of the Requirements for the Degree of Doctor of Philosophy (Electrical, Electronic and Computer Engineering)

December 2021

Visible light communication (VLC) has emerged in the recent years as a new way to communicate using the existing lighting infrastructure. The reason for the attraction of VLC is that conventional radio frequency (RF)-based wireless communication has already arrived at a bottleneck because of the shortage of RF spectrum, the limited potential to exploit, and high power consumption. VLC has great potential to provide high bandwidth and communication security, making it a strong alternative against conventional wireless communication techniques. Therefore, VLC is considered as a potential access option for future fifth generation wireless communications due to its advantages. More specifically, VLC is a technology that takes full advantage of visible light-emitting diodes (LEDs) for the dual purpose of illumination and data communications at very high speeds and is a sustainable and green technology with the potential to revolutionize approaches to how we will use lights in the near

future. Due to reusing the ubiquitous lighting infrastructure, VLC can provide an additional service at a comparably low extra cost. Then it has an unregulated spectrum, specifically from 400 to 800 THz, which provides a huge communication bandwidth to deliver license-free extremely high data rate services. Also, the VLC spectrum can be spatially reused in adjacent communication cells. Lastly, its narrow beam-width and line of sight (LOS) provide VLC with high secrecy and it has immunity to RF interference.

Signal constellation optimization is a well-known research topic, which dates back to the 60s. Although a number of different constellations have been proposed, not many have been considered in VLC systems, which contain some specific signal constraints. Therefore, the main objective of this thesis is to provide a treatment of the symbol designing problem for VLC from both reliability and energy efficiency points of view. In addition to the theoretical concepts, a substantial part of the thesis is devoted to the symbol designing problem, which is a signal design topic that aims at achieving low transmission error probability together with acceptable energy efficiency. Consequently, various problems and how to solve the optimization to achieve a good constellation with better performance are presented. All discussed algorithms involve the use of optimization software and theory of nonlinear optimization but nevertheless can deliver significant performance improvements, which is a very critical issue in the modern communication era.

Contents

List of Figures

List of Tables

Nomenclature

Notation	Description
AE	Autoencoder
AWGN	Additive White Gaussian Noise
BER	Bit Error Rate
BP	Back-propagation
BPSK	Binary Phase-shift Keying
CASCC	Channel-adaptive Space-collaborative Constellation
CC	Collaborative Constellation
CSI	Channel State Information
DL	Deep Learning
DNNs	Deep Neural Network
ED	Euclidean Distance
FC	Fully-connected
FOV	Field of View
GS	Geometrical Shaping
LACC	Layered Adaptive Collaborative Constellation
LED	Light-emitting Diode
LUT	Lookup Table
MIMO	Multiple-input Multiple-output
MISO	Multi-input Single-output
ML	Maximum Likelihood
MMSE	Minimum Mean Square Error
MSE	Mean Square Error
NOMA	Non-orthogonal Multiple Access
OFDM	Orthogonal Frequency Division Multiplexing
OOK	On-off Keying
OWC	Optical Wireless Communication
PD	Photo-diodes
PEP	Pairwise-error Probability
PPM	Pulse Position Modulation
PS	Probabilistic Shaping
PWM	Pulse Width Modulation
QAM	Quadrature Amplitude Modulation
RC	Repetition Coding
RF	Radio Frequency
SER	Symbol Error Rate
SGD	Stochastic Gradient Descent
SISO	Single-input Single-output
SM	Spatial Modulation
SMP	Spatial Multiplexing
SNR	Signal-to-noise
VLC	Visible Light Communication

ZF	Zero Forcing

Chapter 1

Introduction

1.1 Spectrum crunch and motivation to optical wireless communication and visible light communication

The global market for smartphones and tablets has grown tremendously in the last several years while the devices are getting immensely powerful as a result of consumers' desire for constant communication/internet access and continuous data exchange [1]–[3]. Along with the widespread adoption of efficient and always-connected smartphones, the very next major revolution in technology or the internet of things era is nearing, in which all items would be interconnected. Owing to its development and popularization, radio frequency (RF) communications are now the greatest method for wireless communication systems. Nevertheless, as the demand for wireless data traffic and smart mobile devices grows exponentially, serious problems are

appearing from the inside of the RF spectrum [4]. Given this context, the escalating congestion of the electromagnetic spectrum band is a major issue that has received much scientific and corporate attention [5]. Spectrum crunch is a problem that arises in the circumstances with a high demand for wireless resources. This increase results in spectrum crisis conditions such as congestion and poor maximum data rates in comparison to other communication mediums. As a result, the existing infrastructure is incapable of providing sufficient resources for wireless communication.

Numerous possible RF techniques, such as massive multiple-input multiple-output (MIMO) [6], non-orthogonal multiple access (NOMA) [7], and alternative antenna architectures, are yet insufficient or under development. Optical wireless communication (OWC) is one candidate technology that has demonstrated the ability to extend the possibilities of wireless technology [8] that operate in the visible band (390-750 nm). As a result, OWC has attracted significant attention during the last decade. Moreover, OWC is considered as a complementary and potentially interdependence communication technology to the traditional RF technique, which operates within a controlled and licensed electromagnetic spectrum band covering 30 kHz to 300 GHz [9].

Visible light communication (VLC) is a highly promising OWC technology for tackling the spectrum crunch challenge and there has constantly been increasing interest in VLC, motivated by the dramatic development of light-emitting diode (LED) technologies [10], [11] and increasingly scarce spectrum resources [12]–[14]. In addition, VLC offers high security, high data rates, and precise positioning detection, compared with other wireless communications systems [15]. Certainly, research in

this type of wireless optical communication has increased, particularly in light of the prospect of combining with RF systems. Another aspect that draws academics to this emerging area of study is the prospect of working at considerably higher frequencies in VLC that can enable extremely fast wireless communications.

More specifically, the explosive growth of LED has been immense, which makes the possibility of a fully functioning and practical communication system with VLC become more imminent in the near future [16]–[18]. Currently, LEDs are extremely reliable, environment friendly, and have a life expectancy that is much beyond that of conventional light bulbs. Apart from these unique qualities, when combined with a low-cost VLC transceiver circuit, common LEDs can function as VLC transmitters. Due to their various benefits, LEDs have started to be implemented in an increasing number of lighting and communicating applications, and it is expected that they might eventually entirely replace conventional lighting systems. Thus, the unfulfilled potential of ubiquitous LED illumination may be properly utilized. Additionally, growing interest in research of the visible light spectrum has resulted in the development of a variety of inventions that are currently on the market. Therefore, VLC may enable low-cost, high-speed wireless data transmission and its rapid growth demonstrate its promising future [19], [20].

1.2 Fundamental of VLC

1.2.1 The architecture of a VLC system

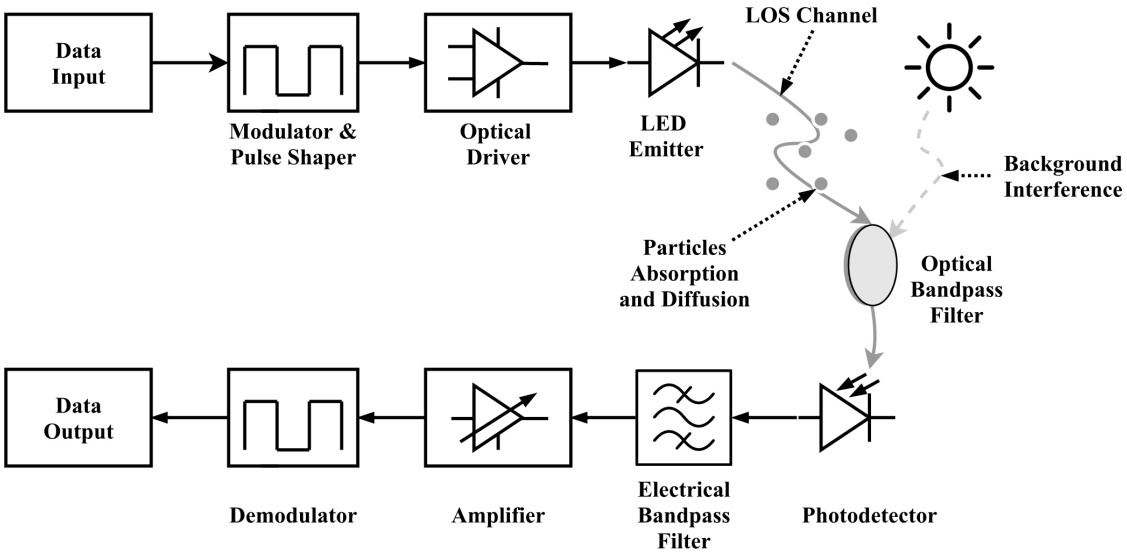

Figure 1.1: VLC System Model.

The principle underlying VLC technologies is to enable illumination and connectivity simultaneously that using light to facilitate communication [21]. As a result, VLC systems would have to include elements capable of transmitting and receiving light. More specifically, LEDs are employed as transmitters in a large portion of published researches to modulate the intensity of light in order to transmit information. Numerous modulation techniques had been studied in the past for optical wireless communication [22]. On-off keying (OOK) is the simplest and most often used modulation technique in communication systems, owing to its simplicity and ability to appropriately utilize bandwidth. Nonetheless, by combining high-order quadrature

amplitude modulation (QAM) [23] with modulation schemes such as orthogonal frequency division multiplexing (OFDM) [24] or discrete multi-tone, the transmission rate may be significantly increased. On the receiver end, photo-diodes (PD) are used to directly detect the received light and convert it to the information stream as the output of the system.

In indoor wireless VLC systems, intensity modulation and direct detection techniques are employed owing to their simplicity and low cost [11]. Signals are modulated to the intensity of the emitted visible light at the transmitter and are directly detected by converting the optical signal received by PDs to an electrical signal. Furthermore, the high data rates can readily be exploited to create optical MIMO communications systems [25].

The Figure 1.1 illustrates the layout of a simplified VLC system. Almost similar to the RF communication system, the data stream is passed through the modulation module and various other coding units before being transmitted using a current-driving LED. Furthermore, the receivers should be in direct line of sight of the LEDs in order to receive the information-carrying beams of light. However, there should be a degradation in the strength of the optical signals during propagation related to particle dispersion and the intrinsic interference of ambient light. Consequently, filters may be used to decrease noise [11]. At the receiving end, light reaches the PD, directly changing the current. Also, the use of amplifiers reduces the vulnerability of information to noise while the signal is demodulated in order to restore its original data.

The VLC transmitter

A VLC transmitter is a unit that converts information to signals that can be transmitted through visible light across a VLC channel [26]. The goal is to simultaneously emit light and send information. Nevertheless, the delivery of information should not impair the principal function of LEDs, that is lighting and signaling. From this perspective, the VLC transmitter must be capable of adapting to changing illumination conditions. That is, it is expected to utilize a certain power level to avoid noticeable flickering and to accommodate for dimming. The encoder or micro-controllers are cost-effective options to transform the information into a modulated stream. More specifically, it controls the LEDs' operation in accordance with the binary data and the required bit rate. Moreover, the VLC transmitter parameters are mostly constrained by the properties of the LEDs. The information rate can be determined by the LEDs' switching capabilities, whereas the coverage region of the emitter is defined by the transmitted energy and the emitting angle.

The VLC receiver

The information from the received beam of light is recovered using the VLC receiver. It converts photons to an electrical current that the integrated decoding unit demodulates and decodes. A PD is a solid-state element that is employed as a detector. It produces a current as a result of the photoelectric effect in the depletion layer caused by incoming intense light on its surfaces. Nevertheless, because the incoming light is not just from the LEDs but also from various sources of light, the receivers are exposed to substantial interference. The interference impact can often be mitigated

by decreasing the field of view (FOV), which has an impact on the coverage areas. A broad FOV requires a greater network coverage, but at the expense of absorbing extra interference, which degrades the SNR [27]. On the other hand, expanding the surface of the PD can improve performance. When the current is converted to a voltage, it is amplified and filtered to remove DC bias, the high, and low-frequency noise. Following these procedures, the signal should coincide with the data-containing light that was sent. the data processing unit extracts the binary information from the received signals.

The VLC channel model

The primary characteristic of the VLC system is interconnected through a free-space optical communication channel. Due to the fact that light waves are electromagnetic waves, their strength diminishes with the square root of the distance, resulting in a quite weak signal level when reaching the recipient. As a result, it is critical to determine if the connection requires an undisturbed line-of-sight (LOS) path between the transmitter and receiver. LOS connections depend on this path, whereas NLOS connections depend on light reflection from diffusely reflecting surfaces. The LOS connection design optimizes energy efficiency and reduces multi-path distortions. Overall, the channel impulse response in indoor VLC systems generally consists of a LOS component and an NLOS component. In many papers, the LOS link is ensured to always exist between any LED and the PD. In practice, the LOS component is commonly assumed to be dominant and the NLOS component is much weaker that can be neglected. However, a distinguishing feature of the theoretical

works related to VLC channels is the strict LOS requirements, which prevent multi-path propagation. Multi-path has a modest impact on VLC, occurring only at the close transmitter-receiver ranges. As previously stated, SNR may be increased at the receiver by employing optical filters, by designing the optical system appropriately, or by utilizing filters.

Additionally, the VLC channels may consist of a variety of types of optical noise, such as disturbance from the sun, noise from other VLC emitters, or any source of light capable of transmitting the information. The quantity of interference, along with the inadequate signal strength, particularly at long ranges, has a major impact on the signal-to-noise ratio (SNR) in VLC systems.

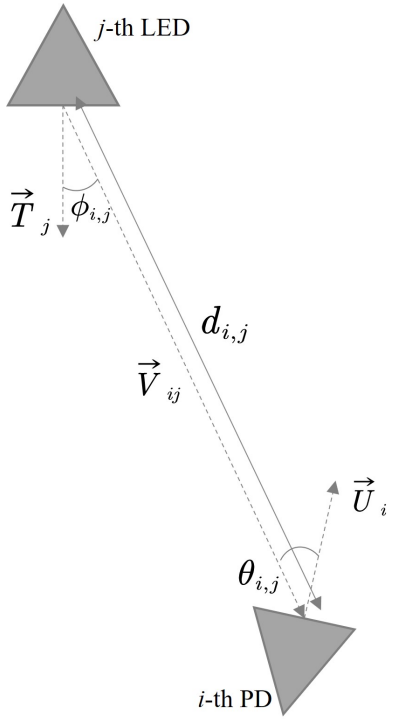

Figure 1.2: The geometry between a pair of LED-PD.

The channel impulse response provides essential information regarding the chan-

nel properties, including channel distortion, optical path loss. The orientation and configuration of the connection between the transmitter and receiver should be taken into account while studying an indoor VLC channel. As an initial exploration and for simplicity, we only consider LOS links between the transmitters and the receiver. In general, an indoor LOS MIMO-VLC system is considered with N_{T} LEDs at the transmitter and N_{R} photo-detectors (PDs) at the receivers. The received signal $\mathbf{y}$ can be represented as follows [28]

$$\mathbf{y} = \mathbf{H}\mathbf{x} + \mathbf{n} \tag{1.1}$$

where $\mathbf{x} = \left[x^{(1)}, x^{(2)}, ..., x^{(N_{\mathrm{T}})}\right]^T$ is a transmitted signal where components are $x^{(i)}$ as the i-th LED signal, $\mathbf{n}$ is the $N_{\mathrm{T}} \times 1$ real valued additive white Gaussian noise (AWGN) that represents the sum of high intensity ambient light shot noise and thermal noise with zero mean and variance σ^2. Moreover, the $N_{\mathrm{R}} \times N_{\mathrm{T}}$ channel matrix $\mathbf{H}$, which represents channel state information (CSI), is assumed to be known at the transmitter through a feedback channel [28]. Each coefficient h_{ji} between the i-th LED and the j-th PD is a non-negative real value and can be determined by [12]

$$h_{ji} = \begin{cases} \frac{(k+1)A_r}{2\pi\rho_{ji}^2}\cos^k(\phi)\cos(\psi) & ,0 \le \psi \le \psi_{1/2} \\ 0 & ,\psi > \psi_{1/2} \end{cases} \tag{1.2}$$

where ϕ is the angle of emergence with respect to the transmitter axis, and ψ is the angle of incidence with respect to its normal axis. The Lambertian mode order k is $k = \frac{-\ln 2}{\ln(\cos \Phi_{1/2})}$ where $\Phi_{1/2}$ is the half-power semi-angle of the LED. A_r and $\psi_{1/2}$ denote the effective area of the detector, and the field-of-view semi-angle of the detector, respectively; ρ_{ji} is the distance between the i-th LED and the j-th PD. In particular, it implies that the channel gain is zero if θ is larger than θ_{fov}, or equivalently the LED

is outside the PD FOV. At the receiver, the maximum-likelihood detector is utilized to detect the received signal and can be expressed as

$$(\bar{\mathbf{e}},\bar{s}) = \arg \min_{\mathbf{x}_i \in \mathcal{S}} \|\mathbf{y} - \mathbf{h}\mathbf{x}_i\|^2. \tag{1.3}$$

Let $\mathcal{X}$ be a given modulation constellation at the transmitter; then, the average electrical power of the constellation $\mathcal{X}$ can be given as $P_e = \mathrm{E}\{\|\mathbf{x}\|_2^2\}/T_s, \mathbf{x} \in \mathcal{X}$ where $\mathrm{E}\{.\}$ is the expectation operation, and T_s is the symbol period. Given that the spectral efficiency of R bits/s/Hz is considered, the cardinality of $\mathcal{X}$ is $|\mathcal{X}| = 2^R$, and therefore, total electrical power at the transmitter can be represented as $P_{\mathcal{X}} = \sum_{\mathbf{x}\in\mathcal{X}} \|\mathbf{x}\|_2^2$.

Moreover, w can be modeled as independent real-valued additive white Gaussian noise with zero mean and a variance of $\sigma_n^2 = \sigma_{\mathrm{sh}}^2 + \sigma_{\mathrm{th}}^2$, where σ_{th}^2 is the thermal noise variance [12]. The signal-dependent shot noise with the main source is the current of the PD can be mathematically described by a stationary Poisson random process and can be approximated by a Gaussian process with a variance of σ_{sh}^2 [22].

1.2.2 VLC advantages, drawbacks, and applications

It is well-known that VLC is anticipated as the next generation of wireless communications because of its distinctive features and benefits. VLC appears to offer the solution to several previously unresolved issues. It has the same features as visible light, including unlimited bandwidth, allowing high transmission rates, unlicensed spectrum, and safety for the body and electrical devices. Additionally, VLC is believed to be much safer than RF, because data transfer is offered in addition to illumination. Apart from these advantages, VLC is a low-cost solution that is simple to deploy. Several pros and disadvantages of the VLC method include the following:

- VLC Advantages
  - Does not have any health risks to human beings
  - Unrestricted technology
  - Security
  - Low-cost implementation
  - Green wireless communication technology with it has low power consumption.
- VLC Disadvantages
  - It requires both source and receiver should be in LOS
  - Limited transmission range
  - VLC based communication has interference issues from other ambient light sources.
  - Beam dispersion
- VLC Applications
  - Li-Fi, which is a bidirectional wireless system that transmits data via LED or infrared light
  - Indoor positioning
  - Forming a smart place with IoT devices
  - Smart transportation
  - RF spectrum crunch alleviation

- Provide communication medium in electromagnetic restricted areas
- Application in underwater or free space communications

1.3 Constellation design methods

The performance of telecommunication systems is highly dependent on a variety of parameters, including bandwidth, energy consumption, and hardware. As a result, several approaches have already been developed to enhance performance [29]. Recently, one of the key solutions has been the construction of optimal modulation techniques. In the literature, much effort has been devoted to construct the most efficient constellation schemes over a wide range of SNR values with the highest spectrum efficiency in terms of bit/s/Hz [30]. Two distinct families of constellation design techniques that can be mentioned are the geometrical shaping (GS) constellation design and the probabilistic shaping (PS) constellation design [31].

1.3.1 Geometrical shaping

The GS is devoted to the geometric representations of the constellation in Euclidean space in order to manipulate it [32]. Typically, the positions of constellation points in Euclidean distance (ED) space are altered in comparison to the frequently utilized cubic structures in communication systems. More precisely, it attempts to optimize the position of the constellation points to imitate a hyper-spherical border by using non-equidistant spacing and uniform distribution of the constellation points.

Generally, GS has been accomplished by optimizing the coordinates of the constel-

lation points in an irregular shape in two-dimensional geometry in order to maximize a metric, and a look-up table can be employed to maintain the symbols' positions. Moreover, $1/M$ is the probability of sending a single constellation symbol, wherein M is the total number of constellation points. Throughout the constellation diagram, the constellation points are not uniformly placed, enabling the improvement of several system parameters, such as the BER or channel capacity. More specifically, constellation design that is based on GS considers two criteria: error probability minimization or channel capacity maximization. The optimal constellation is determined by the SNR and a number of cost functions, such as the lowest possible symbol error rate or signal set capacity. The optimization problem to find the optimized constellation $\mathcal{X}^*$ can be formulated as

$$\begin{aligned} \mathcal{X}^* = \quad & \arg\max \quad \mathrm{R} \\ & st : \mathrm{E}\left[|\mathcal{X}|^2\right] \leq 1 \\ & |\mathcal{X}| = M \end{aligned} \tag{1.4}$$

where R is the objective function of the optimization problem. As a result, many studies utilized restricted non-linear optimization techniques to solve the constellation designing problem, which is usually a non-convex optimization problem. The optimization results achieved using typical interior point methods are initialization-dependent, implying that only locally optimum solutions are identified. Recently, machine learning techniques have garnered considerable attention as a means of replacing the whole transmitter and receiver architecture with neural networks. Similarly, most of the algorithms mentioned in this thesis are referred to as the GS method due to their efficiency in improving the performance of VLC systems.

1.3.2 Probabilistic shaping

The idea of PS is to regulate the probability of occurrence of constellation points in comparison to a uniform probability distribution. Unlike GS, PS employs an asymmetric distribution across equidistant constellation points [33]. Probabilistic shaping imposes an irrational distribution on the constellation points while retaining their equidistant set. There are two distinct strategies: operate the shaping operation after the encoding step or concatenate the encoding and shaping steps into a single step, simplifying the receiver design. In summary, to enhance sensitivity in the AWGN channel, PS enables the transmission symbol probabilities to be altered in order to reduce shaping loss. Additionally, another benefit of PS is the capacity to regulate the transmitted rate for any level of accuracy by changing the probability distribution of the constellation points.

1.4 Contribution and layout of the thesis

The dissertation consists of five chapters structured as follows:

In Chapter 1, we sum up all the motivation and fundamental knowledge relevant to VLC technologies, and related knowledge such as constellation design. Then, we show the outline of the dissertation.

In Chapter 2, we present a novel design of a layered adaptive collaborative constellation (LACC) for MIMO-VLC systems. Specifically, the LACC layered structure based on three fundamental principles simplifies the process of optimally designing constellations of any scale. We incorporate not only the channels in our model,

as well as the relationships between all the constellation points, rather than just a few basic points. The initial non-convex optimization problem is relaxed to a convex problem using a linear approximation approach. Additionally, by adopting the specifically layered constellation construction, the number of constraints in the optimization problem may be significantly decreased. Then, making use of the proposed constellation's identical lattice structure, an enhanced maximum likelihood (ML) detector is developed.

In Chapter 3, we introduce CCNet, a novel DL-based constellation design technique for VLC systems with LACC that significantly reduces complexity in comparison to previous approaches while retaining near-optimal performance. More specifically, the prepossessed channel state information (CSI) is fed to CCNet. Conversely, the presented CCNet architecture requires the implementation of certain hidden fully - connected layers (FC) nonlinear layers. Then, neurons in the hidden layers efficiently achieve the prediction task. On the other hand, CCNet would be first trained offline using synthetic data in order to reduce the mean square error (MSE). The trained model can then be implemented as a low-complexity, low-running-time online estimator.

In Chapter 4, we propose to design the sub-constellations at each LED to enhance the minimum Euclidean distance (MED) of the superposed constellation at the receiver, resulting in a considerable improvement in the system symbol error rate (SER). In particular, an optimization problem is constructed utilizing the constellations at each LED as unknown variables. By tackling the linearized optimization problem iteratively, an optimized solution vector could be used to construct sub-constellations

at each LED in order to maximize the ED while sticking to the constraints on total electrical power and maximum transmitted power. Additionally, we presented the inter-ED and intra-ED terms to minimize the number of constraints in the optimization problem, while utilizing some predetermined shape sub-constellations to significantly increase the ED values and improve symbol error rate (SER) performance.

Finally, in Chapter 5, we conclude the dissertation and discuss possible future research directions.

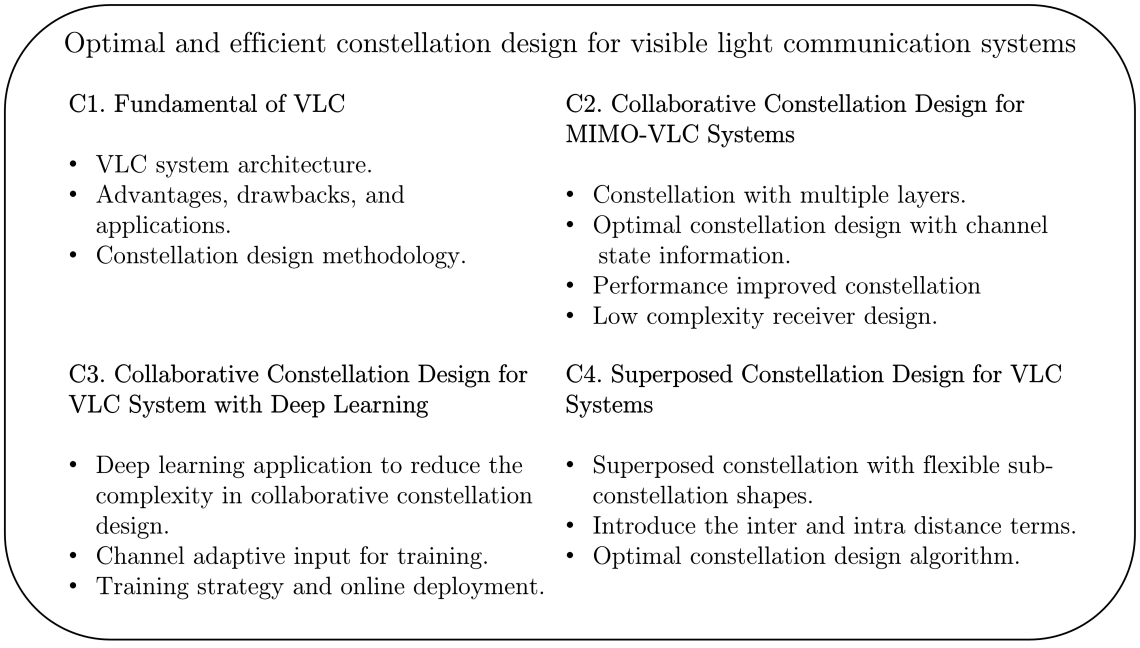

Figure 1.3: Main contributions of this dissertation.

Chapter 2

Collaborative constellation design for MIMO-VLC systems

2.1 Introduction and motivation

As briefly discussed in the Introduction, the channel in an indoor VLC system is typically deterministic, and the performance of MIMO-VLC systems heavily relies on channel correlations [34]. MIMO techniques such as repetition coding (RC) [13], [35], spatial multiplexing (SMP) [34], and spatial modulation (SM) [36] have been proposed for different indoor VLC channel conditions.

For MIMO-VLC systems employing the above-mentioned techniques, there exist two main problems. Firstly, channel correlation is an inevitable feature of MIMO-VLC systems, making the aforementioned techniques sacrifice spatial resources to alleviate the correlation impairment. As a consequence, a promising technique, space-collaborative constellation (CC) for 2×2 MIMO-VLC was proposed [37]. The min-

imum ED in a CC was maximized by designing symbols from multiple transmitter spaces that collaborate as closely as possible under constrained average power. In the CC, by mapping each dimension in the transmitter space to the corresponding LED, the relationships within the LEDs are exploited as spatial resources, and thus, give rise to the design of the space-collaborative constellation. Later, [38] extended the concept of CC to a larger number of LEDs and PDs. Secondly, the mentioned schemes and CC [37] have low mobility of receiver and weak robustness to the MIMO-VLC channel, which is directly related to the geometrical locations of transmitters and receivers. Consequently, the channel-adaptive space-collaborative constellation (CASCC) [39], [28] for MIMO-VLC systems further improved the CC scheme by considering the channel in the system model. Under a particular criterion, a CASCC was designed for 2×2 MIMO-VLC in terms of the basic four-point constellation, and later, was extended to a high-order constellation. More specifically, Xu et al. [28] proposed the design of a constellation that can adapt to different channels due to the changes in geometric locations of transmitters and receivers. An adaptation function is based on the ED of the received constellation at the receiver. However, by optimizing the ED between only four basic points [28], the extension to higher constellations was shown to be inefficient, especially when a significant correlation is present in the channel. On the other hand, the four-point constellation in the receiver space is considered as a diamond shape, which restricts the effectiveness of the channel adaptive constellation.

In this chapter, we follow a different approach and establish a general design for a layered adaptive collaborative constellation (LACC) for MIMO-VLC systems. The

proposed scheme is also based on space collaborative and channel adaptive principles [28]. Specifically, the layered structure of the LACC based on three basic points makes it more convenient and efficient to design constellations of any size. We not only consider the channel in our model, but we also build relations among all the constellation points, instead of a few basic points [28]. In addition, unlike CASCC, the basic constellation at the receiver space is not restricted to a diamond shape. Furthermore, to simplify the design, the number of layers considered in the optimization problem can be varied and depends on the correlation of MIMO-VLC channels. The original optimization problem is non-convex and is relaxed to a convex problem through a linear approximation method. Furthermore, the number of constraints in the optimization problem can be drastically reduced with the help of the specially layered constellation structure. Then, to take advantage of the similar lattice structure in the designed constellation, an improved ML detector is proposed. The idea of the low-complexity detector is to perform ML detection on constellation points inside the sphere centered at an initially estimated point. Simulation results show that LACC can achieve a significant performance gain over different schemes, such as RC, CC, CASCC, SM, and SMP. Therefore, the proposed constellation can be a good candidate for efficient transmission over various MIMO-VLC channels, especially the high-correlation ones. On the other hand, detection complexity is remarkably reduced with the help of the proposed low-complexity detector while maintaining the same performance as the ML detector, even in a very high correlation channel.

2.2 Constellation description

2.2.1 Constellation description

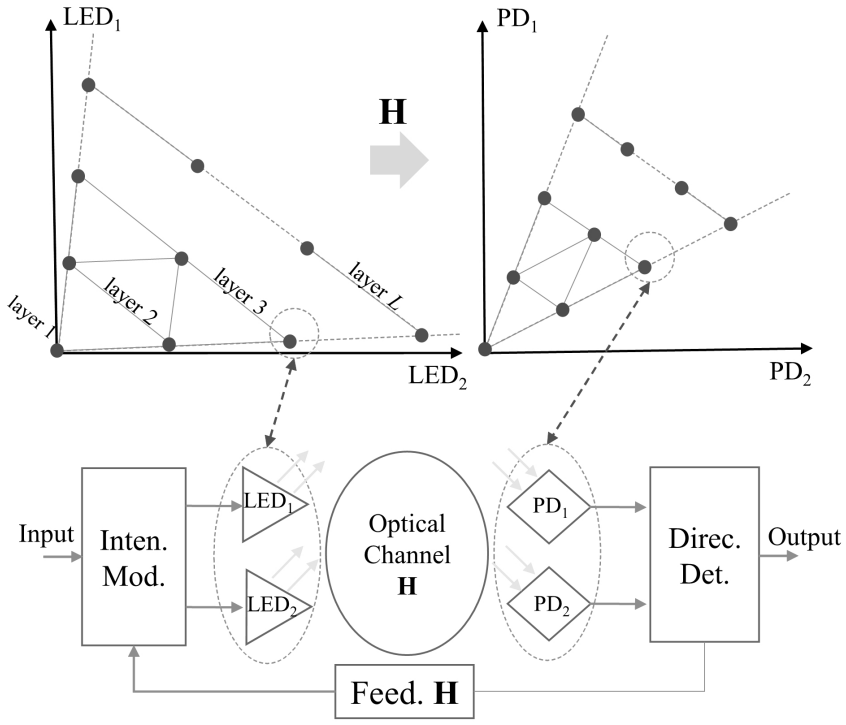

Figure 2.1: Collaborative constellation structure in the transmitter and receiver when $N_{\mathrm{T}} = N_{\mathrm{R}} = 2$.

Let us consider a MIMO-VLC system with a spectral efficiency of R bits/s/Hz, the transmitter constellation $\mathcal{X}$ of $M = 2^R$ symbols is denoted as $\mathcal{X} = [\mathbf{x}_1, ..., \mathbf{x}_M]$ where $\mathbf{x}_i = \left[x_i^{(1)}, x_i^{(2)}, ..., x_i^{(N_{\mathrm{T}})}\right]^T \in \mathcal{X}$ is a signal vector transmitted through the LEDs. As in previous research [37], [28], we describe the structure of the LACC constellation for a 2×2 MIMO-VLC system, or $N_{\mathrm{T}} = N_{\mathrm{R}} = 2$. A discussion of higher numbers of N_{T} and N_{R} will be provided later. Consequently, transmitted signal $\mathbf{x}_i$ can simply be

represented as $\mathbf{x}_i = (x_i^{(1)}, x_i^{(2)})^T \in \mathcal{X}$, where $x_i^{(1)}, x_i^{(2)}$ denote the signal transmitted by LED_1 and LED_2, respectively. Since the number of symbols in $\mathcal{X}$ has to be power of 2, firstly, we give our description to design a layered constellation $\mathcal{S}$. By effectively designing set $\mathcal{S}$, the constellation $\mathcal{X}$ used in transmission can be obtained by selecting 2^R optimal constellation points from $\mathcal{S}$. The detail is given in the followings.

Inspired by the space-collaborative constellation in [37], our goal is to first define a constellation that consist of L layers, as in Fig.2.1. Furthermore, in the l-th layer (l=1, ...,L) there are l constellation points. It can be observed that the L layers constellation can be generated from three basic points $\mathbf{s}_{11} = (0,0)^T$, $\mathbf{s}_{21} = (s_{21}^{(1)}, s_{21}^{(2)})^T$, and $\mathbf{s}_{22} = (s_{22}^{(1)}, s_{22}^{(2)})^T$; with $\mathbf{s}_{mi} = (s_{mi}^{(1)}, s_{mi}^{(2)})^T$ is the i-th constellation point of the m-th layer, and $s_{mi}^{(1)}, s_{mi}^{(2)}$ denote signals collaboratively transmitted by LED_1 and LED_2, respectively. Specifically, constellation $\mathcal{S}$ can be represented by

$$\mathcal{S} = \left\{ \mathbf{s}_{mi} | \mathbf{s}_{mi} = \left(s_{mi}^{(1)}, s_{mi}^{(2)} \right)^T = \left[(m-i)s_{21}^{(1)} + (i-1)\, s_{22}^{(1)}, (m-i)s_{21}^{(2)} + (i-1)\, s_{22}^{(2)} \right]^T \right\}, \tag{2.1}$$

where $1 \leq m \leq L; 1 \leq i \leq m$.

Then, with any constellation $\mathbf{s}_{mi} \in \mathcal{S}$, $\mathcal{S} = [\mathbf{s}_{11}, \mathbf{s}_{21}, \mathbf{s}_{22}, \mathbf{s}_{31}, \mathbf{s}_{32}, \mathbf{s}_{33}, ..., \mathbf{s}_{L1}, \mathbf{s}_{L2}, ...\mathbf{s}_{LL}]$, we define the corresponding received constellation at the two PDs by vector $\mathbf{r}_{mi}$ with $r_{mi}^{(1)}, r_{mi}^{(2)}$ denoting signals received by PD_1 and PD_2 as follows

$$\mathbf{r}_{mi} = \mathbf{H}\mathbf{s}_{mi} \Leftrightarrow \begin{bmatrix} r_{mi}^{(1)} \\ r_{mi}^{(2)} \end{bmatrix} = \begin{bmatrix} h_{11} & h_{12} \\ h_{21} & h_{22} \end{bmatrix} \begin{bmatrix} s_{mi}^{(1)} \\ s_{mi}^{(2)} \end{bmatrix} \tag{2.2}$$

where $\mathbf{H}$ is the 2×2 channel matrix. Therefore, the constellation in the receiver space in Fig.2.1 can be defined as $\mathcal{R} = [\mathbf{r}_{11}, \mathbf{r}_{21}, \mathbf{r}_{22}, \mathbf{r}_{31}, \mathbf{r}_{32}, \mathbf{r}_{33}, ..., \mathbf{r}_{L1}, \mathbf{r}_{L2}, ...\mathbf{r}_{LL}]$ where $\mathcal{R} = \mathbf{H}\mathcal{S}$ and $|\mathcal{R}| = |\mathcal{S}|$. Similar to [28], there is one-to-one mapping between any

pair of constellation points between $\mathcal{S}$ and $\mathcal{R}$. The constellation $\mathcal{R}$ can then be represented as

$$\mathcal{R} = \left\{ \mathbf{r}_{mi} | \mathbf{r}_{mi} = \left(r_{mi}^{(1)}, r_{mi}^{(2)}\right)^T = \left[(m-i)r_{21}^{(1)} + (i-1)\, r_{22}^{(1)}, (m-i)r_{21}^{(2)} + (i-1)\, r_{22}^{(2)}\right]^T \right\}. \tag{2.3}$$

It can be observed that total number of points in L layers collaborative constellation will be $L(L+1)/2$. To design constellation $\mathcal{X}$ of $M = 2^R$ space-collaborative constellation points, the number of layers in $\mathcal{S}$ satisfies $L(L+1)/2 \geq M$, so that $L = \left\lceil \frac{\sqrt{8M+1}-1}{2} \right\rceil$. To select $M = 2^R$ points from equidistant constellation $\mathcal{S}$, one way is to take M points with smallest ED to (0,0) as in [28], since these points will have lowest electrical power level. We give the Algorithm 1 to generate the constellation $\mathcal{X}$ of R bits/s/Hz from three basic points $\mathbf{s}_{11}, \mathbf{s}_{21}, \mathbf{s}_{22}$.

It can be seen that to construct any layered constellation, the optimal three basic points $\mathbf{s}_{11}, \mathbf{s}_{21}, \mathbf{s}_{22}$ are required for Algorithm 1. For example, the space-collaborative constellation in [37] can be generated from three basic points $\mathbf{s}_{11} = (0,0)^T, \mathbf{s}_{21} = (1,0)^T, \mathbf{s}_{22} = (0,1)^T$. The performance of this scheme however, can still be improved with consideration of the channel matrix. In [28], the basic four-point constellation is considered as being adaptive to the channel matrix, and harnesses the spatial resources effectively, compared with the CC in [37]. Specifically, CASCC is mainly based on two major features. First, the space collaborative build relations within the LEDs and thus design a constellation that each dimension maps the corresponding LED. Second, the channel adaptive that optimizing the EDs of constellation at the receiver in stead of the transmitter. It is worth mentioning that the design procedure of the four-point constellation in [28] is basically equivalent to the case with L=3 in

our scheme. However, optimizing the EDs among only four basic points [28] shows the extension to higher constellations is inefficient, especially when a significant correlation is presented in the MIMO-VLC channel. Therefore, the scheme in [28] gives favorable results only when the channel constellation is low enough. Moreover, with a very high correlation channel, the scheme in [28] failed to effectively extend the basic four points to a higher constellation. On the other hand, the received four-point constellation in [28] is restricted to a diamond shape, which reduces the effectiveness of the channel adaptive constellation. In the next section, we address the problem of finding the optimal three basic constellation points $\mathbf{s}_{11}, \mathbf{s}_{21}, \mathbf{s}_{22}$ that can improve system performance by considering the relationship between not only the three basic points but the whole L-layer constellation.

2.3 Collaborative constellation design

In this section, we present our proposed LACC constellation design by flexibly determining the optimal basic points in Algorithm 1 that can maximize the minimum ED between any two constellation points in the receivers. Relying on the structure in Fig. 1, our optimization problem is finding $\mathbf{s}_{11}, \mathbf{s}_{21}, \mathbf{s}_{22}$ that form a constellation $\mathcal{S}$ of L layers through Algorithm 1 and that optimize the distances between any two points of $\mathcal{R} = \mathbf{H}\mathcal{S}$, subject to the fixed total electrical power $P_{\max}$. The optimal points can then be used to generate a constellation of any number of layers L through Algorithm 1. It is worth mentioning that, as simulation results in a later section point out, considering a number of $L^* \leq L$ layers that is high enough can achieve a convergence value of minimum distance, and the consideration of L layers in the

optimization problem is unnecessary when designing an L-layer constellation. This will help lower the complexity of the constellation design process. Before we proceed,

Algorithm 1 Algorithm for Constellation extension

Input: Channel matrix $\{\mathbf{s}_{11}, \mathbf{s}_{21}, \mathbf{s}_{22}\}$ where $\mathbf{s}_{11} = (0,0)^T$, R bits

Output: Set $\mathcal{X}$ of M constellation points

1: calculate L

2: initialize $\mathcal{S} = \{\mathbf{s}_{11}, \mathbf{s}_{21}, \mathbf{s}_{22}\}$

first step is to generate $L(L+1)/2$ points from three basic constellation points

3: **for** $m = 3...L$ **do**

4: **for** $i = 1...m$ **do**

5: set $\mathcal{S} \leftarrow \mathcal{S} + \left\{ \mathbf{s}_{mi} | \mathbf{s}_{mi} = \left(s_{mi}^{(1)}, s_{mi}^{(2)}\right)^T = \left[(m-i)s_{21}^{(1)} + (i-1)\, s_{22}^{(1)}, (m-i)s_{21}^{(2)} + (i-1)\, s_{22}^{(2)}\right]^T \right\}$

6: **end for**

7: **end for**

find optimal constellation $\mathcal{X}$ from $\mathcal{S}$

8: for all $\mathbf{s}_{mi} \in \mathcal{S}$, select $M = 2^R$ points with the smallest ED to (0,0) to construct constellation $\mathcal{X}$

9: normalize the result optimal constellation $\mathcal{X}$ to the required average electrical power.

10: **return** constellation $\mathcal{X}$

we point out that the four basic–point constellation problem in [28] is equivalent to our problem, if we consider only $L^* = 3$. However, as the correlation of channel becomes higher, consideration of only three layers becomes ineffective. Let us define

$d_{\mathcal{R}}$ as the minimum ED between any two points $\mathbf{r}_{mi}, \mathbf{r}_{nj}$ that belong to a specific $\mathcal{R}$; $\mathbf{s}_{11}, \mathbf{s}_{21}, \mathbf{s}_{22}$ can be determined through optimization problem $\mathcal{P}_0$ as follows

$$\begin{aligned}\mathcal{P}_0 : \arg\max_{\mathbf{s}_{21},\mathbf{s}_{22}} \quad d_{\mathcal{R}}^2 &= \min_{\mathbf{r}_{mi}\neq\mathbf{r}_{nj};\mathbf{r}_{mi},\mathbf{r}_{nj}\in\mathcal{R}} d^2\left(\mathbf{r}_{mi},\mathbf{r}_{nj}\right) \\ &= \min_{\mathbf{s}_{mi}\neq\mathbf{s}_{nj};\mathbf{s}_{mi},\mathbf{s}_{nj}\in\mathcal{S}} \left\|\mathbf{H}\mathbf{s}_{mi}-\mathbf{H}\mathbf{s}_{nj}\right\|_2^2 \\ &\text{s.t.: } P_{\mathcal{S}} = \sum_{m=1}^{L}\sum_{i=1}^{m}\left\|\mathbf{s}_{mi}\right\|_2^2 \le P_{\max}\end{aligned} \tag{2.4}$$

Theorem 2.1 *The total electrical power of all constellation points generated from L layers can be calculated by*

$$\begin{aligned}P_{\mathcal{S}} = \sum_{m=1}^{L}\Bigg\{ &\left(\frac{m^3}{3}+\frac{m^2}{2}+\frac{m}{6}\right)\Big[\left(s_{21}^{(1)}\right)^2+\left(s_{21}^{(2)}\right)^2+ \\ &\left(s_{22}^{(1)}\right)^2+\left(s_{22}^{(2)}\right)^2\Big]+\left(\frac{m^3}{3}-\frac{m}{3}\right)\left(s_{21}^{(1)}s_{21}^{(2)}+s_{22}^{(1)}s_{22}^{(2)}\right)\Bigg\}.\end{aligned} \tag{2.5}$$

Proof: Theorem 1 is proven by using (2.1) and Faulhaber's formula [14] with some simple manipulations as follows:

$$\begin{aligned}P_{\mathcal{S}} &= \sum_{m=1}^{L}\sum_{i=1}^{m}\left\|\mathbf{s}_{mi}\right\|_2^2 = \sum_{m=1}^{L}\sum_{i=1}^{m}\left[\left(s_{mi}^{(1)}\right)^2+\left(s_{mi}^{(2)}\right)^2\right] \\ &= \sum_{m=1}^{L}\sum_{i=1}^{m}\Bigg\{\left[(m-i)s_{21}^{(1)}+(i-1)\,s_{22}^{(1)}\right]^2+\Big[(m-i)s_{21}^{(2)} \\ &+(i-1)\,s_{22}^{(2)}\Big]^2\Bigg\} = \sum_{m=1}^{L}\Bigg\{m^2\Big[\left(s_{21}^{(1)}\right)^2+\left(s_{21}^{(2)}\right)^2+\left(s_{22}^{(1)}\right)^2 \\ &+\left(s_{22}^{(2)}\right)^2\Big]+m\,(L-m)\left(s_{21}^{(1)}s_{21}^{(2)}+s_{22}^{(1)}s_{22}^{(2)}\right)\Bigg\} = \sum_{m=1}^{L}\Bigg\{\Bigg(\\ &\frac{m^3}{3}+\frac{m^2}{2}+\frac{m}{6}\Big)\Big[\left(s_{21}^{(1)}\right)^2+\left(s_{21}^{(2)}\right)^2+\left(s_{22}^{(1)}\right)^2+\left(s_{22}^{(2)}\right)^2\Big] \\ &+\left(\frac{m^3}{3}-\frac{m}{3}\right)\left(s_{21}^{(1)}s_{21}^{(2)}+s_{22}^{(1)}s_{22}^{(2)}\right)\Bigg\}\end{aligned} \tag{2.6}$$

Without loss of generality, we can assume $m \geq n \geq 1$, and we set $\alpha = m-n$; $\beta = i-j$. The distance between any two constellation points, $\mathbf{r}_{mi}, \mathbf{r}_{nj} \in \mathcal{R}$, can be represented with the aid of (2.3) as follows

$$\begin{aligned} d^2\left(\mathbf{r}_{mi}, \mathbf{r}_{nj}\right) = \left\|\mathbf{r}_{mi} - \mathbf{r}_{nj}\right\|^2 &= \left\{ \Big[(m-n)-(i-j)\Big] r_{21}^{(1)} \right. \\ &\left. + (i-j) r_{22}^{(1)} \right\}^2 + \left\{ \Big[(m-n)-(i-j)\Big] r_{21}^{(2)} + (i-j) r_{22}^{(2)} \right\}^2 \\ &= \left[(\alpha-\beta)\, r_{21}^{(1)} + \beta r_{22}^{(1)} \right]^2 + \left[(\alpha-\beta)\, r_{21}^{(2)} + \beta r_{22}^{(2)} \right]^2 \\ &= \left\| \begin{bmatrix} \alpha-\beta & \beta & 0 & 0 \\ 0 & 0 & \alpha-\beta & \beta \end{bmatrix} \begin{bmatrix} r_{21}^{(1)} \\ r_{22}^{(1)} \\ r_{21}^{(2)} \\ r_{22}^{(2)} \end{bmatrix} \right\|_2^2 \\ &= \left\| \mathbf{q}_{(\alpha-\beta)\beta} \mathbf{H} \mathbf{t} \right\|_2^2 = \mathbf{t}^T \mathbf{H}^T \mathbf{q}_{(\alpha-\beta)\beta}^T \mathbf{q}_{(\alpha-\beta)\beta} \mathbf{H} \mathbf{t} \\ &= \mathbf{t}^T \mathbf{Q}_{(\alpha-\beta)\beta} \mathbf{t} \end{aligned} \tag{2.7}$$

where $\mathbf{t} = \begin{bmatrix} s_{21}^{(1)} & s_{22}^{(1)} & s_{21}^{(2)} & s_{22}^{(2)} \end{bmatrix}^T$, $\mathbf{q}_{(\alpha-\beta)\beta} = \begin{bmatrix} \alpha-\beta & \beta & 0 & 0 \\ 0 & 0 & \alpha-\beta & \beta \end{bmatrix}$, and $\mathbf{Q}_{(\alpha-\beta)\beta} = \mathbf{H}^T \mathbf{q}_{(\alpha-\beta)\beta}^T \mathbf{q}_{(\alpha-\beta)\beta} \mathbf{H}$.

Assuming $\mathbf{\Phi} = \Big\{ (\alpha-\beta, \beta) \,|\alpha = m-n;\, \beta = i-j; 1 \leq n \leq m \leq L; 1 \leq i \leq m; 1 \leq j \leq n; (m,i) \neq (n,j) \Big\}$, then optimization problem $\mathcal{P}_0$ can be expressed as follows

$$\begin{aligned} \mathcal{P}_1: \quad & \max \min \mathbf{t}^T \mathbf{Q}_{(\alpha-\beta)\beta} \mathbf{t}; (\alpha-\beta, \beta) \in \mathbf{\Phi} \\ \text{s.t.:} \quad & P_{\mathcal{S}} \leq P_{\max} \end{aligned} \tag{2.8}$$

This problem can be rewritten as follows

$$\begin{aligned} \mathcal{P}_2: \quad & \max p \\ \text{s.t.:} \quad & \mathbf{t}^T \mathbf{Q}_{(\alpha-\beta)\beta} \mathbf{t} \geq p; (\alpha-\beta, \beta) \in \mathbf{\Phi} \\ & P_{\mathcal{S}} \leq P_{\max} \end{aligned} \tag{2.9}$$

However, $\mathcal{P}_2$ is a non-convex problem, and therefore, it is extremely hard to find the optimal solution to $\mathcal{P}_2$. A solution was proposed in [40] using leveraging augmented Lagrangian and dual ascent techniques. This method showed an extremely fast convergence rate with very low computational complexity. On the other hand, convex relaxation methods to approximate $\mathcal{P}_2$ were proposed in [41] and [42] and can be used to problem $\mathcal{P}_2$. The core idea of convex relaxation is to linearize $\mathbf{t}^T \mathbf{Q}_{(\alpha-\beta)\beta} \mathbf{t}$ from point $\mathbf{t}_k$ in the solution space. The approximated problem is then given in a different form as follows

$$\begin{aligned} \mathcal{P}_3: \quad & \max p \\ \text{s.t.:} \quad & 2\mathbf{t}_k^T \mathbf{Q}_{(\alpha-\beta)\beta} \mathbf{t} - \mathbf{t}_k^T \mathbf{Q}_{(\alpha-\beta)\beta} \mathbf{t}_k \geq p; (\alpha-\beta, \beta) \in \mathbf{\Phi} \\ & P_{\mathcal{S}} \leq P_{\max} \end{aligned} \tag{2.10}$$

This approximated problem is a convex optimization problem. Therefore, any algorithm or tool useful for solving the convex optimization problem, e.g., the interior point method or CVX tool [43], can be used to solve the approximated maximum minimum ED problem efficiently. The starting point can be randomly generated, but in our simulation, we set the initial points to be the repeat code points (i.e. $\mathbf{s}_{11} = (0,0)^T, \mathbf{s}_{21} = (0.1, 0.1)^T, \mathbf{s}_{22} = (0.2, 0.2)^T$). We can see that the optimization problem comprises only four variables and can be considered a low-complexity prob-

lem. Nevertheless, as the number of considered layers goes higher, so does the number of constraints as the size of set $\mathbf{\Phi}$ also becomes higher. Consequently, the complexity in solving the optimization problem increases significantly. To drastically reduce the number of constraints and to simplify the design process, we propose Theorem 2 in order to obtain set $\mathbf{\Phi}$ with a specific value of L.

Theorem 2.2 *The set* $\mathbf{\Phi}$ *can be defined from* L *as*

$$\mathbf{\Phi} = \{(0,1);(1,0);(a,-b)|1 \leq a,b \leq (L-1)\,;\gcd(a,b)=1\}, \tag{2.11}$$

where gcd*(a,b) is the function to calculate the greatest common divisor between a and b; and*

$$|\mathbf{\Phi}| = 2 + \sum_{k=1}^{L-1} \mu(k) \left\lfloor \frac{L-1}{k} \right\rfloor^2, \tag{2.12}$$

where $\mu(k)$*is the Möbius function.*

Proof: A key issue of constellation design is the high computational complexity of the optimization problem when the number of layers L goes higher. Therefore, some steps are necessary to reduce the number of constraints in the optimization problem. Since the constraints in $\mathcal{P}_3$ are basically generated from set $\mathbf{\Phi} = \{(\alpha-\beta,\beta)\}$, we focus on decreasing the number of elements in $\mathbf{\Phi}$.

Step 1) As the layered structure of the constellation has a lattice property that is closed under addition, we can see that the distance between any two points of two layers will be preserved when we shift both points a same number of layers. To proof this, we observe that, with any $\hat{n},\hat{m},\hat{i},\hat{j}$ satisfy $1 \leq \hat{n} \leq \hat{m} \leq L; 1 \leq \hat{i} \leq \hat{m}; 1 \leq \hat{j} \leq \hat{n}$, since $\hat{m}-\hat{n} = L-(\hat{n}+L-\hat{m})$, based on (2.5), it is easy

to see that $d\left(\mathbf{r}_{\hat{m}\hat{i}}, \mathbf{r}_{\hat{n}\hat{j}}\right) = d\left(\mathbf{r}_{L\hat{i}}, \mathbf{r}_{(\hat{n}+L-\hat{m})\hat{j}}\right)$ where $\hat{n}+L-\hat{m}, L, \hat{m}, \hat{n}$ also satisfies $1 \leq \hat{n}+L-\hat{m} \leq L; 1 \leq \hat{i} \leq \hat{m} \leq L; 1 \leq \hat{j} \leq \hat{n} \leq \hat{n}+L-\hat{m}$.

Therefore, any $d\left(\mathbf{r}_{mi}, \mathbf{r}_{nj}\right)$ can be generated from $\mathbf{\Phi}$ with $m = L$ instead of $1 \leq m \leq L$. Then, with $1 \leq n \leq L; 1 \leq i \leq L; 1 \leq j \leq n$; we can bind $\alpha = L-n$ and $\beta = i-j$ as $-(L-1) \leq (L-i)-(n-j) \leq (L-1); -(L-1) \leq i-j \leq (L-1)$, and we derive $\mathbf{\Phi} = \{(\alpha-\beta, \beta) \,|\, -(L-1) \leq \alpha-\beta, \beta \leq (L-1); (\alpha, \beta) \neq (0,0)\}$

Step 2) Furthermore, since the optimization problem is a maximum minimum ED problem, the constraints represent EDs that are guaranteed to be larger than other ones can be considered to be trivial constraints and should be discarded. That is, we divide $\mathbf{\Phi}$ into two cases:

Case I: If $(\alpha-\beta)\beta \geq 0$ as $0 \leq \alpha-\beta, \beta \leq L-1$ or $-(L-1) \leq \alpha-\beta, \beta \leq 0$, $(\alpha-\beta, \beta) \in \mathbf{\Phi}_1$. Since $(\alpha, \beta) \neq (0,0)$ and $r > 0$, we have, in this case, $d\left(\mathbf{r}_{mi}, \mathbf{r}_{nj}\right) = \left[(\alpha-\beta) r_{21}^{(1)} + \beta r_{22}^{(1)}\right]^2 + \left[(\alpha-\beta) r_{21}^{(2)} + \beta r_{22}^{(2)}\right]^2 \geqslant \left(1 r_{21}^{(1)} + 0 r_{22}^{(1)}\right)^2 + \left(1 r_{21}^{(2)} + 0 r_{22}^{(2)}\right)^2 = \left(r_{21}^{(1)}\right)^2 + \left(r_{21}^{(2)}\right)^2 = \mathbf{t}^T \mathbf{Q}_{10} \mathbf{t}$

Similarly, we have $d\left(\mathbf{r}_{mi}, \mathbf{r}_{nj}\right) \geq \mathbf{t}^T \mathbf{Q}_{01} \mathbf{t}$. Therefore, in this case, $\mathbf{\Phi}_1 = \{(1,0); (0,1)\}$. This case is equivalent to the optimization problem of CASCC in [28], and $\mathbf{\Phi}_1$ can be considered instead of $\mathbf{\Phi}$ in a low-correlation channel without a significant reduction in system performance.

Case II: If $(\alpha-\beta)\beta < 0$ as $0 < \alpha-\beta \leq (L-1), -(L-1) \leq \beta < 0$ or $-(L-1) \leq \alpha-\beta < 0, 0 < \beta \leq (L-1)$; $(\alpha-\beta, \beta) \in \mathbf{\Phi}_2$.

In this case, we can see that $d\left(\mathbf{r}_{mi}, \mathbf{r}_{nj}\right) = \mathbf{t}^T \mathbf{Q}_{(\alpha-\beta)\beta} \mathbf{t} = \left[(\alpha-\beta) r_{21}^{(1)} + \beta r_{22}^{(1)}\right]^2 + \left[(\alpha-\beta) r_{21}^{(2)} + \beta r_{22}^{(2)}\right]^2 = \left[-(\alpha-\beta) r_{21}^{(1)} - \beta r_{22}^{(1)}\right]^2 + \left[-(\alpha-\beta) r_{21}^{(2)} - \beta r_{22}^{(2)}\right]^2 = \mathbf{t}^T \mathbf{Q}_{-(\alpha-\beta)(-\beta)} \mathbf{t}$

Therefore, $\mathbf{t}^T\mathbf{Q}_{(\alpha-\beta)\beta}\mathbf{t} = \mathbf{t}^T\mathbf{Q}_{-(\alpha-\beta)(-\beta)}\mathbf{t}$, and without loss of generality, we consider $\mathbf{\Phi}_2 = \{(\alpha-\beta,\beta)\,|0 < \alpha-\beta \leq (L-1)\,; -(L-1) \leq \beta < 0\}$, consequently, $\mathbf{\Phi} = \mathbf{\Phi}_1 \cup \mathbf{\Phi}_2 = \{(1,0);(0,1);(\alpha-\beta,\beta)\,|0 < \alpha-\beta \leq (L-1)\,; -(L-1) \leq \beta < 0\}$

Step 3) Again, observing that if any pair $(\alpha_1-\beta_1,\ \beta_1), (\alpha_2-\beta_2,\beta_2) \in \mathbf{\Phi}$ that satisfies $\gcd(\alpha_1-\beta_1,-\beta_1) = 1$, $\gcd(\alpha_2-\beta_2,-\beta_2) = \delta > 1$, and $\alpha_2-\beta_2 = \delta \times (\alpha_1-\beta_1)\,; \beta_2 = \delta \times \beta_1$, we only need to consider $(\alpha_1-\beta_1,\beta_1)$ since $\left[(\alpha_2-\beta_2)\,r_{21}^{(1)} + \beta_2 r_{22}^{(1)}\right]^2 + \left[(\alpha_2-\beta_2)\,r_{21}^{(2)} + \beta_2 r_{22}^{(2)}\right]^2 = \delta^2\left[(\alpha_1-\beta_1)\,r_{21}^{(1)} + \beta_1 r_{22}^{(1)}\right]^2 + \delta^2\left[(\alpha_1-\beta_1)\,r_{21}^{(2)} + \beta_1 r_{22}^{(2)}\right]^2 > \left[(\alpha_1-\beta_1)\,r_{21}^{(1)} + \beta_1 r_{22}^{(1)}\right]^2 + \left[(\alpha_1-\beta_1)\,r_{21}^{(2)} + \beta_1 r_{22}^{(2)}\right]^2$ This mean we just consider α_1, β_1, in that $(\alpha_1-\beta_1,\beta_1)$ are co-prime numbers belonging to the pre-determined range $[1; L-1]$. Therefore, the set $\mathbf{\Phi}$ can be simplified into $\mathbf{\Phi} = \{(0,1);(1,0);(a,-b)|1 \leq a,b \leq (L-1)\,; \gcd(a,b) = 1\}$. According to Euler's totient function [44], $\varphi(k)$ is the number of positive integers up to given integer k that are relatively prime to k, and the total number of constraints then is $|\mathbf{\Phi}| = 2 + 2\sum_{k=1}^{L-1}\varphi(k) - 1 = 2 + \sum_{k=1}^{L-1}\mu(k)\left\lfloor\frac{L-1}{k}\right\rfloor^2$, where $\mu(k)$is the Möbius function [44]. That will complete Theorem 2.

With the help of Theorem 2, the number of constraints in $\mathcal{P}_3$ is reduced significantly. We give an example of $\mathbf{\Phi} = \{(0,1);(1,0);(-1,1);(-1,2);(-1,3);(-2,1);(-2,3);(-3,1);(-3,2)\}$ as in the case of eight constellation points. When 256 constellation points are considered, the number of constraints decreases from 32,640 to just 281. With 1,024 constellation points, the number of constraints can be reduced from 523,776 to 1,209, which is capable of being an optimization problem with a low complexity cost. It is worth mentioning that even though $\mathcal{P}_3$ contains a significant number of constraints, there are only four unknown variables that need to be optimized. Hence, the complex-

ity of the maximum minimum ED optimization problem in this chapter is relatively low, compared with the problem elsewhere [40]-[42]. The analysis of the complexity issue will be shown in a later section. Furthermore, our simulation in the next section depends on the correlation value of the channel, and the number of layers that need to be considered can be much lower than L without a significant reduction in the minimum EDs of the constellation.

2.4 Low-complexity ML detector

This section explains the key idea and the algorithm of a low-complexity ML detector. Fast maximum likelihood detection [28] has been proposed. However, by considering just $r_{21}^{(1)}$and $r_{22}^{(2)}$in estimating the initial constellation point, this detector only gave a favorable performance when $r_{21}^{(2)} \ll r_{21}^{(1)}$ and $r_{22}^{(1)} \ll r_{22}^{(2)}$, as in the case where channel correlation is very low. On the other hand, the detector in [28] restricted the search region in nine points, as seen in the blue region in Fig. 2, where it should be all points lying inside the red circle, with the center as the estimated point, and consequently, this detector only works well when the channel correlation is low enough. Therefore, even though fast maximum likelihood detection was proposed in [28] with the idea of narrowing the search region, the detector in [28] showed performance similar to the ML detector only when the channel correlation is very low, and another ML-based detector should be proposed to properly perform under various scenarios. By noticing the structure of the collaborative constellation in this chapter, which can also be considered a lattice [45], [46], it is intuitive to derive a low-complexity detector that takes advantage of this constellation structure. Similar with

[28], the core idea is to only search, in the received constellation, the closest points from initially estimated points. However, the proposed detector improves the initial estimation of transmitted signal and the search region, make it capable of applying to various channels. Specifically, our algorithm considers the following detection process.

2.4.1 Initial estimation

For a given constellation, $\mathcal{S}, \mathcal{R}$, in a MIMO-VLC system, the received signal in (2.1) can be rewritten as

$$\begin{aligned} y = \mathbf{H}\mathbf{s}_{mi} + \mathbf{n} &= \begin{bmatrix} h_{11} & h_{12} \\ h_{21} & h_{22} \end{bmatrix} \begin{bmatrix} (m-i)s_{21}^{(1)} + (i-1)\, s_{22}^{(1)} \\ (m-i)s_{21}^{(2)} + (i-1)\, s_{22}^{(2)} \end{bmatrix} + \mathbf{n} \\ &= \begin{bmatrix} h_{11} & h_{12} \\ h_{21} & h_{22} \end{bmatrix} \begin{bmatrix} s_{21}^{(1)} & s_{22}^{(1)} \\ s_{21}^{(2)} & s_{22}^{(2)} \end{bmatrix} \begin{bmatrix} m-i \\ i-1 \end{bmatrix} + \mathbf{n} \\ &= \mathbf{R}\mathbf{u} + \mathbf{n}, \end{aligned} \tag{2.13}$$

where $\mathbf{R} = \mathbf{H} \begin{bmatrix} \mathbf{s}_{21} & \mathbf{s}_{22} \end{bmatrix} = \begin{bmatrix} \mathbf{r}_{21} & \mathbf{r}_{22} \end{bmatrix}$ and $\mathbf{u} = \begin{bmatrix} m-i & i-1 \end{bmatrix}^T$, which defines the transmitted signal as the i-th point of the m-th layer. The first step of the proposed detector is to find an initial estimate, $\hat{\mathbf{u}}$ of $\mathbf{u}$, by using a linear detection method, such as minimum mean square error (MMSE), or zero forcing (ZF) detection method [47]. Then, $\hat{\mathbf{u}}$ for MMSE and ZF can be determined as

$$\hat{\mathbf{u}} = \left(\mathbf{R}^T\mathbf{R} + \sigma^2\mathbf{I}_{N_\mathrm{T}}\right)^{-1}\mathbf{R}^T\mathbf{y} \tag{2.14}$$

and

$$\hat{\mathbf{u}} = \mathbf{R}^{-1}\mathbf{y} \tag{2.15}$$

Since m and i of $\mathbf{u}$ should be integers, the elements of estimation $\hat{\mathbf{u}}$, are also integers. Let round(a) be a function to return the nearest integer to a. Then, the estimated signal is quantized to the closest point $\mathbf{r}_{\bar{m}\bar{i}}$ in the collaborative constellation by defining $\bar{\mathbf{u}} = \begin{bmatrix} \overline{m-i} & \overline{m-1} \end{bmatrix}^T, \bar{m}, \bar{i} \in \mathbb{Z}$ and $\bar{\mathbf{u}} = \text{round}(\hat{\mathbf{u}}) = \begin{bmatrix} \text{round}(\widehat{m-i}) & \text{round}(\widehat{i-1}) \end{bmatrix}^T$. After this, $\bar{m}, \bar{i}$ can be easily obtained.

2.4.2 Determine the detection region for the ML detector

In this step, we construct a subset $\bar{\mathcal{R}}$ whose elements lie in the sphere centered at the quantization output vector $\mathbf{r}_{\bar{m}\bar{i}}$ with a radius of π_d. The choice of radius will affect the performance of the detector and should be carefully considered, as it provides a trade-off between the BER result and detection complexity. In particular, we set the radius to the largest distance between four constellation points $\mathbf{r}_{11}, \mathbf{r}_{21}, \mathbf{r}_{22}, \mathbf{r}_{32}$, i.e. $\pi_{\text{d}} = \pi_{\text{opt}} = \max\left\{d\left(\mathbf{r}_{11}, \mathbf{r}_{21}\right), d\left(\mathbf{r}_{11}, \mathbf{r}_{22}\right), d\left(\mathbf{r}_{11}, \mathbf{r}_{32}\right), d\left(\mathbf{r}_{21}, \mathbf{r}_{22}\right)\right\}$.
This radius has been shown in simulation results to keep the performance similar to a traditional ML detector while outstandingly decreasing detection complexity. Using the fact that a lattice is closed under addition, we can locate the elements of subset $\bar{\mathcal{R}}$ systematically. Let us define the following set

$$\mathbf{D}_{search} = \left\{(v_1, v_2) \in \mathbb{Z}^2 \middle| \left\|\mathbf{r}_{\bar{m}\bar{i}} - \mathbf{r}_{(\bar{m}-v_1)(\bar{i}-v_2)}\right\|_2 \leq \pi_d\right\} \tag{2.16}$$

as the constellation set with the closest points from $\mathbf{r}_{\bar{m}\bar{i}}$ that lie inside the sphere of radius π_{d}. By the lattice property, it is possible to find the elements of $\bar{\mathcal{R}}$ by shifting the initially estimated point $\bar{\mathbf{u}}$ to the elements of $\mathbf{D}_{search}$, regardless of the value of $\bar{\mathbf{u}}$, and so $\bar{\mathcal{R}}$ can be represented as

$$\bar{\mathcal{R}} = \left\{\mathbf{r}_{\tilde{m}\tilde{i}} | \tilde{m} = \bar{m} - v_1; \tilde{i} = \bar{i} - v_2; (v_1, v_2) \in \mathbf{D}_{search}\right\} \tag{2.17}$$

The key idea of the proposed detector is to take advantage of the lattice property belonging to the collaborative constellation. As the constellation points are closed under addition, we can easily find the closest points inside the sphere centered at an estimated point. The cardinality of $\mathbf{D}_{search}$ depends on the specific channel and the choice of π_{d}, and will be discussed in the next section. Furthermore, set $\mathbf{D}_{search}$ is easy to find via off-line computation, and thanks to the lattice property, by simply shifting initially estimated point $\mathbf{r}_{\bar{m}\bar{i}}$ with the elements of set $\mathbf{D}_{search}$, as in (2.17), the closest constellation points from estimated point $\mathbf{r}_{\bar{m}\bar{i}}$ are obtained. It worth mentioning that if the transmit vector is modulated using conventional methods, the lattice property in the signal set does not hold, and therefore, it is impossible to apply the proposed algorithm. Then, depending on the initial estimated point, the detector only performs a search on the region that belongs to the constellation $\tilde{\mathcal{R}} = \mathcal{R} \cap \bar{\mathcal{R}}$. If $\mathcal{R} \cap \bar{\mathcal{R}} = \emptyset$; then, $\tilde{\mathcal{R}} = \{(0,0)\}$.

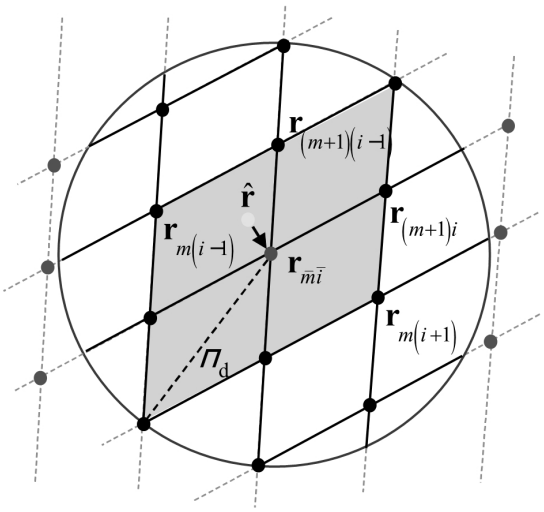

Figure 2.2: An illustration of the proposed detector.

2.4.3 Perform ML detection over the reduced region

After acquiring the reduced search region, the detector uses ML to normally search over the set $\tilde{\mathcal{R}}$ for the point that satisfies (2.18)

$$\{\tilde{\mathbf{s}}, \tilde{\mathbf{r}}\} = \arg\min_{\mathbf{r}_{\tilde{m}\tilde{i}} \in \tilde{\mathcal{R}}} \|\mathbf{y} - \mathbf{r}_{\tilde{m}\tilde{i}}\|_2^2 \tag{2.18}$$

As an example, Fig. 2.2 represents the received signal space, and the yellow mark represents the initial estimate. The yellow mark is quantized to the point that belongs to the constellation (the red mark). Then, we obtain the set inside the sphere that belongs to the region restricted by the red circle, which includes the quantized point $\mathbf{r}_{\bar{m}\bar{i}}$. Finally, we calculate ML metrics over reduced set $\tilde{\mathcal{R}}$. The proposed algorithm is summarized in Algorithm 2.

Algorithm 2 Low-complexity ML detection

Input: Received signal vector $\mathbf{y}$, channel matrix $\mathbf{H}$, constellation set $\mathcal{S}$, $\mathcal{R}$, set $\mathbf{D}_{search}$

Output: estimated input signal point $\tilde{\mathbf{s}}$

1: using MMSE estimator, estimate the initial vector $\hat{\mathbf{u}} = \left(\mathbf{R}^T\mathbf{R} + \sigma^2\mathbf{I}_{N_\mathrm{T}}\right)^{-1}\mathbf{R}^T\mathbf{y}$

2: calculate $\bar{\mathbf{u}} = \begin{bmatrix} \overline{m-i} & \overline{m-1} \end{bmatrix}^T$ as $\bar{\mathbf{u}} = \mathrm{round}(\hat{\mathbf{u}})$

3: determine the reduced set by selecting $\mathbf{r}_{\tilde{m}\tilde{i}}$

$\bar{\mathcal{R}} = \left\{\mathbf{r}_{\tilde{m}\tilde{i}} | \tilde{m} = \bar{m} - v_1; \tilde{i} = \bar{i} - v_2; (v_1, v_2) \in \mathbf{D}_{search}\right\}$

4: find the merged set $\tilde{\mathcal{R}}$

5: perform ML detection: $\{\tilde{\mathbf{s}}, \tilde{\mathbf{r}}\} = \arg\min_{\mathbf{r}_{\tilde{m}\tilde{i}} \in \tilde{\mathcal{R}}} \|\mathbf{y} - \mathbf{r}_{\tilde{m}\tilde{i}}\|_2^2$

6: **return** estimated input signal point $\tilde{\mathbf{s}}$

2.5 Extension to general MIMO-VLC

Due to the limitations of this chapter, the constellation design problem is mainly focused on a 2×2 MIMO-VLC system. This restriction was observed in [37] and [28] due to the complexity and high amount of mathematical content. In this section, we briefly exemplify the concept of LACC for higher numbers of LEDs and PDs. Note that optimization can be derived, and the same design process would be performed without any difficulty. However, the main obstacle in obtaining the optimal constellation for a higher number of transmitters and receivers lies in the high computational complexity of the optimization problem when large numbers of variables and constraints are considered.

Let us again consider a MIMO-VLC system with transmitter constellation $\mathcal{X}$ of $M = 2^R$ symbols, denoted as $\mathcal{X} = [\mathbf{x}_1, ..., \mathbf{x}_M]$ where $\mathbf{x}_i = \left[x_i^{(1)}, x_i^{(2)}, ..., x_i^{(N_\mathrm{T})}\right]^T \in \mathcal{X}$ is a signal vector transmitted through LEDs. With $N_\mathrm{T} = N_\mathrm{R}$ transmitters, we define a multidimensional layered constellation that each N_i-th-dimension (N_i-D) layer comprises all $(N_\mathrm{i} - 1)$-D layers; for example, with $N_\mathrm{T} = N_\mathrm{R} = 2$, an 1-D layer will be a line, as in Fig.2.1; with $N_\mathrm{T} = N_\mathrm{R} = 3$, an 2-D layer contains all 1-D layers belong to it, and each 1-D layer is a line as the case of $N_\mathrm{T} = N_\mathrm{R} = 2$; and so on the collaborative constellation for any $N_\mathrm{T} = N_\mathrm{R}$ can be built by generating all constellation points belong to $(N_\mathrm{T} - 1)$-D layers. Similar to the 2×2 case, a constellation point can be represented as

$$\mathbf{s}_{m_1 m_2 ... m_{N_\mathrm{T}}} = \left(s^{(1)}_{m_1 m_2 ... m_{N_\mathrm{T}}}, s^{(2)}_{m_1 m_2 ... m_{N_\mathrm{T}}}, ... s^{(N_\mathrm{T})}_{m_1 m_2 ... m_{N_\mathrm{T}}}\right)^T, \tag{2.19}$$

where the signal transmitted by the i-th LED can be represented as

$$s^{(i)}_{m_1 m_2 ... m_{N_\mathrm{T}}} = (m_1 - m_2) s^{(i)}_{211...1} + ... + (m_{N_\mathrm{T}-1} - m_{N_\mathrm{T}})$$
$$s^{(i)}_{222...2} + (m_2 - 1)\, s^{(i)}_{211...1} + ... + (m_{N_\mathrm{T}} - 1) s^{(i)}_{222...2} \tag{2.20}$$

where the basic points of the constellation here are $\mathbf{s}_{11...1} = (0, 0, ..., 0)^T$, $\mathbf{s}_{211...1} = \left(s^{(1)}_{211...1}, s^{(2)}_{211...1}, ..., s^{(N_\mathrm{T})}_{211...1}\right)^T$, ..., $\mathbf{s}_{222...2} = \left(s^{(1)}_{222...2}, s^{(2)}_{222...2}, ..., s^{(N_\mathrm{T})}_{222...2}\right)^T$ and $1 \leq m_{N_\mathrm{T}} \leq m_{N_\mathrm{T}-1} \leq ... \leq m_2 \leq m_1 \leq L$.

Furthermore, there are $L!/N_\mathrm{T}!$ points in the constellation. Then, with any transmitted constellation $\mathbf{s}_{m_1 m_2 ... m_{N_\mathrm{T}}} \in \mathcal{S}$,$\mathcal{S} = [\mathbf{s}_{111...1}, \mathbf{s}_{211...1}, ..., \mathbf{s}_{N_\mathrm{T} N_\mathrm{T} N_\mathrm{T} ... N_\mathrm{T}}]$, we define the corresponding received constellation $\mathcal{R}$ at the N_R PDs by vector $\mathbf{r}_{m_1 m_2 ... m_{N_\mathrm{T}}}$ using equation (2.2) and $|\mathcal{R}| = |\mathcal{S}|$. It is observed that the constellation when $N_\mathrm{T} = N_\mathrm{R} = 2$ is a special case, and can be deduced from the above equation.

Although not detailly mentioned in this chapter, the larger dimension constellation $\mathcal{X}$ can be generated from a set of basic points $\{\mathbf{s}_{211...1}, \mathbf{s}_{221...1}, ..., \mathbf{s}_{222...2}\}$ by a generalization of Algorithm 1. After that, the optimization problem of constellation design can be easily formed in the same fashion as problem $\mathcal{P}_0$.

The process of simplifying and solving the optimization problem is possible by systematically extending the method described in this chapter as well as Theorem 1, Theorem 2 without any mathematical difficulty. However, this chapter focus is the 2 $\times$ 2 VLC-MIMO system as previous ones [37], [28] and the extension to system with larger number of LEDs and PDs can be discussed in future research.

Table 2.1: Different channels used in the simulation

Channel matrix	Condition number
$\mathbf{H}_1 = \begin{bmatrix} 1.0000 & 0.0310 \\ 0.0010 & 1.5030 \end{bmatrix}$	1.5042
$\mathbf{H}_2 = \begin{bmatrix} 1.0000 & 0.8000 \\ 0.2000 & 3.0000 \end{bmatrix}$	3.4726
$\mathbf{H}_3 = \begin{bmatrix} 1.0000 & 0.3400 \\ 1.1500 & 0.5120 \end{bmatrix}$	22.2712

2.6 Simulation results and discussion

In this section, we analyze the performance of our scheme, compared with other schemes for MIMO-VLC systems such as CASCC, CC, RC, SMP, and SM. Consider an indoor 2×2 MIMO-VLC scenario with $A_r = 1\text{cm}^2$, $\Phi_{1/2} = 60^o$, and $\psi_{1/2} = 60^o$. The average transmission electrical power is identical in each scheme. By normalizing $\mathbf{H}$ and $\mathbf{s}$, SNR is defined as in [37], [28]. Here, LED_1 and PD_1 are fixed at (0,0,0) and (0,0,3m), and LED_2 and PD_2 are at different locations. We take three channels with different correlation values as the normalized channel matrices shown in the Table 2.1.

We can see that channel H_1 has the smallest condition number, as an insignificant correlation is presented in this channel. In contrast, channel H_3 gets a very large condition number due to a high level of correlation on this channel. We assume

that the receivers in our scheme and other referred schemes use ML detection with complete information about the channel. To compare the performance of our scheme and others, we use BER as the figure of merit.

2.6.1 Constellation design analysis

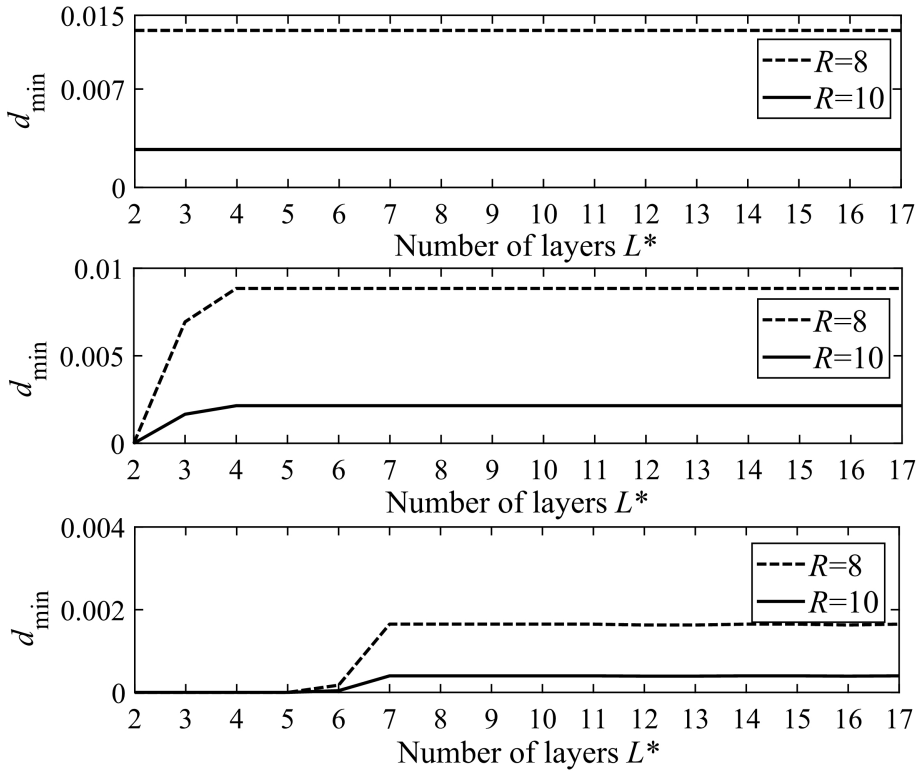

Figure 2.3: The resulting $d_{\min}$ of the proposed scheme on channels $\mathbf{H}_1$, $\mathbf{H}_2$, and $\mathbf{H}_3$ with various L^*.

Fig.2.3 shows the minimum distance, $d_{\min}$, of the R=8,10 bits/s/Hz constellations, versus the number of layers considered in optimization problem $\mathcal{P}_3$ for three channels, i.e. $L^* = 2, 3, ...$ instead of L. We see from this figure that the minimum distance monotonically increases with the number of considered layers, L^*. However, the

minimum distance$d_{\mathcal{R}}$ converges when L^* is high enough, and the speed of convergence depends on the correlation of specific channel. For example, with low correlation channel H_1, only two layers need to be considered when designing a constellation of 256 or 1,024 in size. In another case, with high correlation channel H_3, seven layers is enough. This indicates that with a relatively low complexity, the constellations designed by the proposed scheme with low values of $L^* \leq L$ can guarantee good ED between constellation points.

According to [41], the complexity of the designs is due mainly to the complexity in solving problem $\mathcal{P}_3$, and therefore, should be analyzed from two aspects: i) the computational complexity of solving the optimization at each iteration, and ii) the number of iterations required for convergence. The complexity in solving the optimization problem in each iteration is $\mathcal{O}\left(N_{\mathrm{T}}^2 N_{\mathrm{R}}\right) + \mathcal{O}\left(N_{\mathrm{T}}^3\right) + \mathcal{O}\left(N_{\mathrm{T}}^2 \left|\mathbf{\Phi}\right|\right) + \mathcal{O}\left(N_{\mathrm{T}}^2\right)$ [41], and the number of iterations for the result to converge is about 5$\sim$10 depending on the size of $\mathbf{\Phi}$, according to our simulation results. However, the constellation design is a one-time calculation. Therefore, the complexity is not the focus and should not matter since our proposed algorithm gives improved performance, as shown later in subsequent sections.

2.6.2 Detector analysis

In this section, we compare the traditional ML detector with the proposed low-complexity ML detector. For simplicity, with a large number of constellation points, the complexity of the two detectors can be considered to depend on the number of points belonging to the search region. The complexity of the traditional ML

detector is $\big(2N_{\mathrm{R}}(N_{\mathrm{T}}+1)-1\big)M$ flops or equal to $11M$ flops when $N_{\mathrm{T}} = N_{\mathrm{R}} = 2$. As described in Algorithm 2, the effective search space of the proposed detector is determined by the cardinality of $\mathbf{D}_{search}$, and consequently, $\tilde{\mathcal{R}}$. The cardinality of $\mathbf{D}_{search}$ varies depending on the correlation value of the specific channel, i.e. channel $\mathbf{H}_1$ with low correlation requires $\mathbf{D}_{search}$ with low cardinality. In contrast, a larger set for $\mathbf{D}_{search}$ is necessary in high-correlation channel $\mathbf{H}_3$. The complexity of the proposed detector in Algorithm 2 can be computed, as MMSE requires $4N_{\mathrm{T}}^3 + 12N_{\mathrm{T}}^2N_{\mathrm{R}} + 7N_{\mathrm{T}}^2 + 6N_{\mathrm{T}}N_{\mathrm{R}}$ flops, and quantization complexity is $2N_{\mathrm{T}}$ flops. The construction of set $\bar{\mathcal{R}}$ requires $(2N_{\mathrm{T}}N_{\mathrm{R}} - N_{\mathrm{T}} + 2)\,|\mathbf{D}_{search}|$ flops, and $\|\mathbf{y} - \mathbf{r}_{mi}\|^2$requires $(2N_{\mathrm{R}}(N_{\mathrm{T}}+1)-1)\,|\tilde{\mathcal{R}}|$ flops. Therefore, the total complexity of the proposed detector when $N_{\mathrm{T}} = N_{\mathrm{R}} = 2$ will be 184+5 $\left(|D_{search}| + \left|\tilde{\mathcal{R}}\right|\right)$+3 $|\mathbf{D}_{search}|$ flops.

Fig. 2.4 shows the BER performance comparison between the traditional ML detector and the proposed detector when $\pi_d = \pi_{opt}$ with various channels and spectral efficiencies. We can see that our proposed detector achieves performance similar to the ML detector. It is worth mentioning that the low-complexity detector in [28] showed worse performance with a channel that incurred a high level of correlation. In contrast, our proposed detector, by effectively utilizing the MMSE detector and restricting the search region to a sphere, keeps the BER performance as good as the ML detector while drastically reducing the complexity.

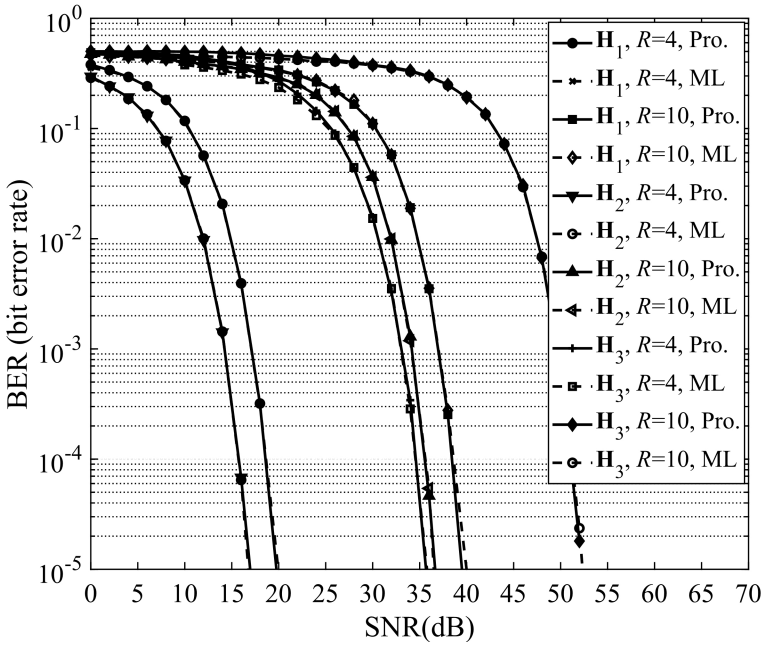

Figure 2.4: Performance comparison of the ML and the proposed detectors under various scenarios.

Table 2.2 shows the complexity comparison of detectors under different scenarios. It is clear that when constellation order increases, the proposed detector can significantly reduce the computational complexity. However, the average number of points inside the search region also increases when the channel correlation is high to a certain value.

Fig. 2.5 shows the performance of the proposed detector when the value of the search radius, π_{d}, decreases. We can see that depending on channel correlation, the BER performance degrades variously. Simultaneously, the complexity of the detector also decreases, however insignificantly, since the choice of optimal $\pi_{\mathrm{d}} = \pi_{\mathrm{opt}}$ mentioned before already drastically reduces the computational complexity while achieving the same performance as ML.

Table 2.2: Complexity comparison for detection algorithms under different conditions and scenarios

Channel and constellation size		ML detector		Proposed detector		
		Average complexity (flops)	Average number of searched points	Average complexity (flops)	Average number of searched points	Compl. reduction (%)
$\mathbf{H}_1$	M=256	2816	256	294.55	7.71	89.54
	M=4096	45056	4096	296.00	8.00	99.34
$\mathbf{H}_2$	M=256	2816	256	476.05	18.41	83.09
	M=4096	45056	4096	498.80	22.96	98.89
$\mathbf{H}_3$	M=256	2816	256	790.20	41.24	71.94
	M=4096	45056	4096	1176.8	70.56	97.39

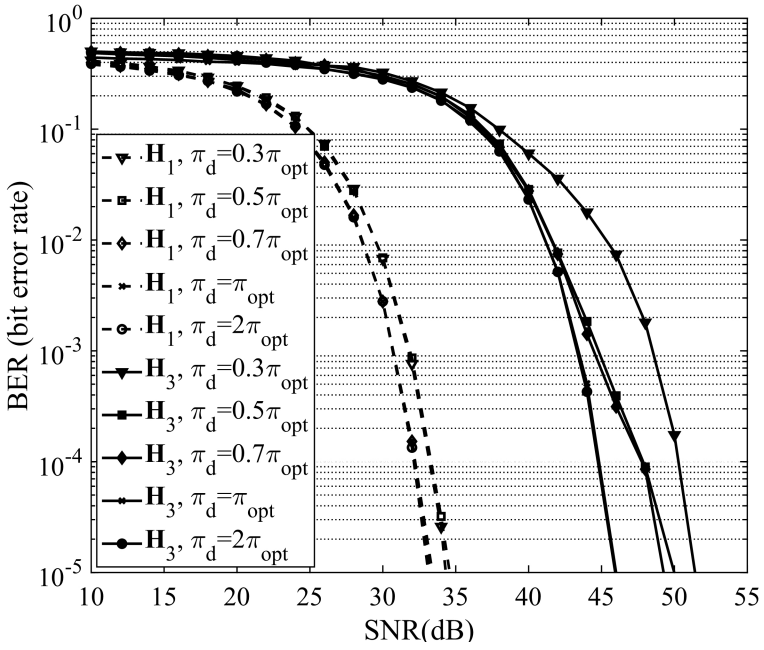

Figure 2.5: Performance of the proposed detector with different values of $\pi_{\mathrm{d}}$with R=8 bits/s/Hz.

2.6.3 Performance analysis under perfect CSI

Fig. 2.6 and Fig. 2.7 show the performance of LACC, CASCC [28], CC [37], RC [35], SMP [34], and SM [36] for low-correlation channel $\mathbf{H}_1$ at different spectral efficiencies of $R = 4, 8, 10$, and 12 bits/s/Hz. In such low-correlation conditions, only the ED impacts the performance of the system. More specifically, our scheme and CASCC [28] perform relatively the same, and both are better than RC, CC, SMP, and SM. Also, the gain between our scheme and CC [37] is significant at low and medium spectral efficiency. Moreover, it is worth mentioning that due to the exceptionally low correlation of channel $\mathbf{H}_1$, RC, SM, and SMP constellations are inappropriate choices in this scenario.

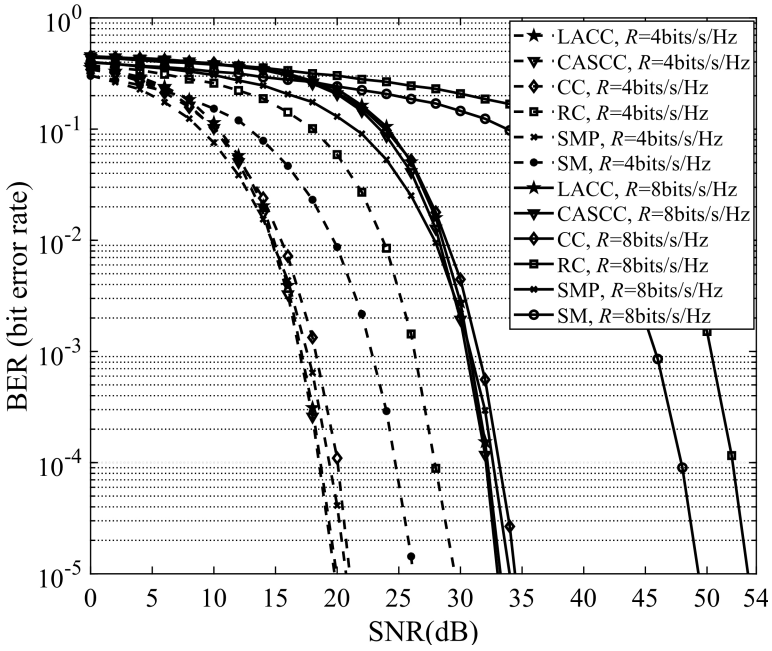

Figure 2.6: Performance at $R = 4$, 8 bits/s/Hz for low-correlation channel $\mathbf{H}_1$.

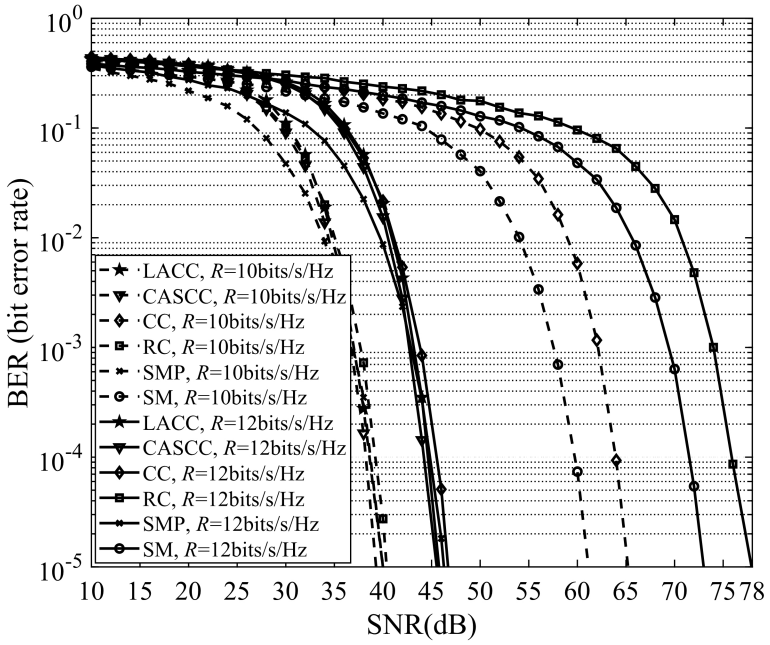

Figure 2.7: Performance at $R = 10$, 12 bits/s/Hz for low-correlation channel $\mathbf{H}_1$.

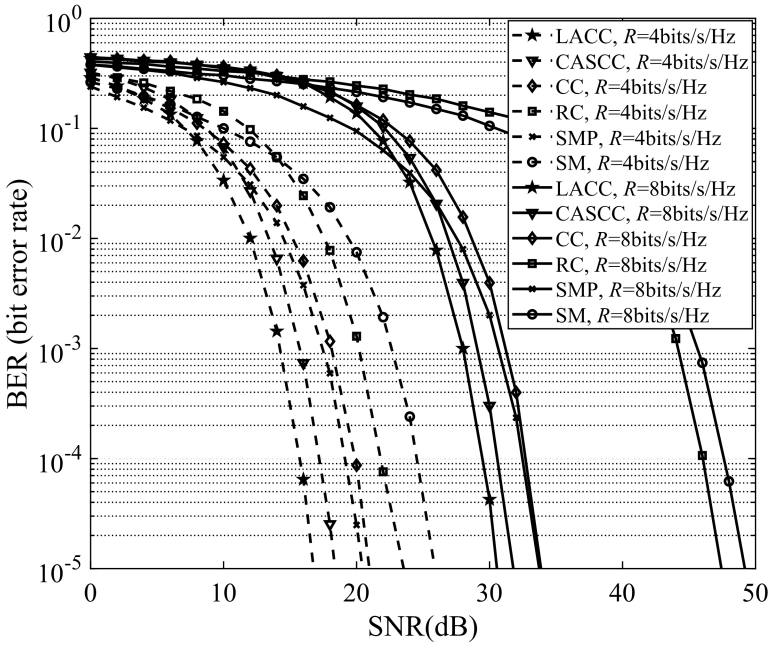

Figure 2.8: Performance at $R = 4$, 8 bits/s/Hz for medium-correlation channel $\mathbf{H}_2$.

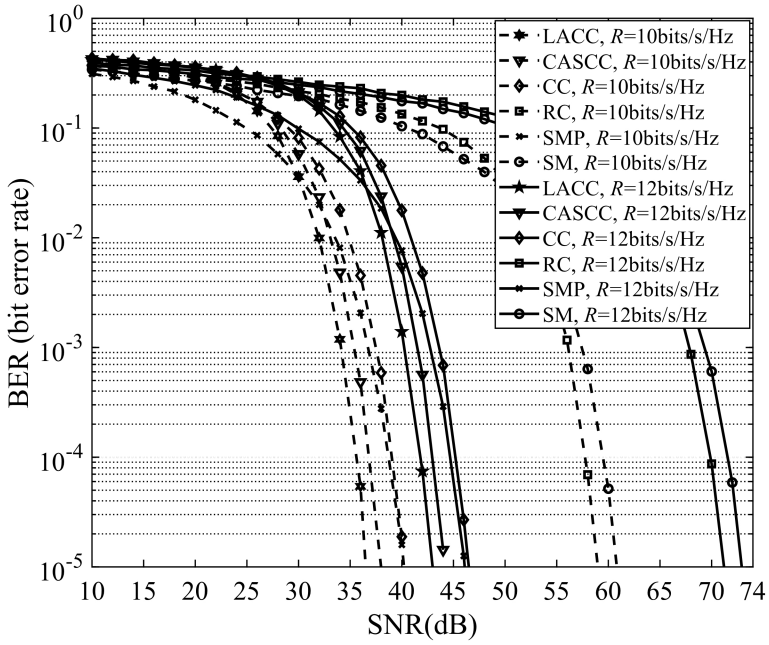

Figure 2.9: Performance at $R = 10$, 12 bits/s/Hz for medium-correlation channel $\mathbf{H}_2$.

Fig. 2.8 and Fig. 2.9 show the performance of LACC, CASCC, CC, RC, SMP, and SM for medium-correlation channel $\mathbf{H}_2$ at different spectral efficiencies of $R = 4, 8, 10,$ and 12 bits/s/Hz. With channel $\mathbf{H}_2$, LACC and CASCC still show better performance in comparison with other schemes, such as RC, CC, and SM. Our proposed scheme shows the best performance, and gain is about 2dB, in comparison with CASCC, since in $\mathbf{H}_2$, both the correlation and ED in the transmitter space affect the performance of MIMO-VLC. LACC, CASCC, and CC achieve some performance gain due to the effectively utilizing the spatial resource. Moreover, by considering the impact of optical channel into constellation design problem, the proposed LACC and CASCC can manage to significantly leverage the interference between transmitting LEDs. On the other hand, our proposed scheme which takes into account the relation between

all constellation points, can further reduce the effect of channel correlation to system performance. Based on this reason, we can firmly state that with the proposed LACC, better performance can be obtained for MIMO-VLC than other schemes with medium and strong correlation channels, while yield similar performances to CASCC for low correlation channel.

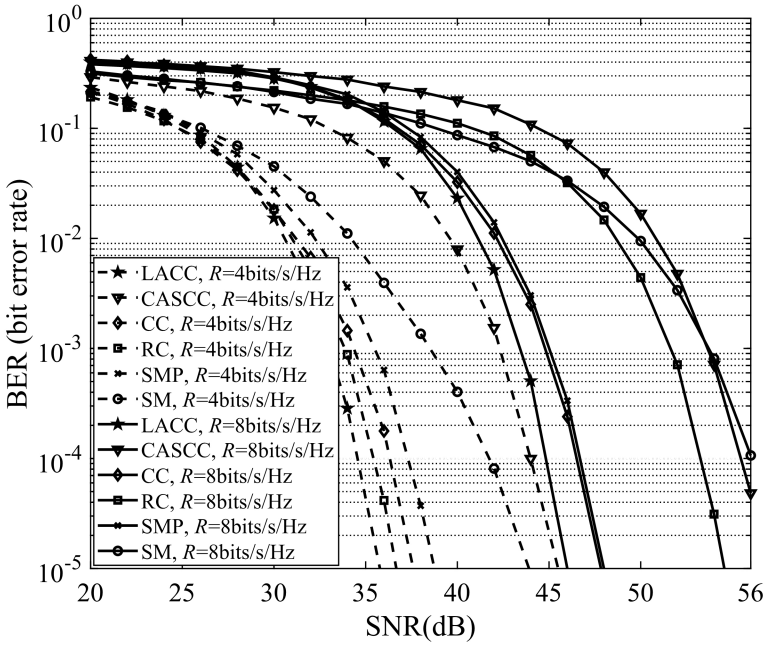

Figure 2.10: Performance at $R = 4$, 8 bits/s/Hz for high-correlation channel $\mathbf{H}_3$.

The benefit of LACC over CASCC, CC, RC, SMP, and SM in high correlation channel $\mathbf{H}_3$ is shown in Fig. 2.10 and Fig. 2.11 at different spectral efficiencies of $R = 4, 8, 10$, and 12 bits/s/Hz. Due to the high correlation of channel $\mathbf{H}_3$, in low spectral efficiency, RC performs well, but our scheme still gains about 1 dB, compared with RC. In medium and high spectral efficiency, RC becomes worse due to inefficient use of power. Moreover, our proposed scheme is still better than CC and the other schemes. It can be observed that, due to the aforementioned design

criterion of CASCC, this scheme hardly maintains the good performance as previous channel configurations.

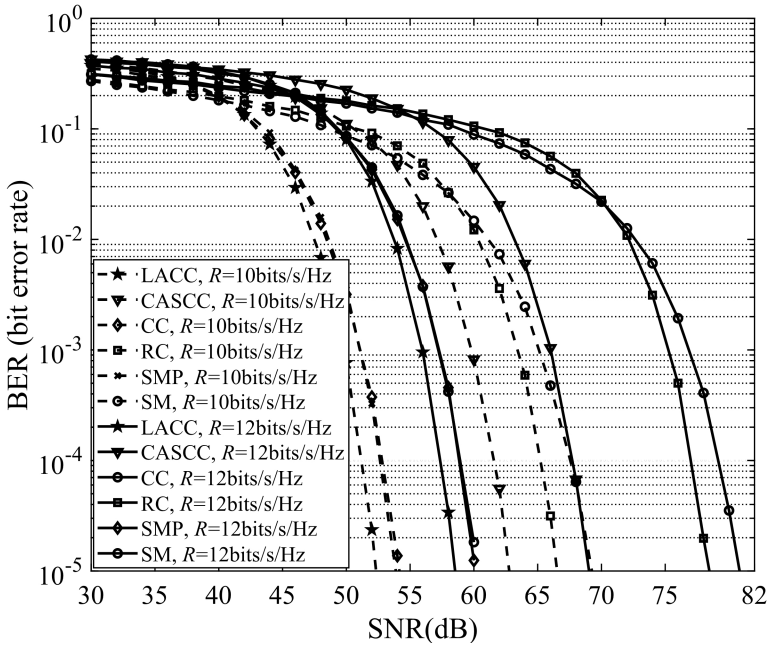

Figure 2.11: Performance at $R = 10$, 12 bits/s/Hz for high-correlation channel $\mathbf{H}_3$.

2.6.4 Performance analysis under imperfect CSI

While the channel in VLC is considered deterministic for given transmitter-receiver specifications and fixed locations, the assumption of perfect CSI at the transmitters is in fact not strongly realistic even for indoor VLC systems [48]. To successfully recover the transmitted symbol with a high degree of confidence, the knowledge of channel coefficients at the receiver side is of paramount importance. Therefore, in order to evaluate and develop insights on the impairment of imperfect CSI on MIMO-VLC system performance with the proposed LACC, in this part, appropriate procedures to emulate the channel estimation errors need to be carried out. Without the loss of

generality, the channel matrix estimated at the receiver can be represented as

$$\mathbf{H}_{\epsilon} = \mathbf{H} + \boldsymbol{\epsilon} \tag{2.21}$$

where $\mathbf{H}_{\epsilon}$ is the estimation for $\mathbf{H}$ with the estimated error matrix $\boldsymbol{\epsilon}$ of dimensions $N_{\mathrm{R}} \times N_{\mathrm{T}}$. The channel estimation error $\boldsymbol{\epsilon}$ which is independent of $\mathbf{H}$ and elements follow $\mathcal{N}(0, \sigma_{\epsilon}^2)$. Under ideal channel estimation conditions, the error is zero, i.e. $\sigma_{\epsilon}^2 = 0$; it is obtained that $\mathbf{H}_{\epsilon} = \mathbf{H}$.

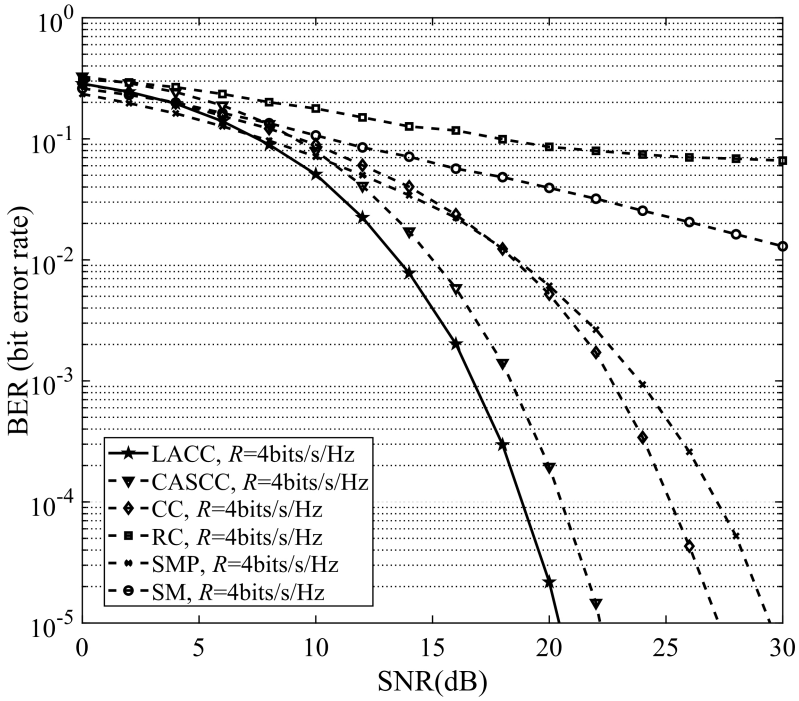

Figure 2.12: Performance at $R = 4$ bits/s/Hz for channel $\mathbf{H}_2$ with $\sigma_{\epsilon}^2 = 0.05$.

In this simulation, we exemplify the case when R=4bits/s/Hz in channel $\mathbf{H}_2$. In order to determine the pure effect of the estimation error on the performance of system, the power of the estimation error σ_{ϵ}^2 was fixed to 0.01, 0.02, and 0.05 values for all SNR values, i.e. corresponding to 1.25%, 2.5%, and 6.25% of the average

channel gains, respectively. Especially with LACC and CASCC in which the imperfect CSI is taken into constellation design process. Moreover, notice that the channel estimation error will also worsen the performance of MIMO-VLC system that employs any aforementioned modulation schemes such as RC, SM, SMP, CC, CASCC, and LACC; since ML detector is utilized. For comparison purposes, the performance of the perfect CSI case ($\sigma_\epsilon^2 = 0$) is also included. Fig.2.12 shows the performance comparison of LACC with other schemes under the highly CSI error where $\sigma_\epsilon^2 = 0.05$. It can be seen that due to the ineffective utilization of power that lead to very small EDs between constellation points, RC and SM become worse. Hence, when channel estimation error is high, both of them perform badly and RC appears to be error floored. In the other hand, LACC still outperforms other schemes.

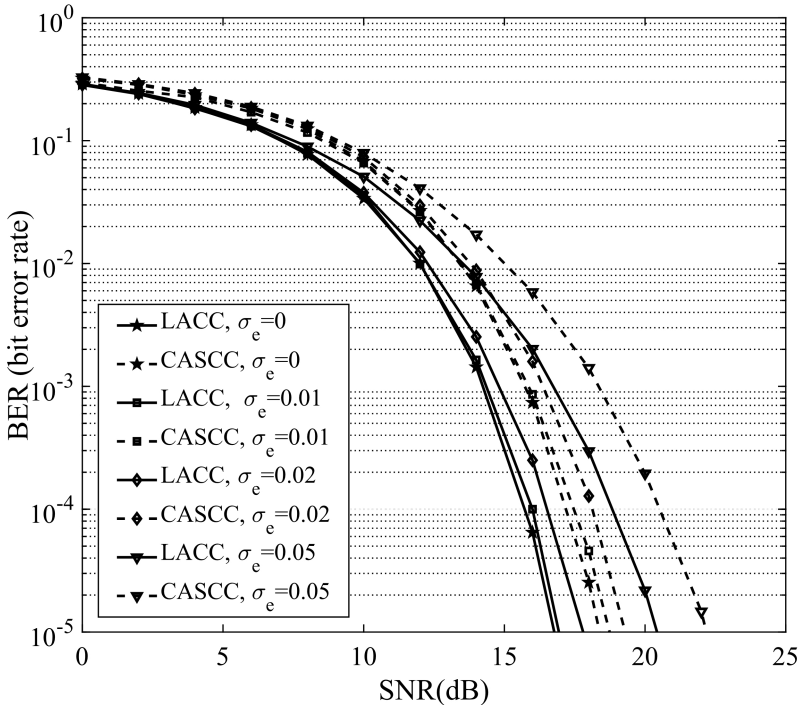

Figure 2.13: Performance of LACC and CASCC at $R = 4$ bits/s/Hz for $\mathbf{H}_2$.

Since the imperfect CSI directly impacts the constellation design procedure of LACC and CASCC, we then give a detail comparison between those two schemes in various imperfect CSI scenarios in Fig.2.13.

According to Fig.2.13, LACC is able to achieve at leat 2dB of SNR gain in comparison with CASCC with low to high CSI imperfection. It also worth mentioning that the performance of both schemes rapidly degrade when CSI error increasing.

Chapter 3

Collaborative constellation design with deep learning

3.1 Introduction and motivation

Despite having better performance, the designing algorithm in the previous chapter suffers from high complexity due to the optimization-solving process. The total number of constraints in the optimization problem depends on the constellation size. Consequently, the complexity cost and running time needed to determine the optimal constellation set becomes prohibitively large when the required transmission rate is relatively high. In fact, due to the high mobility of the receiver, contemporary constellation design schemes such as [49], [42] are unable to be employed practically in real-time high-speed communication scenarios. In this context, deep learning (DL) can be exploited to mitigate the fundamental drawbacks of the conventional constellation design schemes.

Furthermore, DL and deep neural networks (DNNs) have been successfully employed in communication systems, especially in VLC systems [50]–[57]. For example, [58] introduced optical signal constraints into the training process to regulate the operation of DNNs and to analyze the practicability of the autoencoder (AE) in dimmable VLC systems. An AE VLC system was proposed in [53], which yielded an efficient OOK transceiver for common optical channels. To the best of our knowledge, there are no existing works that investigate the potential of employing DL in the constellation designing problem, not to mention the CC designing in a MIMO VLC system.

This chapter proposes a DL-based constellation design scheme for MIMO VLC systems with CC, called CCNet, which can significantly reduce complexity compared to existing schemes while maintaining a near-optimal performance. More specifically, the preprocessed channel state information (CSI) is fed to CCNet. Meanwhile, the proposed CCNet structure requires a small number of hidden fully connected (FC) nonlinear layers. Neurons in the hidden layers perform the prediction task efficiently. On the other hand, using simulated data, CCNet is first trained offline to minimize the mean square error (MSE). Then, the trained model can be deployed as an online predictor with low complexity and running time. It is confirmed via numerical results that CCNet can provide a satisfactory performance that approaches the performance of the conventional high complexity scheme. Moreover, the number of neurons in the hidden layer can be adaptively adjusted to fine-tune the trade-off between performance and complexity.

3.2 System model and problem formulation

3.2.1 System model

The performance of the CC scheme was evaluated in [37] where it was found that CC is able to achieve the minimum average optical power with a fixed minimum Euclidean distance (ED) between any two constellation points. Consequently, the bit error rate (BER) performance is improved in comparison with previous modulation techniques. Layered adaptive CC (LACC) was introduced in [49], in which an efficient symbol design principle and a low-complexity maximum likelihood (ML)-based detection algorithm was proposed and analyzed. Generally, all of the constellation points of CC can be represented by four basic constellation points. The optimal basic points can be efficiently determined using the algorithm [49].

In [37], instead of separately considering the signal transmitted by each LED, the transmitter exploits the available spatial resources by forming relations within the LEDs to design a CC, with each LED maps to a corresponding dimension of the constellation. Later, authors in [49] effectively optimized the CC using additional channel state information (CSI). Similarly, we consider a MIMO VLC system with N_t LEDs and N_r photodetectors (PDs) that employs a CC. Without loss of generality, we assume that $N_t = N_r = N$. For a spectral efficiency of R bits, the transmitter constellation $\mathcal{U}$ of $M = 2^R$ symbols is denoted as $\mathcal{U} = \{\mathbf{u}_1, ..., \mathbf{u}_M\}$. More specifically, the signal vector $\mathbf{u}_i$ can be represented as $\mathbf{u}_i = \left[u_i^{(1)}, ..., u_i^{(n)}, ..., u_i^{(N)}\right]^T$ where $u_i^{(n)}$ denotes the signals respectively conveyed by $n-$th LED. The received signal $\mathbf{r}$ can be

described as

$$\mathbf{r} = \mathbf{H}\mathbf{u}_i + \mathbf{n}, \tag{3.1}$$

where $\mathbf{n}$ is the real-valued additive white Gaussian noise (AWGN) with zero mean and variance σ^2. Moreover, we consider the channel matrix $\mathbf{H}$ in [12] for the MIMO VLC system. On the receiver side, we consider the ML detector. With the assumption that $\mathbf{H}$ is correctly estimated at the receiver, the ML detector of the received signal in (3.1) leads to the following detecting problem

$$\hat{\mathbf{u}}_i = \arg\min_{\mathbf{u}_i \in \mathcal{U}} \|\mathbf{r} - \mathbf{H}\mathbf{u}_i\|. \tag{3.2}$$

3.2.2 Problem Formulation

With a specific constellation $\mathcal{U}$, the error probability in transmission can be bounded as

$$P \leq \frac{1}{2M} \sum_{i=1}^{M} \sum_{j=1, j\neq i}^{M} Q\left(\frac{\|\mathbf{H}\left(\mathbf{u}_i - \mathbf{u}_j\right)\|}{\sqrt{2}\sigma}\right), \tag{3.3}$$

where Q is the tail distribution function of the standard normal distribution [59]. The error probability solely depends on the ED between any two constellation points $d_{\mathbf{H}}\left(\mathbf{u}_i, \mathbf{u}_j\right) = \|\mathbf{H}\left(\mathbf{u}_i - \mathbf{u}_j\right)\|$.

Consequently, for a high SNR value, the performance of the system can be improved by the optimization problem $\mathcal{P}_0$ as

$$\begin{aligned} \mathcal{P}_0 : \max_{\mathcal{U}} \min_{\mathbf{u}_i, \mathbf{u}_j \in \mathcal{U}} & d_{\mathbf{H}}\left(\mathbf{u}_i, \mathbf{u}_j\right) \\ \text{s.t.} : & \sum_{i=1}^{M} \|\mathbf{u}_i\| \leq P_{\max}. \end{aligned} \tag{3.4}$$

The problem $\mathcal{P}_0$ of finding the optimal constellation has been discussed in various researches. The authors in [42] proposed a simple technique to minimize the constel-

lation energy while keeping the EDs between different constellation points greater or equal to a certain threshold. All the EDs constraints as nonconvex quadratic functions can be iteratively linearized around an original feasible point so the optimization problem can be solved efficiently to produce a new feasible point with an improved objective value. However, by considering all the possible pairs of $\mathbf{u}_i$ and $\mathbf{u}_j$, the method in [42] has high complexity cost, making it less attractive for large-sized constellations and only a good solution for small to medium-size constellations. On the other hand, for the special case of the CC, the set $\mathcal{U}$ with M constellation points can be represented as basic constellation points and affine combinations of basic constellation points. From $N+1$ basic constellation points $\mathbf{u}_1 = [0, ..., 0]^T$, $\mathbf{u}_i = \left[u_i^{(1)}, ..., u_i^{(n)}, ..., u_i^{(N)}\right]^T$ for $i = 2, ..., N+1$, we have $\mathbf{u}_i = \left[\sum_{\tau=2}^{N+1} \phi_\tau^{(i)} u_\tau^{(1)}, ..., \sum_{\tau=2}^{N+1} \phi_\tau^{(i)} u_\tau^{(n)}, ..., \sum_{\tau=2}^{N+1} \phi_\tau^{(i)} u_\tau^{(N)}\right]^T$ for $i > N+1$, where $\phi_\tau^{(i)} \in \mathbb{N}$ and $\mathbb{N}$ is the set of natural number. Consequently, we have

$$\mathbf{u}_i - \mathbf{u}_j = \left[\sum_{\tau=2}^{N+1} \left(\phi_\tau^{(i)} - \phi_\tau^{(j)}\right) u_\tau^{(1)}, ..., \sum_{\tau=2}^{N+1} \left(\phi_\tau^{(i)} - \phi_\tau^{(j)}\right) u_\tau^{(N)}\right]^T. \tag{3.5}$$

Set $\alpha_\tau^{(ij)} = \phi_\tau^{(i)} - \phi_\tau^{(j)}$, we have

$$\mathbf{u}_i - \mathbf{u}_j = \begin{bmatrix} \mathbf{q}^{(ij)} & \cdots & \mathbf{0}_{1\times N} \\ \vdots & \ddots & \vdots \\ \mathbf{0}_{1\times N} & \cdots & \mathbf{q}^{(ij)} \end{bmatrix} \cdot \mathbf{t}, \tag{3.6}$$

where $\mathbf{q}^{(ij)} = [\alpha_2^{(ij)}, ..., \alpha_{N+1}^{(ij)}]$, $\mathbf{0}_{1\times N}$ is all zeros vector of size $1 \times N$, and $\mathbf{t} = \begin{bmatrix} u_2^{(1)} & , ..., & u_{N+1}^{(1)} & , ..., & u_2^{(N)} & , ..., & u_{N+1}^{(N)} \end{bmatrix}^T$ is a vector of size N^2. Consequently the

optimization problem $\mathcal{P}_0$ can be expressed as

$$\begin{aligned} \mathcal{P}_1 : &\max_{\boldsymbol{t}} \quad p \\ &\text{s.t.} : \mathbf{t}^T \mathbf{Q}^{(ij)} \mathbf{t} \geq p \\ &P_{\mathcal{U}} \leq P_{\max} \end{aligned} \tag{3.7}$$

where $\mathbf{Q}^{(ij)} = \left(\mathbf{q}^{ij}\right)^T \mathbf{H}^T \mathbf{H} \mathbf{q}^{ij}$ and $P_{\mathcal{U}}$ is the total electrical power of the constellation. Since $\mathcal{P}_1$ is a non-convex optimization problem due to the set of constraints in (3.7) for all pairs of (i, j), the iterative linearizing and approximating technique can be employed to approximate $\mathcal{P}_1$ by linearizing $\mathbf{t}^T \mathbf{Q}_{\alpha,\beta} \mathbf{t}$ from an initial solution in the solution space. After that, any tool for solving the convex optimization problem can be used to solve the approximated problem of $\mathcal{P}_1$. Furthermore, the initial solution can be randomly generated, while the optimization problem can be solved with different initial solutions to increase the quality of the optimal solution. As an example, for the case of $N = 2$, three basic constellation points are $\mathbf{u}_1 = [0, 0]^T$, $\mathbf{u}_2 = \left[u_2^{(1)}, u_2^{(2)}\right]^T$, and $\mathbf{u}_3 = \left[u_3^{(1)}, u_3^{(2)}\right]^T$. Then we have $\mathbf{t} = \left[u_2^{(1)}, \quad u_3^{(1)}, \quad u_2^{(2)}, \quad u_3^{(2)}\right]^T$ and $\mathbf{q}^{(ij)} = \left[\alpha_2, \quad \alpha_3\right]$. According to [49], we have $(\alpha_2, \alpha_3) \in \mathbf{\Phi}$ where the set $\mathbf{\Phi} = \left\{ (0, 1) ; (1, 0) ; (a, -b) \,|1 \leq a, b \leq \left(\lceil \frac{\sqrt{8M+1}-1}{2} \rceil - 1 \right) ; \gcd(a, b) = 1 \right\}$ while $\gcd(a, b)$ is the function used to calculate the greatest common divisor between a and b.

In comparison with the solution in [42], by optimizing the constellation using just $N + 1$ basic constellation points instead of M [49], the complexity cost in solving the optimization problem $\mathcal{P}_0$ is significantly reduced. However, as an unavoidable cost, when the constellation size M becomes higher, so does the size of the set $\mathbf{\Phi}$. Therefore, the number of constraints in $\mathcal{P}_1$ also increases, and consequently, the complexity of solving the optimization problem $\mathcal{P}_1$ increases dramatically. Therefore, we provide

here a constellation design approach based on DL techniques. Interestingly, the DL has never been investigated in the constellation design scheme in part because the size of the output is usually equivalent to the number of constellation points M. Hence, the application of DL for a high rate communication system is impractical. However, as the size of the unknown variable $\mathbf{t}$ in CC is just N^2, regardless of constellation size M, the feasibility of applying DL improves because a DNN can be used to predict the optimal basic constellation with little complexity cost and a low running time. In the next section, we present a practical approach to solve $\mathcal{P}_1$ based on the DL technique.

3.3 Proposed deep-learning-based collaborative constellation design

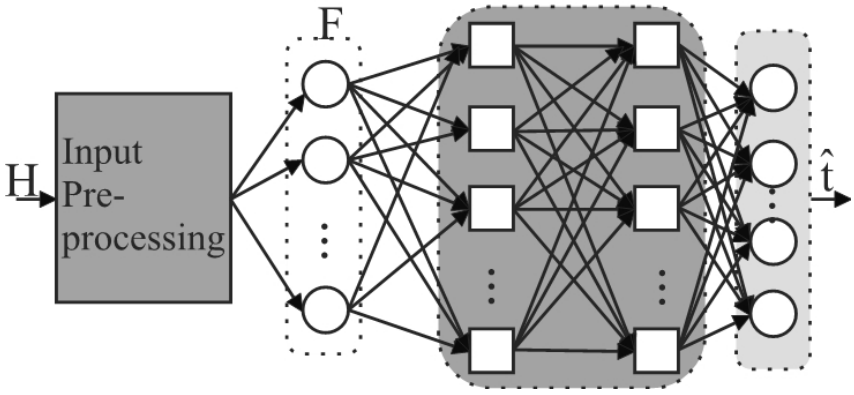

Figure 3.1: The CCNet structure.

In this section, we first present the network structure of the proposed CCNet, then input preprocessing with data generation will be detailed, finally the training procedure and online deployment of CCNet will be described.

3.3.1 Network structure

The proposed CCNet structure is basically a fully connected DNN, with hidden layers that act as a nonlinear programming solver of the optimization problem $\mathcal{P}_0$. More specifically, CCNet consists of an input layer, several hidden layers, and an output layer [57]. The neurons are connected between adjacent layers, while in the same layer, the neurons are independent. Moreover, the input is multiplied by weights, and a bias corresponding to each neuron is added. Specifically, if the input of the FC layer is $\mathbf{x} = [x_1, x_2, ..., x_F]^T \in \mathbb{R}^F$, then the output of the FC layer can be expressed as $y_p^{(k)} = \sum_{q=1}^{N} w_{pq}^{(k)} x_i + b_p^{(k)}$, where $w_{pq}^{(k)}$ is the weight of the $q-$th input in the k-th weight matrix layer connected to the $p-$th hidden layer neuron. At each hidden layer, the signal is processed through a nonlinear activation function such as sigmoid, tanh, or ReLU, while the output layer is processed without an activation function.

3.3.2 Input features

The optimization of the basic constellation points $\mathbf{t}$ can be interpreted as a nonlinear mapping from the CSI matrix $\mathbf{H}$ onto the optimal $\mathbf{t}$. The input features $\mathbf{x} = [x_1, x_2, ..., x_F]^T$ with F inputs are significant to the performance of the CCNet learning process. Since the choice of input feature is of the utmost importance, the proposed CCNet takes advantage of expert knowledge to extract meaningful features instead of directly relying on the original channel matrix to enhance prediction performance.

Feature selection

First, it is intuitive that the vectorization channel matrix should be the network input. Since the optimization solely depends on $\mathbf{H}$, the most straightforward feature input should be a vector of length N^2, as $\mathbf{x} = [h_{11}, h_{12}, ..., h_{NN}]^T$. However, as in [60], the squared distances between any pair of symbols can be represented as a function of the basic constellation points as

$$\begin{aligned} d^2_{\mathbf{H}}(\mathbf{u}_i, \mathbf{u}_j) = \|\mathbf{H}(\mathbf{u}_i - \mathbf{u}_j)\| = \sum_{n=1}^{N} \left(\Delta_{i,j}^{(n)} \|\mathbf{h}_{\mathrm{c}}^{(n)}\| \right)^2 \\ + \sum_{n=1}^{N} \sum_{m=1, n\neq m}^{N} \Delta_{i,j}^{(n)} \Delta_{i,j}^{(m)} \left(\mathbf{h}_{\mathrm{c}}^{(n)}\right)^T \mathbf{h}_{\mathrm{c}}^{(m)} \end{aligned} \tag{3.8}$$

where $\boldsymbol{\Delta}_{i,j} = \mathbf{u}_i - \mathbf{u}_j$; $\mathbf{h}_{\mathrm{c}}^{(n)}$ and $\mathbf{h}_{\mathrm{c}}^{(m)}$ are the $n-$th and $m-$th columns of the channel matrix $\mathbf{H}$. Consequently, for a particular constellation, the distance between received signals depends on the channel matrix information $\mathbf{H}$. With particular values of $\mathbf{t}$ and i, j, several real values are required to describe the dependence of the distance on the channel matrix $\mathbf{H}$, namely $\|\mathbf{h}_{\mathrm{c}}^{(n)}\|$, and the scalar products $\left(\mathbf{h}_{\mathrm{c}}^{(n)}\right)^T \mathbf{h}_{\mathrm{c}}^{(m)}$. Later, it will be demonstrated that the input features with columns and rows of the channel matrix instead of just using channel coefficients, can significantly improve the performance of CCNet.

Moreover, in DL, data augmentation is a useful tool to create a robust dataset and is crucial for the performance of the model [61], [62]. The most popular form of data augmentation is the elastic transformation or traditional affine. Throughout the simulations, we observed that the performance was further improved with a particular data-augmentation-like trick. Similar to (3.8), the distance between received signals also depends on the norm of row vectors $\|\mathbf{h}_{\mathrm{r}}^{(n)}\|$ of the channel matrix $\mathbf{H}$, and the scalar

products $\left(\mathbf{h}_{\mathrm{r}}^{(n)}\right)^{T}\mathbf{h}_{\mathrm{r}}^{(m)}$, it turns out that the input features of size $F = N^2 + N$, $\mathbf{x} = \left[\|\mathbf{h}_{\mathrm{c}}^{(n)}\|, \frac{\left(\mathbf{h}_{\mathrm{c}}^{(n)}\right)^{T}\mathbf{h}_{\mathrm{c}}^{(m)}}{\|\mathbf{h}_{\mathrm{c}}^{(n)}\|\|\mathbf{h}_{\mathrm{c}}^{(m)}\|}, \|\mathbf{h}_{\mathrm{r}}^{(n)}\|, \frac{\left(\mathbf{h}_{\mathrm{r}}^{(n)}\right)^{T}\mathbf{h}_{\mathrm{r}}^{(m)}}{\|\mathbf{h}_{\mathrm{r}}^{(n)}\|\|\mathbf{h}_{\mathrm{r}}^{(m)}\|}\right]^{T}, n = 1, 2, ..., N; m \in \{1, 2, ..., N\}; m \neq n$ are sufficient for CCNet to predict an optimal $\mathbf{t}$ for any constellation size M, even though the number of ED increases with the size M of the constellation. For example, in a system with $N = 2$, the size of the input feature vector for the former case $\mathbf{x} = [h_{11}, h_{12}, ..., h_{NN}]^{T}$ is $F = 4$ while the size of the input feature vector for the later proposed one is $F = 6$. When $N = 4$, the corresponding feature vectors have the sizes of $F = 16$ and $F = 20$, respectively. On the other hand, the output size of the CCNet is N^2 for any constellation of size M. For the cases of $N = 2$ and $N = 4$, with any M, the sizes of the estimated $\hat{\mathbf{t}}$ are just 4 and 8, respectively.

Data generation

First, we design the training and testing samples. Each sample contains input feature $\mathbf{x}$ and basic output constellation $\mathbf{t}$. Various receiver locations are randomly generated to obtain a corresponding set of channel coefficients. For a particular channel matrix $\mathbf{H}$ corresponding to a specific receiver location, the feature vector $\mathbf{x}$ is calculated and denoted as $\mathbf{x}_k$. Consequently, the basic constellation, denoted as vector $\mathbf{t}_k$ is obtained by solving $\mathcal{P}_1$ using the convex optimization solving process as in [49] or [42]. The obtained suboptimal solutions from both methods have similar minimum ED values and are able to achieve a favorable error performance in the simulations in comparison with conventional one [37]. This can be observed later in the simulation result. Besides, the complexity cost to generate training data in [49] is lower than one in [42]. Therefore, we consider the data generated using [49] and the

$k-$th sample can be expressed as $\mathbf{z}_k = (\mathbf{x}_k, \mathbf{t}_k)$. Then, we generate the normalized data set as

$$\mathbf{d}_k^{(l)} = \frac{\mathbf{z}_k^{(l)} - \mathbb{E}\{z_k\}}{\max(z_k) - \min(z_k)}, \tag{3.9}$$

where $\mathbb{E}$ denotes the expectation operator and $l = 1...(N^2 + N)$. Since the output $\mathbf{t}_k$ depends on the absolute values of the channel coefficients instead of the relative ratio between them, the use of a normalized dataset can help to effectively reduce the MSE and speed up the training process without compromising the performance of CCNet. Furthermore, as mentioned in [49], the optimized constellation was normalized to meet the power constraints. Using the training data set generated from [49], the predicting output of the network does not vary much from the total power constrains $P_{\max}$. Nevertheless, the resultant constellation should be normalized again without any significant impact on the performance.

3.3.3 Training strategy and online deployment

In the input layer of CCNet, each value in the training sample $\mathbf{d}_k$ corresponds to each neuron as either input or output. During training, we simply adopt the MSE loss function as

$$\mathcal{L}(\mathbf{W}, \mathbf{b}, \mathbf{t}, \hat{\mathbf{t}}) = \|\mathbf{t} - \hat{\mathbf{t}}\|^2. \tag{3.10}$$

Furthermore, as implemented by Tensorflow and Keras, we employ a mini-batch stochastic gradient descent (SGD) algorithm, such as the Adam algorithm, to train CCNet. More specifically, to minimize the MSE loss function, the weight values between the neurons are adjusted and updated accordingly using the back-propagation (BP) algorithm. After evaluating the generalization of the trained CCNet using the

validation, the learning rate is adapted by monitoring the validation loss function to avert overfitting or underfitting. More specifically, the learning rate is reduced by a factor of four every time learning stagnates until it is smaller than 10^{-4}.

As in previous research on DNN, since the training requires a significant amount of computing power without the need for real-time processing, CCNet training can be executed offline [63]. After that, the trained CCNet can be deployed in the receiver at any random location to rapidly determine the optimal constellation based on the estimated channel gain.

3.4 Numerical results

In this section, we provide simulation results of the MSE, BER, and the running time of the proposed CCNet in comparison with previous schemes, including the method in [42], [49]. For a fair comparison, we consider here a 2×2 MIMO VLC system. Later, some results are also presented for the cases of 4×4 and 8×8. The proposed CCNet is trained over 300 iterations with a batch size of 314 samples. Each sample is generated using the method in [49] with five initial solutions to the optimization problem. Moreover, for each iteration, the network is trained with 1000 epochs. The learning rate is reduced by a factor of 1/4 when the validation loss does not improve after four epochs, until it reaches the minimum value of 0.0002. Also, an iteration is terminated early, and the training stops when the validation loss value stops improving. Meanwhile, parameters such as F, the number of layers, and the number of neurons are scenario-specific. For example, $F = N^2$ with the input feature vector of $\mathbf{x} = [h_{11}, h_{12}, ..., h_{NN}]^T$ while $F = N^2 + N$ when the proposed input

Table 3.1: MSE comparison of CCNet for $N = 2$ and $F = 4, 6$.

	1 hidden layer		2 hidden layers		3 hidden layers	
Neurons	10	20	10/10	20/20	10/10/10	20/20/20
$F = 4$	9.28e-3	5.22e-3	9.73e-4	5.32e-4	4.83e-4	8.31e-5
$F = 6$	8.31e-4	1.19e-4	1.76e-4	4.11e-5	7.24e-5	9.23e-6

feature vector is utilized. In both cases, the size of the network output is fixed at N^2. Consequently, with $N = 2$, while the output size is just four neurons, the input features have sizes of four and six, respectively.

In Table I, the comparison of MSE for CCNet with different inputs and different network parameters is shown. Overall, the preprocessing of input features with $F = 6$ always outperforms the case when $F = 4$. Also, more hidden layers can provide a better MSE. However, throughout many simulations, CCNet tends to overfit when the number of hidden layers is more than four, and it was found that the optimal number of layers is three. Finally, the MSE reaches a minimum value of about 9.23^{-6} with three hidden layers of 20 neurons and six input features.

Next, we compare the BER performances of the proposed CCNet with the previous algorithms in [49],[42] and the conventional CC [37] in Fig. 3.2. It can be seen that CCNet achieves results similar to the high complexity algorithms in [49],[42], and outperforms the conventional CC. Moreover, the gap increases when the number of constellation points is larger, which demonstrates that the proposed CCNet can be effectively applied with any constellation size.

In Fig. 3.3, we present the BER performance results of systems with $N = 4$ and $N = 8$ for two different constellation sizes, $M = 64$ and $M = 128$, respectively. Similar with the case of $N = 2$, for each data sample, the receiver is randomly positioned

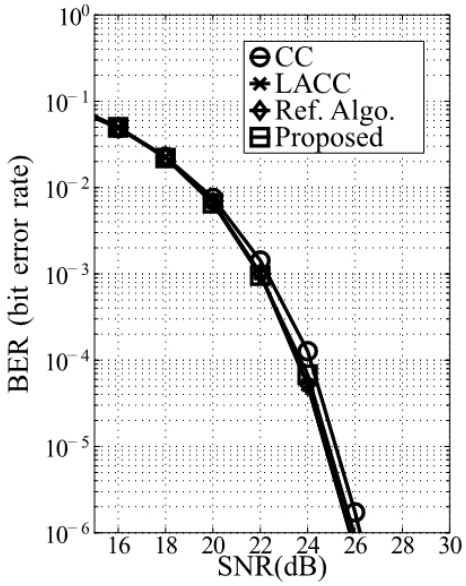

(a) $M = 8$

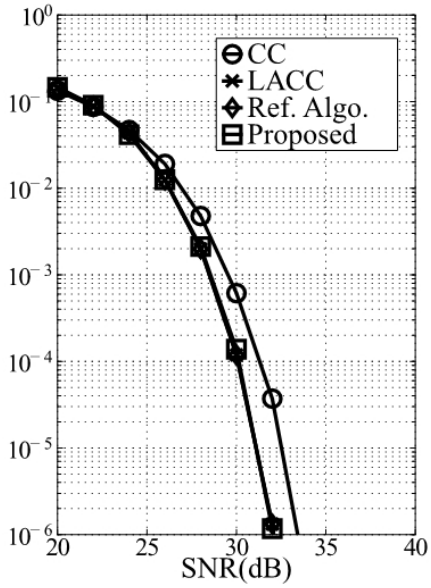

(b) $M = 32$

Figure 3.2: BER comparison of 2×2 system for the constellations of sizes.

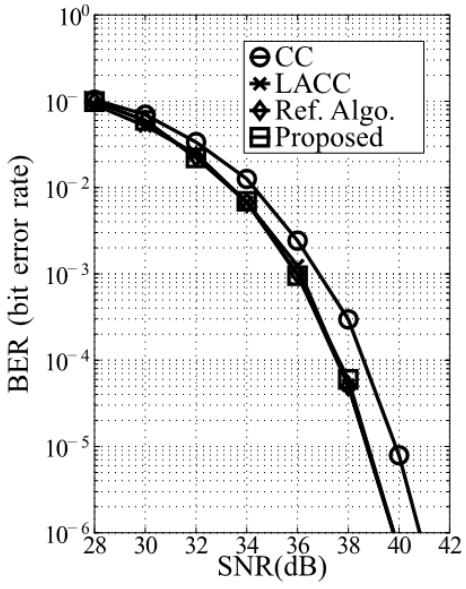

(a) $M = 64$, 4×4 system

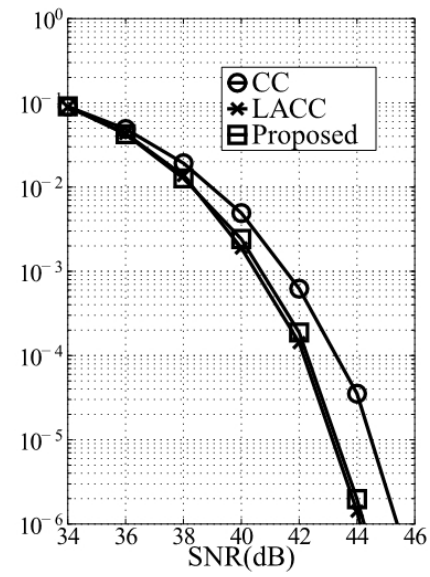

(b) $M = 128$, 8×8 system

Figure 3.3: BER comparison for the constellations of sizes.

and the optimal constellation is computed using either [49] or [42]. However, when $M = 128$, the number of constraints in optimization problem [42] is 8192, which is extremely larger than 108 in [49]. In fact, this issue of complexity has been mentioned in [42] and the result for 8×8 system is shown without the method in [42]. It can be seen from Fig. 3.3 that a similar network behavior is expected when increasing the value of N. The proposed CCNet still provides a similar performance with the algorithm in [42], [49] and the gap between the optimized constellation with the original one in [37] still persists. This is explained by the valuable spatial resource that can be freely exploited with a larger number of LEDs, which is neglected in the original constellation in [37].

Table 3.2: Execution time comparison.

M	CCNet		Ref.[49]	Ref.[42]
	2 layers	3 layers		
8 ($N = 2$)	0.055s	0.062s	1.173s	1.929s
32 ($N = 2$)	0.060s	0.065s	2.657s	5.862s
64 ($N = 4$)	0.188s	0.190s	5.200s	13.187s
128 ($N = 8$)	0.326s	0.335s	12.209s	-

Finally, to compare the complexity cost of the proposed CCNet with the method provided in [49] and [42], we show the running time of an input sample in Table II. To evaluate the run time of CCNet and for a fair comparison, we use MATLAB 2019a to convert the trained model from Keras to estimate the run time for each sample, using a workstation with an Intel Xeon CPU at 3.47 GHz and 24 GB of memory storage. For all cases, the run time values are increasing with the size of the constellation and the number of LEDs. The algorithms in [49] and [42] require much more time to

calculate and become impractical to be employed when the size of the constellation are large. More specifically, the conventional method in [42] requires a higher complexity than [49] since the number of constraints in the optimization problem is higher. On the other hand, with simple input preprocessing and a network structure, CCNet can estimate the optimal constellation in an extremely short amount of time with little compromise to BER performance. Moreover, the complexity mainly depends on the numbers of input and output neurons, which are increase as N increases.

Chapter 4

Superposed constellation design for VLC systems

4.1 Introduction and motivation

Although several modulation schemes can mitigate the nonlinearity of LEDs by sacrificing spectral efficiency, such as on-off keying (OOK) modulation [11], pulse width modulation (PWM) [64], and pulse position modulation (PPM) [65], all of these binary signals modulations have very limited spectral efficiency and are not good in high rate transmission systems [66]. On the other hand, various modulation schemes have been proposed for VLC systems with multiple LED transmissions, such as spatial multiplexing (SMP) [67] and repetition coding (RC) [68]. Despite its simple design principle, spatial modulation (SM) [59] has been envisioned as one prospective digital modulation approach among the various technologies to achieve high spectral efficiency and energy efficiency. Even so, SM performance is also impaired by the

high-level correlation of the optical channel, especially when the channel links are identical, thus making it very difficult to identify the active LEDs in the SM VLC system [69].

It has been proved that spatial summing is useful in mitigating LED nonlinearity with ideal LED devices when the channel correlation is high. Coincidentally, low-order constellations are more appropriate at the transmitters whereas higher-order constellations are acceptable at the receivers [70]. Therefore, higher-order modulation can be employed without non-linear distortion in VLC systems. The promising approach of an SMP scheme using the principle of superposed signals has recently been suggested for a 2×1 multi-input single-output (MISO) VLC system [71]. In the proposed method, two data streams multiplied by various power ratios are transmitted from two LEDs and then uniquely superposed modulations are recreated in the receiving PD. Consequently, multiplexing gains can be achieved in the highly correlated MISO channels. In [72], the authors suggested a novel 2×2 VLC system with a superposed 32 quadrature amplitude modulation (QAM) constellation scheme with the conclusion that only low-order constellations are required at LEDs to have a reasonable minimum Euclidean distance (ED). Previous studies such as [71]–[73] mainly focused on an effective algorithm to separate and detect a signal transmitted by individual LEDs while an optimal power allocation coefficient was exhaustively determined to improve the transmission performance. The power allocation is one way of reducing the error probability at the receiver side by increasing the minimum ED between the received superposed constellation points. This has proved to be remarkably effective since different values of coefficients generate different error probabilities. However,

this strategy has the inherent limitation of low optimization dimensions and can only improve the transmission performance up to a certain point.

In this chapter, instead of the conventional way of optimizing the power allocation for individual LEDs in the superposed constellations of a multi-dimensional VLC system [72], [73], we propose designing the sub-constellations at each LED to increase the minimum ED of the superposed constellation at the receiver side, resulting in a significant improvement in the symbol error rate (SER) of the system. More specifically, an optimization problem formed by using the constellations at individual LEDs as unknown parameters is linearized and iteratively solved. The optimal result vector is then used to construct the sub-constellations at each LED so that the minimum ED is as large as possible according to the constraints on total electrical power and maximum transmitted power. Furthermore, we propose the inter-ED and intra-ED terms to reduce the number of constraints in the optimization problem, while some pre-defined shape sub-constellations are utilized to remarkably enhance the minimum ED values and improve the SER performance. The simulation results demonstrate the advantages of the proposed constellation design method. The superposed constellation at the receiver can have different minimum ED values (and thus different error rate probabilities) depending on the pre-defined shape of the sub-constellations. Our approach promises to deliver favorable performance and affordable complexity costs with appropriately chosen parameter values such as constellation size and shape.

4.2 System model

First, we consider a VLC system consisting of N LEDs as the transmitter and one PD as the receiver. At each period t, the input information bits are modulated into the input signal vector that will later be emitted by all LEDs, $\left[s_1(t), s_2(t), ..., s_N(t)\right]^T$. On the receiver side, after the propagation of the signal through the optical channel, it can be assumed that the signals received at the PD are superpositions of those transmitted from each LED. For example, as in [72], [73], the 32-QAM constellation on the receiver can be obtained using 4-QAM and 8-QAM on the two LEDs on the transmitter side. The relationship between the received superposed signals at the PD and the independent transmitted signals from the LEDs can then be defined as

$$r(t) = \sum_{n=1}^{N} h_n(t) \otimes s_n(t) + w(t), \tag{4.1}$$

where $h_n(t)$ represents the channel coefficient between the n-th LED and the PD, and $w(t)$ denotes the additive white Gaussian noise (AWGN). More specifically, since we can choose any modulation for each LED (such as QAM), the real and imaginary parts of the constellation of the n-th LED can be represented as

$$\mathcal{S}_n = \left\{ \left(x_n^{(1)}, y_n^{(1)}\right), \left(x_n^{(2)}, y_n^{(2)}\right), ..., \left(x_n^{(m_n)}, y_n^{(m_n)}\right), ..., \left(x_n^{(M_n)}, y_n^{(M_n)}\right) \right\}, \tag{4.2}$$

where $x_n^{(m_n)}$ and $y_n^{(m_n)}$ denote the real and imaginary parts of the m-th constellation of the n-th LED, respectively, under the condition that $1 \leq n \leq N$ and $1 \leq m_n \leq M_n$. Here, M_n is the modulation order of the n-th LED, and the pseudo-random binary sequence is modulated in each LED by one of the symbols in $\mathcal{S}_n$. Therefore, the bit rate of the system with N LEDs can be calculated as $\log_2\left(\prod_{n=1}^{N} M_n\right)$.

Any particular superposed constellation composition can be defined by the corresponding power ratio of the LEDs. For example, in the case of a VLC system with two LEDs and without the loss of generality, the real and imaginary components of the LED_1 constellation are kept as invariant, with scaling factor α to express the power ratio between the two LEDs. Therefore, α can be multiplied by the real and imaginary components of the LED_2 to adjust its amplitude. Consequently, the optimal constellation with favorable performance can be obtained by exhaustively searching for the optimal value of α. On the other hand, specific receivers have been suggested to recognize the original symbols conveyed by LEDs, with the maximum likelihood (ML) or lookup table (LUT) detector being by far the most straightforward and fundamental signal detector. Notably, the ML detector algorithm is used to estimate the received mixture from various transmitted combinations as via the ML algorithm, it tries to find a combination that generates the minimum ED with the obtained signal. The successive interference cancellation-LUT (SIC-LUT) was proposed by [72], while in [73], the least-squares algorithm is utilized in the frequency domain to separate the superposed signals. Moreover, the ED is commonly used as a distance measure in signal processing. In the present study, the ED between any two received constellation points is defined as

$$d\left(\left(x^{(i)}, y^{(i)}\right), \left(x^{(i')}, y^{(i')}\right)\right) = \left(\left|x^{(i)} - x^{(i')}\right|^2 + \left|y^{(i)} - y^{(i')}\right|^2\right)^{1/2}. \tag{4.3}$$

The overall pairwise-error probability (PEP) for all available pairs of superposed symbols is generally employed as the upper limit for the system SER performance.

4.3 The proposed constellation design scheme

Without the loss of generality, the real part of the received signal in (1), $r_x(t)$, can be rewritten by using the vector form as

$$r_x(t) = \mathbf{h}(t)\,\mathbf{x}(t) + w_x(t) \tag{4.4}$$

where $\mathbf{h}(t) = [h_1(t) ... h_n(t) ... h_N(t)]$ and $\mathbf{x}(t) = [x_1(t) ... x_n(t) ... x_N(t)]^{\mathrm{T}}$ represent the channel gain and the real parts of the transmitted symbols, respectively. Using the presumption in [72], [73], when the propagation distance and range between the positioned LEDs are relatively small, we can presume that in an ideal scenario, all of the channel gains have approximately the same values. Subsequently, signals from all of the LEDs are superposed in the PD, and the system can be simplified as the single-input single-output (SISO) model. Therefore, the difference between the channel coefficients is very small, and the received symbols in Eq. (4.2) can be expressed as

$$r_x(t) = \mathbf{x}_{\mathrm{sup}}\mathbf{p}(t) + w_x(t) \tag{4.5}$$

where $\mathbf{x}_{\mathrm{sup}} = \left[x_1^{(1)} ... x_1^{(M_1)} x_n^{(1)} ... x_n^{(M_n)} x_N^{(1)} ... x_N^{(M_N)}\right]$ is the $\sum_{n=1}^{N} M_n$-length vector which composed of all real parts of symbols set $\mathcal{S}$. Besides, $\mathbf{p}(t) = \begin{bmatrix} \mathbf{p}_1 & ... & \mathbf{p}_n & ... & \mathbf{p}_N \end{bmatrix}^{\mathrm{T}}$ is a vector of the same length whereas each individual $\mathbf{p}_n$ is an M_n-length vector in which all of the elements are zero except for the one at the position of the transmitted symbol of the n-th LED. For example, if the first symbol of the LED_1 and the second symbol of the LED_2 with 4-QAM constellation are chosen, we have $\mathbf{x}_{\mathrm{sup}} = \left[x_1^{(1)} x_1^{(2)} x_1^{(3)} x_1^{(4)} x_2^{(1)} x_2^{(2)} x_2^{(3)} x_2^{(4)}\right]$ and $\mathbf{p}(t) = [1 \quad 0 \quad 0 \quad 0 \quad 0 \quad 1 \quad 0 \quad 0]^T$. Notice that we denote the imaginary part of the transmitted symbol $y_n(t)$ as $(x_n(t), y_n(t)) \in \mathcal{S}_n$.

Therefore, with the imaginary part of the transmitted signal, we can represent the superposed constellation at the receiver as

$$\begin{aligned}&\mathbf{r}\left(t\right)\\&=\begin{bmatrix}r_x\left(t\right) & r_y\left(t\right)\end{bmatrix}=\begin{bmatrix}\mathbf{x}_{\text{sup}}\mathbf{p}\left(t\right) & \mathbf{y}_{\text{sup}}\mathbf{p}\left(t\right)\end{bmatrix}=\begin{bmatrix}\mathbf{x}_{\text{sup}} & \mathbf{y}_{\text{sup}}\end{bmatrix}\begin{bmatrix}\mathbf{p}\left(t\right) & \mathbf{0}_{\sum_{n=1}^{N}M_n\times 1}\\ \mathbf{0}_{\sum_{n=1}^{N}M_n\times 1} & \mathbf{p}\left(t\right)\end{bmatrix}.\end{aligned} \tag{4.6}$$

On the other hand, we can rewrite the ED between any two different received superposed constellation points $\mathbf{r}^{i},\mathbf{r}^{i'}$ as

$$\begin{aligned}d^2\left(\mathbf{r}^{(i)},\mathbf{r}^{(i')}\right)&=\left(r_x^{(i)}-r_x^{(i')}\right)^2+\left(r_y^{(i)}-r_y^{(i')}\right)^2\\&=\begin{bmatrix}\mathbf{x}_{\text{sup}}\mathbf{p}^{(i,i')} & \mathbf{y}_{\text{sup}}\mathbf{p}^{\left(\ i,i'\ \right)}\end{bmatrix}\begin{bmatrix}\mathbf{x}_{\text{sup}}\mathbf{p}^{\left(\ i,i'\ \right)} & \mathbf{y}_{\text{sup}}\mathbf{p}^{\left(\ i,i'\ \right)}\end{bmatrix}^{\text{T}}\\&=\mathbf{t}\mathbf{Q}^{(i,i')}\mathbf{t}^{\text{T}},\end{aligned} \tag{4.7}$$

where $\mathbf{Q}^{(i,i')}=\begin{bmatrix}\mathbf{p}^{\left(\ i,i'\ \right)} & \mathbf{0}_{\sum_{n=1}^{N}M_n\times 1}\\ \mathbf{0}_{\sum_{n=1}^{N}M_n\times 1} & \mathbf{p}^{\left(\ i,i'\ \right)}\end{bmatrix}\begin{bmatrix}\mathbf{p}^{\left(\ i,i'\ \right)} & \mathbf{0}_{\sum_{n=1}^{N}M_n\times 1}\\ \mathbf{0}_{\sum_{n=1}^{N}M_n\times 1} & \mathbf{p}^{\left(\ i,i'\ \right)}\end{bmatrix}^{\text{T}}$,

$\mathbf{t}=\begin{bmatrix}\mathbf{x}_{\text{sup}} & \mathbf{y}_{\text{sup}}\end{bmatrix}$, $\mathbf{p}^{(i,i')}=\mathbf{p}^{\left(\ i\ \right)}-\mathbf{p}^{\left(\ i'\ \right)}$, and $\mathbf{p}^{\left(\ i\ \right)}$ is the vector represents the index of the transmitted symbol at the transmitter. Intuitively, at a high signal-to-noise (SNR) level, the minimum ED between any two received constellation points is the predominant factor in the average error probability. To design a constellation that maximizes the minimum of all of the pair-wise distances among the constellation symbol set, optimal vector $\mathbf{t}$ can be determined through an optimization problem $\mathcal{P}_0$

as

$$\mathcal{P}_0 : \max_{\mathbf{t}} \min_{i,i'} \quad d^2\left(\mathbf{r}^{(i)}, \mathbf{r}^{(i')}\right) \tag{4.8a}$$

$$s.t. \quad 0 \leq \mathbf{t} \leq I_{\max} \tag{4.8b}$$

$$\|\mathbf{t}\| \leq P_{\max}, \tag{4.8c}$$

where the first constrain $0 \leq \mathbf{t} \leq I_{\max}$ ensures the transmitted signal level meets the maximum transmission power of the LED while the second constraint $\|\mathbf{t}\| \leq P_{\max}$ ensures that the total electrical transmitted power of all LEDs is smaller than $P_{\max}$. Thus, the problem $\mathcal{P}_0$ can be rewritten as follows

$$\mathcal{P}_1 : \max_{\mathbf{t}} \quad q \tag{4.9a}$$

$$s.t. \quad \mathbf{t}\mathbf{Q}^{(i,i')}\mathbf{t}^{\mathrm{T}} \geq q, \forall i \neq i' \tag{4.9b}$$

$$0 \leq \mathbf{t} \leq I_{\max} \tag{4.9c}$$

$$\|\mathbf{t}\| \leq P_{\max}. \tag{4.9d}$$

The fundamental principle of the optimization approach is to maximize q as the minimum ED between the constellation points (the maximization of q is known as the maximum-minimum ED problem). When the maximum-minimum ED problem is non-convex, a method called the approximated maximum-minimum ED, which has a fairly quick convergence rate with relatively low computational complexity, can be used to transform this problem into a convex form. Nevertheless, convex relaxation methods were introduced in [41], [74] to approximate $\mathcal{P}_1$, the main concept of which is the linearization of $\mathbf{t}\mathbf{Q}^{(i,i')}\mathbf{t}^{\mathrm{T}}$ from point $\mathbf{t}^{(k)}$ in the solution space. The approximate

problem can be defined as

$$\mathcal{P}_2 : \max_{\mathbf{t}} \quad q \tag{4.10a}$$

$$s.t. \quad 2\mathbf{t}^{(k)}\mathbf{Q}^{(i,i')}\mathbf{t}^{\mathrm{T}} - \mathbf{t}^{(k)}\mathbf{Q}^{(i,i')}\left(\mathbf{t}^{(k)}\right)^{\mathrm{T}} \geq q, \forall i \neq i' \tag{4.10b}$$

$$0 \leq \mathbf{t} \leq I_{\max} \tag{4.10c}$$

$$\|\mathbf{t}\| \leq P_{\max}. \tag{4.10d}$$

Since the approximated optimization problem is a convex one, any algorithm or technique such as an internal point method can be employed to solve the maximum-minimum ED problem effectively within several iterations. However, to solve $\mathcal{P}_2$, we try to solve multiple convex optimization sub-problems iteratively before reaching convergence. Our simulation results show that the convergence rate is very slow, which will result in high computational complexity. Moreover, it becomes more difficult to find a good constellation as the size of the constellation increases. In the next part, we present the notations of intra-ED and inter-ED between the constellation points to reduce the number of constraints in $\mathcal{P}_2$. Conversely, as mentioned in [73], the constellation employed in each individual LED can be chosen as any QAM shape (such as a square, rectangle, or circle), which can help to reduce the size of the unknown vector $\mathbf{t}$ and, consequently, reduce the complexity of solving the optimization problem.

4.4 The low complexity constellation design

In this section, we explain the low complexity constellation design principle with some examples. Moreover, we (1) define the intra-ED and inter-ED to reduce the

number of constraints and (2) propose using the pre-defined sub-constellation shapes to reduce the total unknown variables in the optimization problem.

4.4.1 The principles of intra-ED and inter-ED

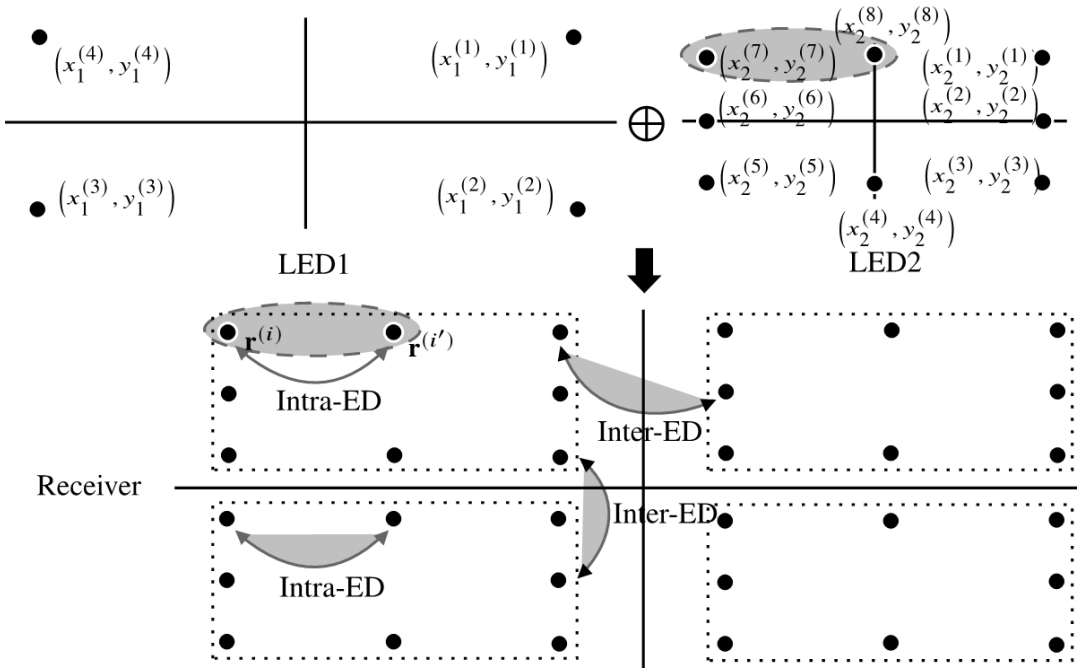

Figure 4.1: Intra-ED and inter-ED examples.

Consider a simple case of 32-QAM superposed constellation $\mathcal{S}$ using two LEDs with the constellation $\mathcal{S}_1$ as 4-QAM at LED_1, and $\mathcal{S}_2$ as 8-QAM at LED_2. We can define the intra-ED between two superposed constellation points $\mathbf{r}^{(i)}$ and $\mathbf{r}^{(i')}$ which comprise the same signal from one LED (either LED_1 or LED_2). For example, as illustrated in Fig. 4.1, constellation points $\mathbf{r}^{(i)}$ or $\mathbf{r}^{(i')}$ of $\mathcal{S}$ are both superposed from $\left(x_1^{(4)}, y_1^{(4)}\right)$ of LED_1 with either $\left(x_2^{(7)}, y_2^{(7)}\right)$ or $\left(x_2^{(8)}, y_2^{(8)}\right)$ of LED_2, respectively. As a result, the ED between these two constellation points $\mathbf{r}^{(i)}, \mathbf{r}^{(i')} \in \mathcal{S}$ can be computed

as

$$d^2\left(\mathbf{r}^{(i)},\mathbf{r}^{(i')}\right)=\left[\left(x_1^{(4)}+x_2^{(7)}\right)-\left(x_1^{(4)}+x_2^{(8)}\right)\right]^2+\left[\left(y_1^{(4)}+y_2^{(7)}\right)-\left(y_1^{(4)}+y_2^{(8)}\right)\right]^2$$
$$=\left[x_2^{(7)}-x_2^{(8)}\right]^2+\left[y_2^{(7)}-y_2^{(8)}\right]^2=d^2\left(\mathbf{s}_2^{(7)},\mathbf{s}_2^{(8)}\right). \tag{4.11}$$

Therefore, regardless of the transmitted signal in LED_1, the distance between the two superposed constellation points with the intra-ED property always equals $d^2\left(\mathbf{s}_2^{(7)},\mathbf{s}_2^{(8)}\right)$, which is equivalent to the ED between the transmitted symbols at LED_2. In this way, all of the intra-ED constraints with the same transmitted symbols at LED_1 can be reduced to just one constraint. On the other hand, the inter-ED constraints that are the ED between two superposed constellation points $\mathbf{r}^{(i)}$ and $\mathbf{r}^{(i')}$ belonging to $\mathcal{S}$ composed of different symbols from all of the LEDs can be considered as nontrivial. In this way, the $\sum_n M_n\left(\sum_n M_n-1\right)/2$ constraints in the optimization problem $\mathcal{P}_2$ can be reduced to $\sum_{k=0}^{N-2}\left[\prod_{l=0}^{k}\left(M_{N-l}\right)^2\times M_{N-k-1}\left(M_{N-k-1}-1\right)\right]$ and comprises both the inter-ED and intra-ED constraints.

4.4.2 The pre-defined shaped sub-constellations

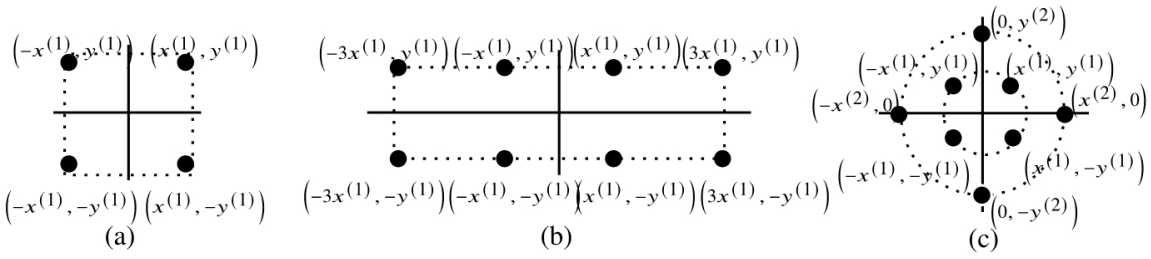

Figure 4.2: Sub-constellation examples: (a) square-shaped (4-sQAM), (b) rectangular-shaped (8-rQAM), and (c) circular-shaped (8-cQAM).

As mentioned before, the unknown vector $\mathbf{t}$ has a total of $2\sum_{n=1}^{N} M_n$ variables that becomes obstructively large as the number of LEDs and the constellation size increase. For example, for $N = 3$, a 64-point constellation with all of the LEDs using 4-QAM constellation, $\mathbf{t}$ contains 24 variables. Besides, the approximated optimization problem with a large number of variables becomes ineffective since the random initial vectors of $\mathbf{t}$ pose a huge degree of uncertainty in the solving process, thereby leading to a poor quality solution and degradation in the system performance. Therefore, to further reduce the complexity cost on the optimization problem-solving process and improve the optimal solutions, we further modify the optimization problem using pre-defined shaped sub-constellations for each LED. As illustrated in the simulation results, comparisons are made between the pre-defined shaped sub-constellation QAM combinations, such as square-shaped (sQAM), rectangular-shaped (rQAM), and circular-shaped (cQAM). A comparison with conventional and the aforementioned proposed high complexity method clearly shows that the pre-defined shape constellation of the LED helps to reduce the complexity cost of the optimization problem-solving process while significantly improving the quality of the resulting constellation.

Example: $N = 2$, $M = 32$ using rQAM constellations

In this scenario, the transmitter is equipped with two LEDs, LED_1 and LED_2, with rQAM constellations, denoted as M_1-rQAM and M_2-rQAM, respectively. For example, 4-rQAM at LED_1 and 8-rQAM at LED_2 can be employed to obtain a 32-QAM superposed constellation at the receiver. The unknown 4-rQAM constellation at LED_1

can be denoted as $\mathcal{S}_1 = \left\{\left(x_1^{(1)}, y_1^{(1)}\right), \left(x_1^{(1)}, -y_1^{(1)}\right), \left(-x_1^{(1)}, y_1^{(1)}\right), \left(-x_1^{(1)}, -y_1^{(1)}\right)\right\}$ while 8-rQAM at LED_2 can be denoted as $\mathcal{S}_2 = \Big\{ \left(3x_2^{(1)}, y_2^{(1)}\right), \left(3x_2^{(1)}, -y_2^{(1)}\right), \left(x_2^{(1)}, -y_2^{(1)}\right), \left(-x_2^{(1)}, -y_2^{(1)}\right), \left(-3x_2^{(1)}, -y_2^{(1)}\right), \left(-3x_2^{(1)}, y_2^{(1)}\right), \left(-x_2^{(1)}, y_2^{(1)}\right), \left(x_2^{(1)}, y_2^{(1)}\right) \Big\}$. Consequentially, $\mathbf{x}_{\text{sup}}$ can be expressed as

$$\begin{aligned}\mathbf{x}_{\text{sup}} &= \begin{bmatrix} x_1^{(1)} & x_1^{(1)} & -x_1^{(1)} & -x_1^{(1)} & 3x_2^{(1)} & 3x_2^{(1)} & x_2^{(1)} & -x_2^{(1)} & -3x_2^{(1)} & -3x_2^{(1)} & -x_2^{(1)} & x_2^{(1)} \end{bmatrix} \\ &= \begin{bmatrix} x_1^{(1)} & x_2^{(1)} \end{bmatrix} \begin{bmatrix} \mathbf{q}_x^{(1)} & \mathbf{0}_{1\times M_2} \\ \mathbf{0}_{1\times M_1} & \mathbf{q}_x^{(2)} \end{bmatrix}, \end{aligned} \tag{4.12}$$

where $\mathbf{q}_x^{(2)} = [3 \quad 3 \quad 1 \quad -1 \quad -3 \quad -3 \quad -1 \quad 1]$ and $\mathbf{q}_x^{(1)} = [1 \quad 1 \quad -1 \quad -1]$. Similarly, $\mathbf{y}_{\text{sup}}$ can be expressed using just two unknown variables: $\begin{bmatrix} y_1^{(1)} & y_2^{(1)} \end{bmatrix}$ with $\mathbf{q}_y^{(1)} = [1 \quad -1 \quad 1 \quad -1]$ and $\mathbf{q}_y^{(2)} = [1 \quad -1 \quad -1 \quad -1 \quad -1 \quad 1 \quad 1 \quad 1]$. Consequently, $\mathbf{t} = \begin{bmatrix} x_1^{(1)} & x_2^{(1)} & y_1^{(1)} & y_2^{(1)} \end{bmatrix} \mathbf{U}$, where $\mathbf{U} = \begin{bmatrix} \mathbf{q}_x^{(1)} & \mathbf{0}_{1\times M_2} & \mathbf{0}_{1\times M_1} & \mathbf{0}_{1\times M_2} \\ \mathbf{0}_{1\times M_1} & \mathbf{q}_x^{(2)} & \mathbf{0}_{1\times M_1} & \mathbf{0}_{1\times M_2} \\ \mathbf{0}_{1\times M_1} & \mathbf{0}_{1\times M_2} & \mathbf{q}_y^{(1)} & \mathbf{0}_{1\times M_2} \\ \mathbf{0}_{1\times M_1} & \mathbf{0}_{1\times M_2} & \mathbf{0}_{1\times M_1} & \mathbf{q}_y^{(2)} \end{bmatrix}$. Finally, the constraint (8b) can be expressed as

$$2\overline{\mathbf{t}}^{(k)} \bar{\mathbf{Q}}^{(i,i')} \overline{\mathbf{t}}^{\mathrm{T}} - \overline{\mathbf{t}}^{(k)} \bar{\mathbf{Q}}^{(i,i')} \left(\overline{\mathbf{t}}^{(k)}\right)^{\mathrm{T}} \geq q, \forall i \neq i', \tag{4.13}$$

where $\bar{\mathbf{Q}}^{i,i'} = \mathbf{U}\mathbf{Q}^{i,i'}\mathbf{U}^{\mathrm{T}}$ and $\overline{\mathbf{t}} = \begin{bmatrix} x_1^{(1)} & x_2^{(1)} & y_1^{(1)} & y_2^{(1)} \end{bmatrix}$. This obviously helps to alleviate the computational cost as the number of unknown values is just 4 instead of 24.

Example: $N = 2$, $M = 32$ using 4-rQAM and 8-cQAM constellations

A 4-rQAM constellation is used at LED_1 and an 8–cQAM constellation is used at LED_2. Similarly, we have

$$\begin{aligned}\mathbf{x}_{\text{sup}} &= \left[x_1^{(1)}\ x_1^{(1)}\ -x_1^{(1)}\ -x_1^{(1)}\ x_2^{(1)}\ 0\ -x_2^{(1)}\ 0x_2^{(2)}\ -x_2^{(2)}\ -x_2^{(2)}\ x_2^{(2)}\right] \\ &= \left[x_1^{(1)}\ x_2^{(1)}\ x_2^{(2)}\right]\begin{bmatrix}\mathbf{q}_{1x}^{(1)} & \mathbf{0}_{1\times 4} & \mathbf{0}_{1\times 4} \\ \mathbf{0}_{1\times 4} & \mathbf{q}_{2x}^{(1)} & \mathbf{0}_{1\times 4} \\ \mathbf{0}_{1\times 4} & \mathbf{0}_{1\times 4} & \mathbf{q}_{2x}^{(2)}\end{bmatrix}\end{aligned} \tag{4.14}$$

with $\mathbf{q}_{1x}^{(1)} = [1 \quad 1 \quad -1 \quad -1]$, $\mathbf{q}_{1x}^{(1)} = [1 \quad 0 \quad -1 \quad 0]$, and $\mathbf{q}_{1x}^{(2)} = [1 \quad -1 \quad -1 \quad 1]$. Similarly, $\mathbf{y}_{\text{sup}}$ can be expressed using just three unknown variables: $[y_1^{(1)}\ y_2^{(1)}\ y_2^{(2)}]$ with $\mathbf{q}_{1y}^{(1)} = [1 \quad -1 \quad 1 \quad -1]$, $\mathbf{q}_{2y}^{(1)} = [0 \quad 1 \quad 0 \quad -1]$, and $\mathbf{q}_{2y}^{(2)} = [1 \quad 1 \quad -1 \quad -1]$. Consequently, the optimization problem $\mathcal{P}_2$ can be reformed using a similar form where $\overline{\mathbf{t}} = \left[x_1^{(1)}\ x_2^{(1)}\ x_2^{(2)}\ y_1^{(1)}\ y_2^{(1)}\ y_2^{(2)}\right]$.

Example: $N = 3, M = 64$ using 4-rQAM constellations

Similar to the previous scenario, when $N = 3$ and $M = 64$, we assume that all three LEDs use 4-rQAMs in the transmission. For example, with LED_1, the selected constellation is $\mathcal{S}_1 = \left\{\left(x_1^{(1)}, y_1^{(1)}\right), \left(x_1^{(1)}, -y_1^{(1)}\right), \left(-x_1^{(1)}, y_1^{(1)}\right), \left(-x_1^{(1)}, -y_1^{(1)}\right)\right\}$. Consequently, the unknown vector can be denoted as $\overline{\mathbf{t}} = \left[x_1^{(1)}\ x_2^{(1)}\ x_3^{(1)}\ y_1^{(1)}\ y_2^{(1)}\ y_3^{(1)}\right]$.

4.5 Numerical results

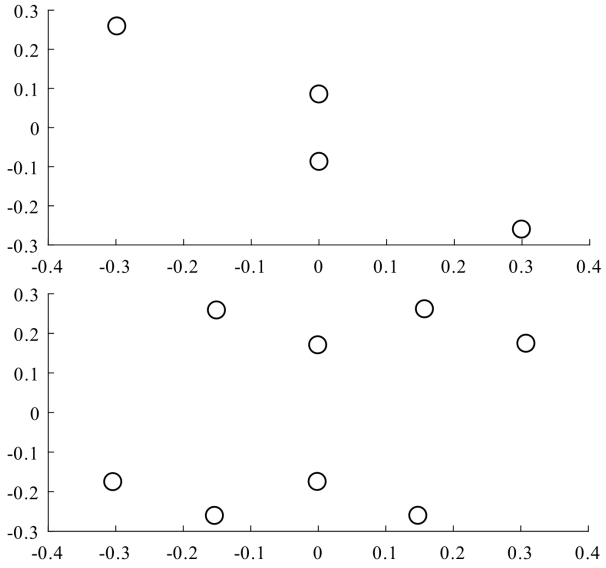

(a)

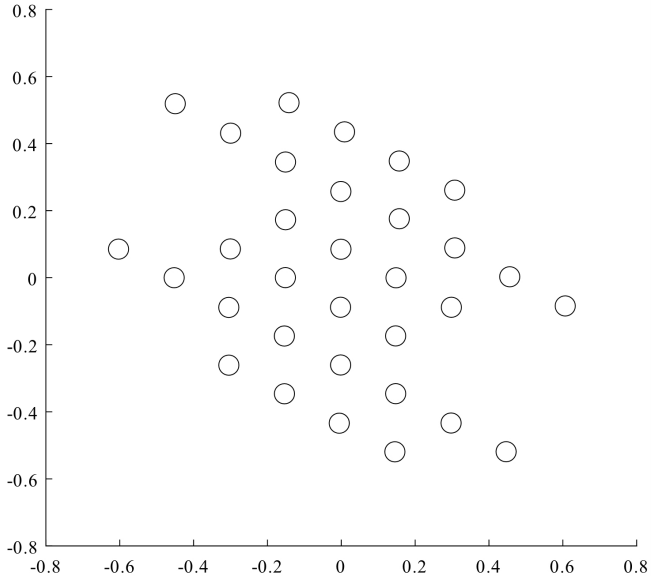

(b)

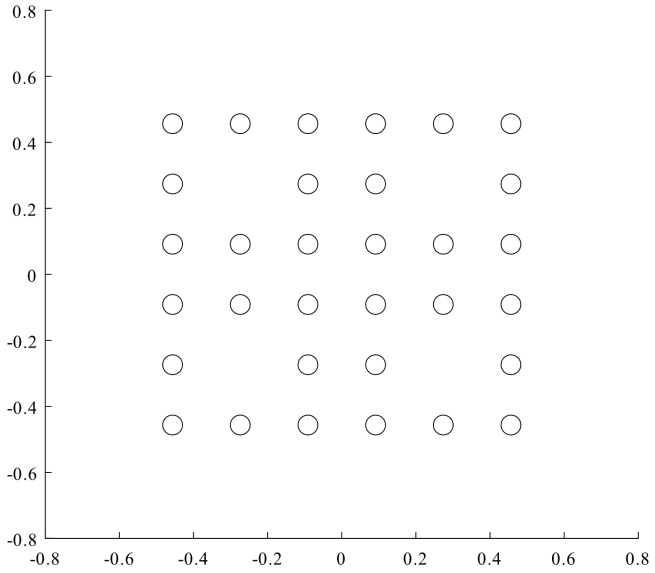
0.8
0.6
0.4
0.2
0
-0.2
-0.4
-0.6
-0.8
-0.8 -0.6 -0.4 -0.2 0 0.2 0.4 0.6 0.8

(c)

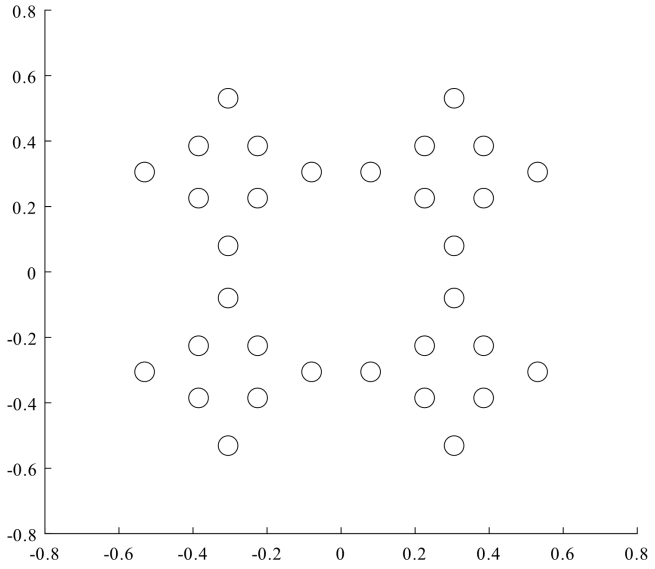
0.8
0.6
0.4
0.2
0
-0.2
-0.4
-0.6
-0.8
-0.8 -0.6 -0.4 -0.2 0 0.2 0.4 0.6 0.8

(d)

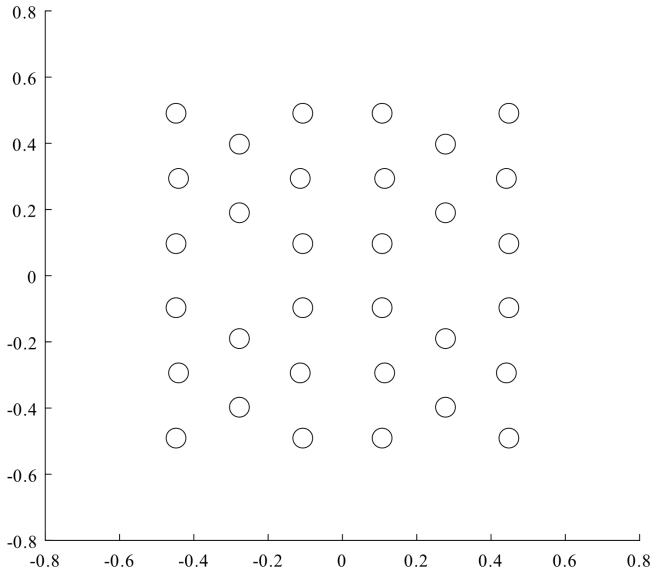

(e)

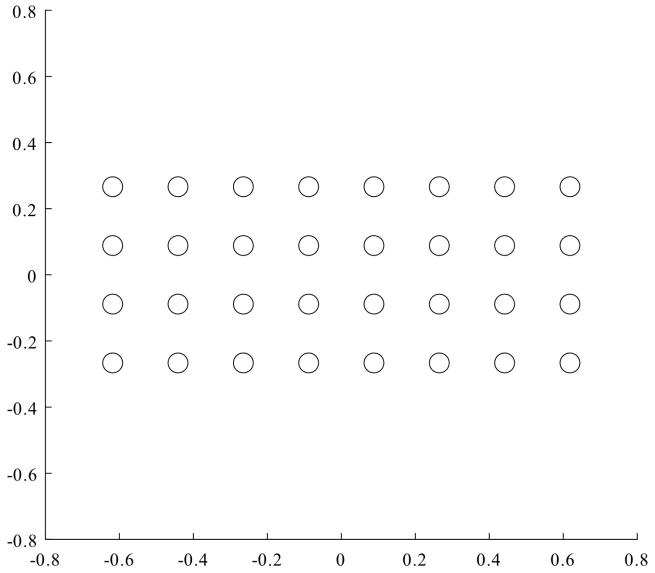

(f)

Figure 4.3: Superposed 32-point: (a) w/o pre-defined shaped, (b) pro. (4-QAM, 8-QAM), (c) con. (4-sQAM, 8-sQAM), (d) con. (4-sQAM, 8-cQAM), (e) pro. (4-rQAM, 8-cQAM), (f) pro. (4-rQAM, 8-rQAM).

The performance of the proposed constellation was evaluated via simulation studies. Similar to previous researches [71], [72], we assume that the channel coefficients are the same between all of the LEDs and the receiver. A conventional constellation was utilized with optimal power allocation coefficients at the LEDs while the proposed ones were employed without the need for power allocation. More specifically, both the conventional and proposed low complexity constellations were built using the resulting optimal vector $\mathbf{t}$ from the optimization solving process. With each of 50 random initial vectors $\mathbf{t}^{(1)}$, the solver iteratively solved $\mathcal{P}_2$ within 5 loops. Last, the optimal $\mathbf{t}$ was the one that gave the largest ED value.

The resulting constellations for the case of $N = 2$ and $M = 32$, where the cardinalities of $\mathcal{S}_1$ and $\mathcal{S}_2$ are 4 and 8, respectively, are shown in Fig. 4.3. With the case of proposed method without pre-defined shaped sub-constellations, the constellations of the individual LEDs are shown in Fig. 4.3a, while the resulting superposed constellation at the receiver side is shown in Fig. 4.3b. It is clear that with a large number of constraints and without any restraint on the shape of the sub-constellations, it is difficult to find an acceptable constellation that can provide a sufficiently large minimum ED. This issue was confirmed later by the error probability of the constellations using this method being worse than the proposed pre-defined shaped sub-constellations. On the other hand, the conventional superposed constellations of 4-sQAM at LED_1 and 8-sQAM at LED_2 (Fig. 4.3c), and 4-sQAM at LED_1 and 8-cQAM at LED_2 (Fig. 4.3d), had optimal power allocation coefficients at the two LEDs. Finally, the constellations from the proposed low complexity method of 4-rQAM at LED_1 and 8-cQAM at LED_2, and 4-rQAM at LED_1 and 8-rQAM at LED_2, are shown in Fig. 4.3e and

Table 4.1: Minimum ED comparison of the 32-point superposed constellations.

Scheme	Size	Constellation Set	Minimum ED
Con. [71]	32	LED_1: 4-sQAM, LED_2: 8-sQAM	0.0333
Con. [71]	32	LED_1: 4-sQAM, LED_2: 8-rQAM	0.0260
Con. [71]	32	LED_1: 4-sQAM, LED_2: 8-cirQAM	0.0284
Pro. (w/o pre-define.)	32	LED_1: 4-QAM, LED_2: 8-QAM	0.0294
Pro. (w/ pre-define.)	32	LED_1: 4-rQAM, LED_2: 8-cQAM	0.0373
Pro. (w/ pre-define.)	32	LED_1: 4-rQAM, LED_2: 8-rQAM	0.0324

4.3f, respectively.

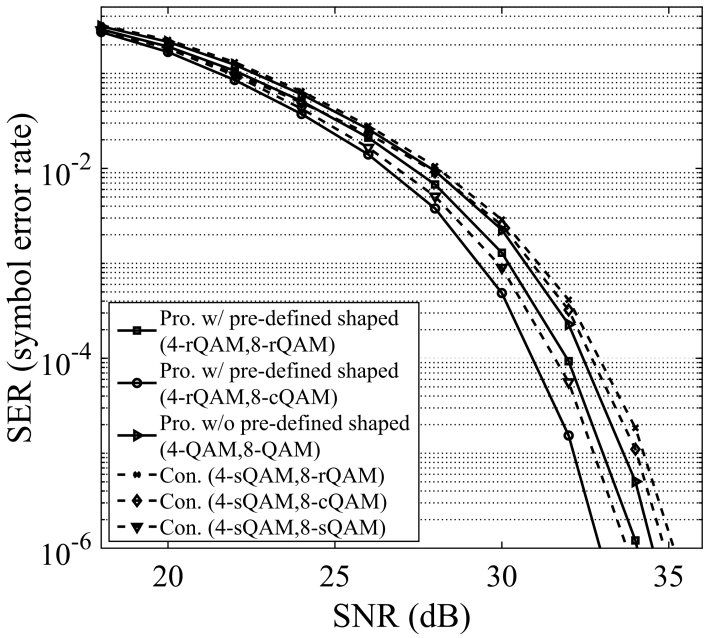

Figure 4.4: SER for a 2-LED system with 32-point superposed constellations.

A minimum ED value comparison between the conventional constellations and the proposed ones is summarized in Table 4.1. It can be seen that the proposed low complexity method with the pre-defined shape of 4-rQAM and 8-cQAM obtained the largest minimum ED values, while those of the proposed method without the

Table 4.2: Minimum ED comparison of 64- and 128-point superposed constellations.

Scheme	S.	Constellation Set	ED
Con. [71]	64	L_1: 4-sQAM, L_2: 4-sQAM, L_3: 4-sQAM	0.0167
Pro. (w/o)	64	L_1: BPSK, L_2: 4-QAM, L_3: 8-QAM	0.0151
Pro. (w/)	64	L_1: BPSK, L_2: 4-rQAM, L_3: 8-cQAM	0.0193
Pro. (w/)	64	L_1: 4-rQAM, L_2: 4-rQAM, L_3: 4-rQAM	0.0165
Con. [71]	128	L_1: 4-sQAM, L_2: 4-sQAM, L_3: 4-sQAM, L_4: BPSK	0.0122
Pro. (w/o)	128	L_1: 4-QAM, L_2: 4-QAM, L_3: 4-QAM, L_4: BPSK	0.0109
Pro. (w/)	128	L_1: 4-rQAM, L_2: 4-rQAM, L_3: 4-rQAM, L_4: BPSK	0.0126
Pro. (w/)	128	L_1: 4-rQAM, L_2: 8-cQAM, L_3: BPSK, L_4: BPSK	0.0140

pre-defined shapes provided relatively small. Besides, the proposed low complexity method with 4-rQAM and 8-rQAM achieved a similar minimum ED value to the conventional one while the conventional 4-sQAM and 8-rQAM obtained the worst minimum ED value. This means that the choice of the shape of the constellation for the individual LEDs matters as it decides the minimum ED values.

The SER performances of the various configurations detailed in Table 4.1 are exhibited in Fig. 4.4, in which it is evident that the constellation combination with the largest minimum ED value had the best SER performance. While the proposed low complexity constellation with a 4-rQAM at LED_1 and 8-cQAM at LED_2 achieved the best performance, the proposed (4-rQAM, 8-rQAM) and conventional (4-sQAM, 8-sQAM) configurations gave performances with SNR gaps similar to the best one at around 1 dB. Moreover, it is not surprising that the proposed method without a pre-defined shape constellation obtained a poor SER result, although a little better than the conventional (4-sQAM, 8-rQAM) and conventional (4-sQAM, 8-cirQAM) configurations. The minimum EDs for the scenario of 3 and 4 LEDs at the transmitter are reported in Table 4.2. The first four entries are for 3-LED systems used to generate

a 64-point superposed constellation of at the receiver. Various sub-constellations were used at each LED. For example, the best conventional constellation was 3 4-sQAMs at 3 LEDs while the proposed one can use constellations range from binary phase-shift keying (BPSK) to an 8-QAM to ensure that the resulting constellation would have 64 distinguishable superposed points at the receiver side. In a similar case with a system of 4 LEDs, a 128-point superposed constellation was generated at the receiver. For both the 64-and 128-point constellations, the choice of pre-defined shape constellation at the transmitter dominated the performance of the superposed constellations at the receiver, which was similar to the previous cases with two LEDs. The best constellations were still the low complexity ones involving cQAMs.

Finally, Figs. 4.5a and 4.5b exhibit the SER performances for the 64-point and 128-point constellations, respectively. Similar to the 32-point constellations, the SER performance with a high SNR level closely followed the minimum ED values: constellations with the largest minimum ED values had the lowest error probability whereas the one with the smallest minimum ED value (the proposed high complexity method) had the worst performance in comparison with others. Moreover, the findings in [73] indicate that square-shaped sub-constellations of LEDs in combination with optimum power allocation coefficients can provide a good superposed constellation. Nevertheless, it is clear that with the help of pre-defined formed sub-constellations, solving the optimization problem can generate constellations with better performance. Hence, the circle-shaped constellation is a potential candidate to construct excellent superposed constellations for many scenarios with various numbers of LEDs and constellation sizes.

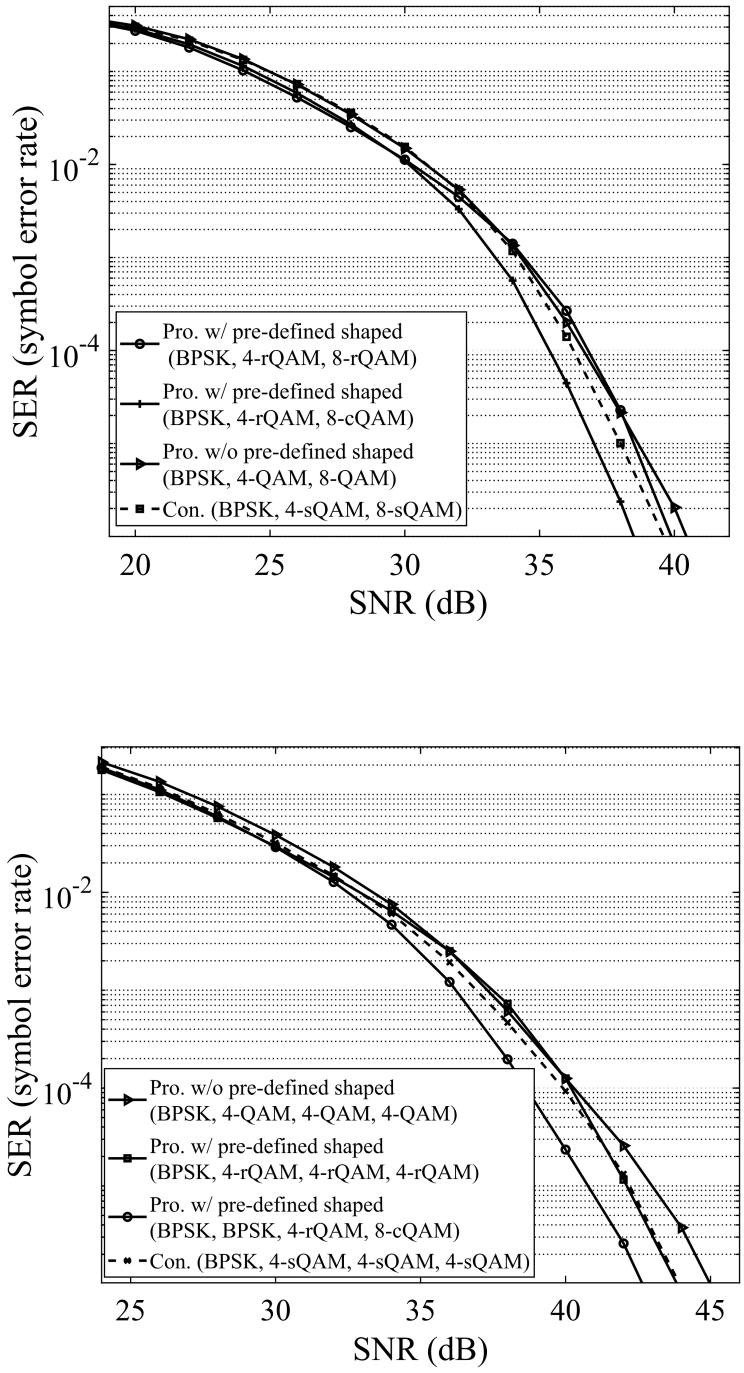

Figure 4.5: SER comparison: (a) 3-LED, 64-point (b) 4-LED, 128-point.

Chapter 5

Summary of contributions and future works

5.1 Thesis conclusion

Future mobile networks would involve considerable increment capacity due to the rapidly growing in the number of wireless devices such as smartphones, tablets, and internet of things devices. With the RF spectrum becoming increasingly congested, an alternate form of wireless communication is required to meet the constantly growing demand for wireless traffic.

As a result, numerous researchers have engaged in and explored VLC technologies during the last few years. Visible light has been regarded as a wireless communication medium due to several benefits it provides over other common wireless transmissions mediums. Having greater bandwidth, it is feasible to accommodate more users and perhaps achieve a better transmission rate, since each user may be allocated a bigger

percentage of the available bandwidth for data transmission. Additionally, the VLC system has a great advantage over other communication systems in that they are ubiquitous in any location. Thus, VLC may be more efficiently utilized by expanding its contemporaneous capabilities to include data transmission in conjunction with illuminating an area.

Apart from the undeniable benefits, VLC technologies do have certain drawbacks that must be thoroughly studied and minimized. We must evaluate the system's weaknesses and limitations, which can include noise from ambient light and the line-of-sight. Because when the noise is stronger than the light from the system, the SNR becomes insufficient, causing data transmission to be disrupted. To compensate for this and improve the system error rate, the transmitted signal should be optimized sufficiently. More precisely, we focused on symbol design issues in this thesis. The primary contributions of this dissertation are mentioned below.

- First, we investigate the symbol designing problem in MIMO-VLC systems with the collaborative constellation. The collaborative constellations try to reduce the impact of channel correlation by effectively increasing the distances between symbols in the constellation under the same power constraint. Consequently, the proposed constellation is able to achieve better power efficiency and spectral efficiency. The proposed LACC scheme with the aid of space collaborative and channel adaptive features was shown to give better performance. Consequently, in comparison with conventional constellations, LACC can be shown to achieve some gain as our proposed scheme smartly take advantage of extra spatial resource and channel state information.

- Next, we study the collaborative constellation problem with the application of deep learning. The neural network is used to approximate the optimal basic constellation points of a MIMO system with CC, which depends on the channel matrix for channel adaptation purposes. More specifically, we explore how to select the right neural network input features to obtain a good performance since the direct use of the channel coefficients does not provide good results. In this sense, we compare different feature choices based on the performance they achieve. From our point of view, the use of parametric function approximation technology that is behind nearly all modern practical applications of deep learning is very useful to deal with the nonlinear and non-convex functions. Therefore, the deep learning approach is an effective solution for the purpose of improving the accuracy and reducing the complexity when optimizing the constellation for the MIMO system.

- Finally, we observed that previous studies on the VLC system with superposed constellation only focused on improving the demodulation part while in the transmitter, the power allocation coefficients were exhaustively chosen to obtain a good minimum Euclidean distance between the received signals at the PD. Our paper focuses explicitly on the sub-constellation at the LED of the VLC system and uses optimization problem solving to achieve a constellation with a significantly larger value of minimum ED. Moreover, we also define the intra-ED and inter-ED notations to reduce the number of constraints in the optimization problem. With different pre-defined shaped sub-constellations at the LEDs, the improvement in minimum ED value consequently can improve the SER

performance of the VLC system with the superposed constellation.

5.2 Future research directions

Recently, VLC is a very advanced technique, and as such, it has enormous potential. As a result, significant research is required in this subject. When VLC techniques become more efficient, we may soon see something analogous to VLC hot-spots anywhere a light bulb is accessible. It will be cleaner and greener, and the technology in the future will be more secure. Due to the limited quantity of available bandwidth, the wireless communication spectrum gets increasingly congested, making it increasingly difficult to obtain a reliable, high-speed transmission. VLC technology has the potential to resolve this problem. When it comes to deploying VLC systems in industrial contexts, there are several specific problems that might be deemed a study subject.

The optimal constellation design and resource allocation for multi-user facilitation in a multi-access VLC network is an important VLC-related issue. In a traditional VLC network, each LED serves as an access point and is integrated with the rest of the network via a power grid and a data infrastructure. Additionally, the implementation of adaptive beam-forming and NOMA protocols in VLC systems and networks has inspired many studies.

Another emerging area of study is the application of machine learning and deep learning to numerous VLC issues, such as multi-path reflection mitigation or multiple position estimation, or to further improve the solution to constellation design and power allocation problems in an even more effective and efficient manner.

Currently, we are conducting research to identify whether there are any alternative approaches for such proposed constellation design techniques. Our objective is to develop a new solution that is more precise and less complicated in order to operate faster and adapt better to the mobility properties of indoor VLC systems. Additionally, we are investigating the issue of integrating VLC transmission with other communication techniques such as RF or free-space optical (FSO) in order to improve the system's capability. Additionally, physical layer security has lately developed as a less computationally expensive and more flexible level of protection in comparison to the other layers' established security features. This prompted an investigation into the somewhat safe but yet susceptible VLC channels.

Publications

SCI(E) Journals

[1] **M. Le-Tran**, S. Kim, T. Ketseoglou, and E. Ayanoglu, "LED selection and MAP detection for generalized LED index modulation," *IEEE Photon. Technol. Lett.*, vol. 30, no. 19, pp. 1695–1698, Oct. 2018.

[2] **M. Le-Tran** and S. Kim, "Layered adaptive collaborative constellation for MIMO visible light communication," *IEEE Access*, vol. 6, pp. 74895–74907, 2018.

[3] **M. Le-Tran** and S. Kim, "Effective receiver design for MIMO visible light communication with quadrichromatic LEDs," *Elec.*, vol. 8, no. 12, p. 1383, Dec. 2019.

[4] **M. Le-Tran** and S. Kim, "Receiver-oriented spatial modulation in visible light communication system," *IEEE Access*, vol. 7, pp. 129666–129677, 2019.

[5] **M. Le-Tran** and S. Kim, "Novel bit mapping for generalized spatial modulation in VLC systems," *IEEE Photon. Technol. Lett.*, vol. 31, no. 15, pp. 1257–1260, Aug. 2019.

[6] **M. Le-Tran** and S. Kim, "Joint power allocation and orientation for uniform

illuminance in indoor visible light communication," *Opt. Express*, vol. 27, no. 20, pp. 28575–28587, Sep. 2019.

[7] **M. Le-Tran** and S. Kim, "Enhanced multi-level multi-pulse modulation for MIMO visible light communication," *IEEE Access*, vol. 8, pp. 210116–210126, 2020.

[8] **M. Le-Tran** and S. Kim, "Orientation-induced link-blocked receiver for MIMO visible light communication," *Opt. Express*, vol. 28, no. 8, p. 12157, Apr. 2020.

[9] **M. Le-Tran** and S. Kim, "Deep learning-based collaborative constellation design for visible light communication," *IEEE Commun. Lett.*, vol. 24, no. 11, pp. 2522–2526, Nov. 2020.

[10] **M. Le-Tran** and S. Kim, "Superposed constellation design for spatial multiplexing visible light communication systems," *Opt. Express*, vol. 28, no. 25, p. 38293, Dec. 2020.

[11] **M. Le-Tran** and S. Kim, "Deep learning-assisted index estimator for generalized LED index modulation OFDM in visible light communication," *Photon.*, vol. 8, no. 5, Art. no. 5, May 2021.

[12] **M. Le-Tran** and S. Kim, "Performance analysis of dual-hop mixed power line Communication/Free-space optical cooperative systems," *Photon.*, vol. 8, no. 6, Art. no. 6, Jun. 2021.

[13] **M. Le-Tran**, T.-H. Vu, and S. Kim, "Performance analysis of optical backhauled

cooperative NOMA visible light communication," Early access in *IEEE Trans. Vehi. Technol.*

International Conferences

[14] **M. Le-Tran** and S. Kim, "Improved GLIM in multiple-input multiple-output OFDM VLC," in Frontiers in Intelligent Computing: Theory and Applications, Singapore, 2020, pp. 123–130.

[15] **M. Le-Tran** and S. Kim, "Multilayer collaborative constellation for MIMO visible light communication," in Proc. 2019 International Conference on Advanced Technologies for Communications (ATC), Oct. 2019, Hanoi, Vietnam pp. 278–281.

Bibliography

[1] Z. Hasan, H. Boostanimehr, and V. K. Bhargava, "Green cellular networks: A survey, some research issues and challenges," *IEEE Commun. Surv. Tutor.*, vol. 13, no. 4, pp. 524–540, 2011.

[2] Daquan Feng, Chenzi Jiang, Gubong Lim, L. Cimini, Gang Feng, and G. Li, "A survey of energy-efficient wireless communications," *IEEE Commun. Surv. Tutor.*, vol. 15, no. 1, pp. 167–178, 2020.

[3] Y. S. Eroğlu, İ. Güvenç, A. Şahin, Y. Yapıcı, N. Pala, and M. Yüksel, "Multi-element VLC networks: LED assignment, power control, and optimum combining," *IEEE J. Sel. Areas Commun.*, vol. 36, no. 1, pp. 121–135, Jan. 2018.

[4] M. Agiwal, A. Roy, and N. Saxena, "Next generation 5G wireless networks: A comprehensive survey," *IEEE Commun. Surv. Tutor.*, vol. 18, no. 3, pp. 1617–1655, 2016.

[5] T. O. Olwal, K. Djouani, and A. M. Kurien, "A survey of resource management toward 5G radio access networks," *IEEE Commun. Surv. Tutor.*, vol. 18, no. 3, pp. 1656–1686, 2016.

[6] S. Yang and L. Hanzo, "Fifty years of MIMO detection: The road to large-scale MIMOs," *IEEE Commun. Surv. Tutor.*, vol. 17, no. 4, pp. 1941–1988, 2019.

[7] L. Dai, B. Wang, Z. Ding, Z. Wang, S. Chen, and L. Hanzo, "A survey of non-orthogonal multiple access for 5G," *IEEE Commun. Surv. Tutor.*, vol. 20, no. 3, pp. 2294–2323, 2018.

[8] M. A. Khalighi and M. Uysal, "Survey on free space optical communication: A communication theory perspective," *IEEE Commun. Surv. Tutor.*, vol. 16, no. 4, pp. 2231–2258, 2019.

[9] S. Arnon, Ed., *Visible Light Communication*. Cambridge, United Kingdom: Cambridge University Press, 2015.

[10] D. Karunatilaka, F. Zafar, V. Kalavally, and R. Parthiban, "LED based indoor visible lght communications: State of the art," *IEEE Commun. Surv. Tutor.*, vol. 17, no. 3, pp. 1649–1678, 2020.

[11] P. H. Pathak, X. Feng, P. Hu, and P. Mohapatra, "Visible light communication, networking, and sensing: A survey, potential and challenges," *IEEE Commun. Surv. Tutor.*, vol. 17, no. 4, pp. 2047–2077, Sep. 2015.

[12] T. Komine and M. Nakagawa, "Fundamental analysis for visible-light communication system using LED lights," *IEEE Trans. Consum. Electron.*, vol. 50, no. 1, pp. 100–107, Feb. 2004.

[13] J. M. Kahn and J. R. Barry, "Wireless infrared communications," in *Proc. IEEE*, Feb. 1997, pp. 265–298.

[14] A. Jovicic, J. Li, and T. Richardson, "Visible light communication: Opportunities, challenges and the path to market," *IEEE Commun. Mag.*, vol. 51, no. 12, pp. 26–32, Dec. 2013.

[15] M. Z. Chowdhury, M. T. Hossan, A. Islam, and Y. M. Jang, "A comparative survey of optical wireless technologies: Architectures and applications," *IEEE Access*, vol. 6, pp. 9819–9840, Jan. 2018.

[16] S. Zhang, S. Watson, J. J. D. McKendry, D. Massoubre, A. Cogman, E. Gu, R. K. Henderson, A. E. Kelly, and M. D. Dawson, "1.5 gbit/s multi-channel visible light communications using CMOS-controlled GaN-based LEDs," *J. Light. Technol.*, vol. 31, no. 8, pp. 1211–1216, Apr. 2013.

[17] D. F. Zhang, Y. J. Zhu, and Y. Y. Zhang, "Multi-LED phase-shifted OOK modulation based visible light communication systems," *IEEE photon, Technol. Lett.*, vol. 25, no. 23, pp. 2251–2254, Dec. 2013.

[18] J. Xu, C. Gong, J. Luo, and Z. Xu, "LED half-power angle optimization for ultra-dense indoor visible light communication network deployment," *IEEE Open J. Commun. Soc.*, vol. 1, pp. 835–848, 2020.

[19] M. Obeed, A. M. Salhab, M. Alouini, and S. A. Zummo, "On optimizing VLC networks for downlink multi-user transmission: A survey," *IEEE Commun. Surv. Tutor.*, vol. 21, no. 3, pp. 2947–2976, Mar. 2019.

[20] A. Memedi and F. Dressler, "Vehicular visible light communications: A survey," *IEEE Commun. Surv. Tutor.*, vol. 21, no. 4, pp. 1342–11 365, 2020.

[21] Q. Wang, D. Giustiniano, and M. Zuniga, "In light and in darkness, in motion and in stillness: A reliable and adaptive receiver for the internet of lights," *IEEE J. Sel. Areas Commun.*, vol. 36, no. 1, pp. 149–161, Jan. 2018.

[22] S. Dimitrov and H. Haas, *Principles of LED Light Communications*. Cambridge University Press, Mar. 2015.

[23] A. Svensson, "An introduction to adaptive QAM modulation schemes for known and predicted channels," *Proc. IEEE*, vol. 95, no. 12, pp. 2322–2336, Dec. 2007.

[24] J. Zhao and P. D. Townsend, "Detection and equalization of set-partitioned offset-QAM OFDM in IMDD systems," *IEEE photon, Technol. Lett.*, vol. 31, no. 1, pp. 70–73, Jan. 2019.

[25] C. Xu, S. Sugiura, S. X. Ng, P. Zhang, L. Wang, and L. Hanzo, "Two decades of MIMO design tradeoffs and reduced-complexity MIMO detection in near-capacity systems," *IEEE Access*, vol. 5, pp. 18 564–18 632, May 2017.

[26] N. Chi, *LED-Based Visible Light Communications*, ser. Signals and Communication Technology. Berlin Heidelberg: Springer-Verlag, 2018.

[27] Z. Ghassemlooy, L. N. Alves, S. Zvanovec, and M.-A. Khalighi, *Visible Light Communications : Theory and Applications*, First. CRC Press, 2017.

[28] K. Xu, H.-Y. Yu, Y.-J. Zhu, and H.-B. Cai, "Channel-adaptive space-collaborative constellation design for MIMO VLC with fast maximum likelihood detection," *IEEE Access*, vol. 5, pp. 842–852, Jan. 2017.

[29] S. G. Wilson, *Digital Modulation and Coding*, 1 edition. Upper Saddle River, N.J: Pearson, Aug. 1995.

[30] Z. Mheich, P. Duhamel, L. Szczecinski, and M.-L. A. Morel, "Constellation shaping for broadcast channels in practical situations," in *Proc. 2011 19th European Signal Processing Conference*, Aug. 2011, pp. 96–100.

[31] M. Stark, F. Ait Aoudia, and J. Hoydis, "Joint learning of geometric and probabilistic constellation shaping," in *Proc. 2019 IEEE Globecom Workshops (GC Wkshps)*, Dec. 2019, pp. 1–6.

[32] S. Zhang and F. Yaman, "Constellation design with geometric and probabilistic shaping," *Optics Communications*, Advances in Modulation and DSP for Optical Transmission Systems, vol. 409, pp. 7–12, Feb. 2018.

[33] J. Cho and P. J. Winzer, "Probabilistic constellation shaping for optical fiber communications," *J. Light. Technol.*, vol. 37, no. 6, pp. 1590–1607, Mar. 2019.

[34] T. Fath and H. Haas, "Performance comparison of MIMO techniques for optical wireless communications in indoor environments," *IEEE Trans. Commun.*, vol. 61, no. 2, pp. 733–742, Feb. 2013.

[35] M. Safari and M. Uysal, "Do we really need OSTBCs for free-space optical communication with direct detection?" *IEEE Trans. Wirel. Commun*, vol. 7, no. 11, pp. 4445–4448, Nov. 2008.

[36] R. Mesleh, H. Elgala, and H. Haas, "Optical spatial modulation," *J Opt Commun Netw.*, vol. 3, no. 3, pp. 234–244, Mar. 2011.

[37] Yi-Jun Zhu, Wang-Feng Liang, Jian-Kang Zhang, and Yan-Yu Zhang, "Space-collaborative constellation designs for MIMO indoor visible light communications," *IEEE photon, Technol Lett*, vol. 27, no. 15, pp. 1667–1670, Aug. 2015.

[38] Y.-J. Zhu, W.-F. Liang, C. Wang, and W.-Y. Wang, "Energy-efficient constellations design and fast decoding for space-collaborative MIMO visible light communications," *Optics Communications*, vol. 383, pp. 260–273, Jan. 2017.

[39] K. Xu, H. Yu, Y. J. Zhu, and Y. Yang, "Channel-adapted space-collaborative constellation design for MIMO visible light communication," in *Proc. 2016 IEEE Global Communications Conference (GLOBECOM)*, Dec. 2016, pp. 1–7.

[40] P. Cheng, Z. Chen, J. A. Zhang, Y. Li, and B. Vucetic, "A unified precoding scheme for generalized spatial modulation," *IEEE Trans. Commun*, vol. 16, no. 99, pp. 1453–1465, Jan. 2018.

[41] M. C. Lee, W. H. Chung, and T. S. Lee, "Generalized precoder design formulation and iterative algorithm for spatial modulation in MIMO systems with CSIT," *IEEE Trans. Commun.*, vol. 63, no. 4, pp. 1230–1244, Apr. 2015.

[42] M. Beko and R. Dinis, "Designing good multi-dimensional constellations," *IEEE Wirel. Commun. Lett.*, vol. 1, no. 3, pp. 221–224, Jun. 2012.

[43] *CVX: Matlab software for disciplined convex programming*, September 2013, http://cvxr.com/cvx.

[44] S. Wolfram, *The Mathematica Book*, 4th ed. Champaign, IL : New York: Cambridge University Press, 1999.

[45] J. H. Conway and N. J. A. Sloane, *Sphere Packings, Lattices, and Groups*. New York: Springer, 1999.

[46] J. Choi, Y. Nam, and N. Lee, "Spatial lattice modulation for MIMO systems," *IEEE Trans. Signal Process*, vol. 66, no. 12, pp. 3185–3198, Jun. 2018.

[47] D. Tse and P. Viswanath, *Fundamentals of Wireless Communication*. Cambridge: Cambridge University Press, 2005.

[48] H. Marshoud, P. C. Sofotasios, S. Muhaidat, B. S. Sharif, and G. K. Karagiannidis, "Optical adaptive precoding for visible light communications," *IEEE Access*, vol. 6, pp. 22 121–22 130, Mar. 2018.

[49] M. L. Tran and S. Kim, "Layered adaptive collaborative constellation for MIMO visible light communication," *IEEE Access*, vol. 6, pp. 74 895–74 907, 2018.

[50] X. Lin and L. Zhang, "Intelligent and practical deep learning aided positioning design for visible light communication receivers," *IEEE Commun. Lett.*, pp. 577–580, Dec. 2019.

[51] L. Xiao, G. Sheng, S. Liu, H. Dai, M. Peng, and J. Song, "Deep reinforcement learning-enabled secure visible light communication against eavesdropping," *IEEE Trans. Commun.*, vol. 67, no. 10, pp. 6994–7005, Oct. 2019.

[52] M. Le-Tran and S. Kim, "Deep learning-assisted index estimator for generalized LED index modulation OFDM in visible light communication," *Photon.*, vol. 8, no. 5, p. 168, May 2021.

[53] H. Lee, I. Lee, and S. H. Lee, "Deep learning based transceiver design for multi-colored VLC systems," *Opt. Express*, vol. 26, no. 5, pp. 6222–6238, Mar. 2018.

[54] S. Ma, J. Dai, S. Lu, H. Li, H. Zhang, C. Du, and S. Li, "Signal demodulation with machine learning methods for physical layer visible light communications: Prototype platform, open dataset, and algorithms," *IEEE Access*, vol. 7, pp. 30 588–30 598, 2019.

[55] P. Miao, B. Zhu, C. Qi, Y. Jin, and C. Lin, "A model-driven deep learning method for LED nonlinearity mitigation in OFDM-based optical communications," *IEEE Access*, vol. 7, pp. 71 436–71 446, 2019.

[56] T. Wang, F. Yang, F. Yang, J. Song, and J. Song, "Deep learning-based detection scheme for visible light communication with generalized spatial modulation," *Opt. Express*, vol. 28, no. 20, pp. 28 906–28 915, Sep. 2020.

[57] T. V. Luong, Y. Ko, N. A. Vien, D. H. N. Nguyen, and M. Matthaiou, "Deep learning-based detector for OFDM-IM," *IEEE Wirel. Commun. Lett.*, vol. 8, no. 4, pp. 1159–1162, Aug. 2019.

[58] H. Lee, I. Lee, T. Q. S. Quek, and S. H. Lee, "Binary signaling design for visible light communication: A deep learning framework," *Opt. Express*, vol. 26, no. 14, p. 18 131, Jul. 2018.

[59] M. L. Tran and S. Kim, "Novel bit mapping for generalized spatial modulation in VLC systems," *IEEE Photon, Technol. Lett.*, vol. 31, no. 15, pp. 1257–1260, Aug. 2019.

[60] A. Tato, C. Mosquera, P. Henarejos, and A. Perez-Neira, "Neural network aided computation of mutual information for adaptation of spatial modulation," *IEEE Trans. Commun.*, vol. 68, no. 5, pp. 2809–2822, May 2020.

[61] Y. Wang, M. Chen, Z. Yang, T. Luo, and W. Saad, "Deep learning for optimal deployment of UAVs with visible light communications," *IEEE Trans. Wirel. Commun.*, pp. 10 715–10 790, May 2020.

[62] Z.-Y. Wu, M. Ismail, E. Serpedin, and J. Wang, "Efficient prediction of link outage in mobile optical wireless communications," *IEEE Trans. Wirel. Commun.*, vol. 20, no. 2, pp. 882–896, Oct. 2020.

[63] C. Zou and F. Yang, "Dimming-aware deep learning approach for OOK-based visible light communication," *J. Light. Technol.*, vol. 38, no. 20, pp. 5733–5743, Oct. 2020.

[64] J. Okumura, Y. Kozawa, Y. Umeda, and H. Habuchi, "Hybrid PWM/DPAM dimming control for digital color shift keying using RGB-LED array," *IEEE J. Sel. Areas Commun.*, vol. 36, no. 1, pp. 45–52, Jan. 2018.

[65] S. Wilson, M. Brandt-Pearce, Qianling Cao, and M. Baedke, "Optical repetition MIMO transmission with multipulse PPM," *IEEE J. Sel. Areas Commun.*, vol. 23, no. 9, pp. 1901–1910, Sep. 2005.

[66] X. Li, L. Wu, Z. Liu, B. Hussain, W. C. Chong, K. M. Lau, and C. P. Yue, "Design and characterization of active matrix LED microdisplays with embedded visible light communication transmitter," *J. Light. Technol.*, vol. 34, no. 14, pp. 3449–3457, Jul. 2016.

[67] M. L. Tran and S. Kim, "Orientation-induced link-blocked receiver for MIMO visible light communication," *Opt. Express*, vol. 28, no. 8, pp. 12 157–12 173, Apr. 2020.

[68] H. B. Cai, J. Zhang, Y. J. Zhu, J. K. Zhang, and X. Yang, "Optimal constellation design for indoor 2x2 MIMO visible light communications," *IEEE Commun. Lett.*, vol. 20, no. 2, pp. 264–267, Feb. 2016.

[69] J. Zhang, Y. Wang, L. Ding, and N. Zhang, "Bit error probability of spatial modulation over measured indoor channels," *IEEE Trans. Wirel. Commun.*, vol. 13, no. 3, pp. 1380–1387, Mar. 2014.

[70] Y.-Y. Zhang, H.-Y. Yu, J.-K. Zhang, Y.-J. Zhu, and T. Wang, "Energy-efficient space-time modulation for indoor MISO visible light communications," *Opt Lett*, vol. 41, no. 2, pp. 329–332, Jan. 2016.

[71] L. Qiao, X. Lu, S. Liang, J. Zhang, and N. Chi, "Performance analysis of space multiplexing by superposed signal in multi-dimensional VLC system," *Opt. Express*, vol. 26, no. 16, pp. 19 762–19 770, Aug. 2018.

[72] X. Guo and N. Chi, "Superposed 32QAM constellation design for 2×2 spatial multiplexing MIMO VLC systems," *J. Light. Technol.*, vol. 13, no. 4, pp. 1121–1129, 2019.

[73] Z. Wang, S. Han, and N. Chi, "Performance enhancement based on machine learning scheme for space multiplexing 2×2 MIMO VLC system employing joint IQ independent component analysis," *Opt. Commun.*, vol. 458, pp. 124 733–124 742, Mar. 2020.

[74] M. L. Tran and S. Kim, "Joint power allocation and orientation for uniform illuminance in indoor visible light communication," *Opt. Express*, vol. 27, no. 20, pp. 28 575–28 587, Sep. 2019.